Autonomous Optimization of Repurposed Electric Vehicle Batteries for Grid Balancing

Bernhard Fäßler

Autonomous Optimization of Repurposed Electric Vehicle Batteries for Grid Balancing

Doctoral Dissertation for the Degree of Doctor of Philosophy (PhD) at the Faculty of Engineering and Science, Specialization in Renewable Energy

University of Agder
Faculty of Engineering and Science
2018

Doctoral Dissertations at the University of Agder 193

ISSN: 1504-9272
ISBN: 978-82-7117-892-5

Printed by the Wittusen & Jensen
Oslo

To my girlfriend, Verena Lechner,
to my parents, Gabriele and Norbert Fäßler,
to my brothers, Andreas and Tobias Fäßler,
and to all my friends.

Acknowledgements

This thesis was made possible through the PhD cooperation agreement between Vorarlberg, University of Applied Sciences (FHV), Dornbirn, Austria and University of Agder (UiA), Grimstad, Norway. I would like to thank all parties involved in this arrangement as a result of which I was allowed to participate in the PhD program of UiA, while the project financing was arranged by the FHV.

My thanks go particularly to my adviser, Dr. Mohan Lal Kolhe (UiA), whose guidance has been valuable throughout the development of this thesis. I am deeply grateful to Dr. Jörg Petrasch (FHV), my co-adviser, for, besides enabling this project, he has contributed immensely to the quality of this thesis through his numerous, valuable insights. I would also like to thank the examiners for their objective assessment of this thesis.

Special thanks go to Dr. Markus Preißinger, the Illwerke VKW Professor for Energy Efficiency and the head of the Energy Research Center at FHV, for his prompt and valuable additions.

I would also like to express my gratitude to the administrators Emma Hornemann (UiA) and Helena Gössler (FHV). Their countless hours of work are, unfortunately, often not visible, but this thesis would not have been possible without their assistance.

I appreciate the feedback, discussions, advice and comments I got from my colleagues, the members of the Energy Research Center at FHV. Above all, Peter Kepplinger, whose ideas, technical inputs, and co-operation made this thesis possible. Huge thanks to Gerhard Huber, who kept me grounded and kept his eyes on the bigger picture. My co-worker Michael Schuler always partook in enriching discussions. I have received generous support from Anupam Akolkar and Nima Rahmatian, who contributed, as reviewers to making my thesis and my publications clearer. Thanks to all other members of the Energy Research Center, Bettina Friedel, Stefan Arzbacher and Johannes Haag. They have been helpful throughout my thesis work.

Special thanks to my family and friends for their continued support throughout my studies. Last, but not least, my deepest, heartfelt appreciation goes to my girlfriend, Verena Lechner, who has always believed in me and supported me through difficult times. Whether in moments of simple self-doubt or in more desperate situations, her encouragement ensured the continuity of my efforts and the resulting success is owed as much to her persistence with me as mine with my tasks.

Abstract

Battery storage systems are increasingly being used as grid-balancing measures to ensure smooth operation of the electrical grid due to their compactness, practical environment-independence, high efficiencies, and wide-ranging power and energy capacities. Currently, battery storage systems for grid balancing are facing high lifecycle costs as well as high energy and material requirements. To reduce costs, the reuse of electric vehicle batteries as stationary storage has been proposed. Such batteries are typically replaced if their capacity drops below 70–80% of their initial capacity. However, they may still have sufficient capacity for stationary applications. An advantage of reusing is that less active bulk material is wasted and thus, the ecological footprint of such batteries is improved.

In this thesis, a theoretical and experimental investigation of a decommissioned and repurposed electric vehicle ZEBRA (Zero Emission Battery Research Activities) battery as stationary storage for autonomous grid balancing is presented. Therein, the battery operation mode (charge, discharge, or idle) is determined by an autonomous optimization routine based on a one-way communicated incentive, which represents the intention of the operator to achieve a certain goal, e.g. grid balancing. In a first attempt, the historic Austrian day-ahead stock market price for electricity serves as the incentive. A mathematical model of the molten-salt, high-temperature ZEBRA battery is developed to simulate battery dynamics.

For the implementation of the approach on a physical system, steps are taken towards developing highly efficient simulation and optimization routines, which can be executed on hardware with limited computational resources. To this end, different nonlinear and linear optimization approaches are compared with respect to computational costs and resulting control optimality. It is shown that linear programs using linear models yield comparable results to more complex optimization routines and models. In addition, the simulations indicate that the temporal resolution of the incentive strongly influences the battery dynamics and is thus crucial for an optimal battery operation.

To validate the simulations, a linear optimization routine driven by the Austrian electricity spot-market price for electricity is implemented on a decommissioned ZEBRA battery. The experimental results prove the general findings of the previous simulations, i.e. it is not possible to gain a profitable operation based on present economic boundary conditions, given the low variation currently seen in day-ahead prices. Additionally, the reuse of a ZEBRA battery showed significant hardware and software related challenges. Specifically, some technical details of the ZEBRA battery are difficult to model, e.g. the internal battery system check. These challenges result in a high discrepancy between the predicted theoretical and the observed physical potential of grid-balancing measures, which underlines the urgent need for field test implementations. The results obtained in this scientific contribution are valuable for the repurposing of other electric vehicle batteries, because many similar challenges may also be encountered for other battery types. The findings of this study show that it is crucial to plan the second use of electric vehicle batteries for grid balancing even prior to their commissioning.

In order to investigate the consequences of battery storage systems as grid-balancing measures in a low-voltage distribution grid penetrated by distributed generation, a simulation study that shows the impacts of different battery positions and incentives is conducted.

Compared to available studies in the literature, a real, low-voltage distribution grid topology, real smart meter household load profiles, and real photovoltaics load data are used. The study incorporates: 1) a baseline simulation without storage; 2) a single, central battery storage; and 3) multiple, distributed battery storages which together have the same power and capacity as the central storage. The incentives address either market conditions, grid balancing, optimal photovoltaic utilization, load shifting, or self-consumption. The impacts on power quality are assessed by the peak-to-average power ratio at the feed-in node and the maximum voltage drop/rise at all grid nodes. The investigated cases showed that incentives that reflect more general conditions, such as supraregional markets, may even deteriorate power quality. Thus, it was proved that it is crucial to assess the impact of grid-balancing measures on all voltage levels of the electrical grid. This means that to improve the power quality of low-voltage distribution grids using autonomously optimized devices, incentives reflecting load conditions are preferable.

Table of Contents

Structure of the Thesis

This thesis is a collection of four technical publications addressing autonomous optimization of repurposed electric vehicle batteries for grid balancing. The thesis is split into two parts. PART I gives an introduction into the topic, shows the authors motivation, the problem statement and discusses the general approach. In addition, a detailed summary report of all scientific contributions of the author is given followed by a general conclusion of the main findings of this thesis and a short outlook on relevant future research. In PART II, all thesis related scientific contributions are given in a modified format in order to detail the scientific content.

Publications

All listed publications are an outcome of the research work carried out by the author of this thesis, including three published and one submitted scientific contribution. The following publications are included in this thesis:

Paper A: B. Fäßler, P. Kepplinger, M. L. Kolhe, and J. Petrasch, "Decentralized on-site optimization of a battery storage system using one-way communication," presented at the International Conference on Renewable Power Generation, 2015, pp. 1–6.
Digital object identifier: https://doi.org/10.1049/cp.2015.0304

Paper B: B. Faessler, P. Kepplinger, and J. Petrasch, "Decentralized price-driven grid balancing via repurposed electric vehicle batteries," *Energy*, vol. 118, pp. 446–455, Jan. 2017.
Digital object identifier: https://doi.org/10.1016/j.energy.2016.12.013

Paper C: B. Faessler, P. Kepplinger, and J. Petrasch, "Field testing of repurposed electric vehicle batteries for price-driven grid balancing," (Submitted to Elsevier Energy Journal, Manuscript Number: EGY-D-17-05788)

Paper D: B. Faessler, M. Schuler, M. Preißinger, and P. Kepplinger, "Battery storage systems as grid-balancing measure in low-voltage distribution grids with distributed generation," *Energies*, vol. 10, no. 12, pp. 1–14, Dec. 2017.
Digital object identifier: https://doi.org/10.3390/en10122161

PART I

List of Figures

List of Tables

Nomenclature

C	Heat capacity (J/K)
c	Pseudo-cost function (–)
E_{el}	Electrical energy content (J)
E_{losses}	Cumulative distribution losses (Wh)
PAPR	Peak-to-average power ratio (–)
P_{AC}	Alternating power (W)
P_{DC}	Direct power (W)
P_{fan}	Cooling fan power (W)
P_{h}	Auxiliary heating power (W)
P_{loss}	Linearized battery losses (W)
P_{Ri}	Dissipated heat transfer rate due to internal resistance (W)
$\dot{Q}_{\mathrm{cool}}$	Heat transfer rate due to cooling (W)
$\dot{Q}_{\mathrm{loss}}$	Heat loss via the insulation (W)
S_{slack}	Power at the slack node (VA)
SOC	State of charge (%)
T	Battery temperature (°C)
t	Time (s)
$U_{\mathrm{d/r}}$	Alternating voltage drop/rise (V)
u	Decision variable
η_{in}	Charging converter efficiency (–)
η_{out}	Discharging converter efficiency (–)

1. Introduction

Batteries have become an integral part of our lives and can be found practically everywhere, from day-to-day gadgets such as wristwatches, mobile phones, electric vehicle (EV) batteries, to very specialized devices such as heart pacemakers. Batteries have many advantages compared to other storage technologies [1]. They can be built with wide ranges of power and energy capacities, as well as voltage and current outputs, by appropriately combining cells based on various cell chemistries [2]. Most batteries can be operated at room temperatures. The individual battery cells are usually sealed, emit no exhaust gases, do not require cooling fans, operate noiselessly, produce no vibrations, and have good shock and vibration resistance. Additionally, many battery types are practically maintenance free [3] and very efficient since they can typically deliver 90% of input energy as output energy [4]. Batteries have high responsiveness [5] and their operating time scales can range from seconds to days [2]. This means they can be used to cover a wide spectrum of applications, ranging from instantaneous to long-term operation.

Due to their compactness, location-independence, and wide-ranging power and energy capacities, battery storage systems are increasingly applied in the electrical power system, with a variety of cell chemistries [6]–[8]. The electrical power grid consists of several voltage levels between the point of electrical energy generation and the point of consumption to ensure minimal distribution losses and associated insulation efforts, handling issues, and costs [9]. The voltage levels range from several thousand to some hundred volts. Traditionally, the electrical energy is mainly fed in at higher voltage levels, transmitted over several voltage levels, and consumed mainly at the lowest voltage level. Conversely, renewables tend to participate in the feed-in at all voltage levels of the electrical grid [9]. Battery storage systems can be integrated at all these voltage levels and can support the grid by buffering electrical energy [10]. The round-trip efficiencies achieved in commercial battery storage solutions, including converters, range from 65% to almost 90% [11]. Batteries can be used for:

- Uninterruptible power supply: Batteries have already been used as an auxiliary source for years to ensure an uninterrupted supply of critical electrical loads in the event of a fault like power outage or anomalies in the electrical power system [12].
- Island grids: Such grids consist only of a few energy sources, are spatially limited, and are not connected to other grids. Commercial solutions are already available for isolated grids in which batteries are used as buffers [13] and to compensate for power fluctuations [2], [14].
- Residential storage: Batteries are used to increase self-sufficiency by storing surplus electrical energy, mainly generated by renewables, and supporting demand in times of deficits [15].
- Grid support: Batteries can provide real, active, and reactive power and therefore help control the amount of reactive power in the electrical grid [9].
- Black start capability: In case of a full or partial blackout of the electrical grid, power sources are needed to return the energy system to normal operation [16]. Simulations have shown that batteries are able to provide black start capacities [2], [16], [17].

In addition, balancing strategies [18], [19] as well as energy buffers are necessary [6], [20] to keep electrical energy generation and demand in balance. To compensate for that, grid-

balancing approaches based on different types of batteries have already been investigated [21]–[25]. Energy fluctuations, caused by imbalances, occur on the generation side as well as on the demand side. Balancing energy is already a challenge and will be an increasing issue in the near future, which can be attributed to continuously progressive effects on the generation and the demand side.

On the generation side, grid operation can be severely affected by renewables since most of the energy generated from renewables comes from transient sources such as wind and solar [18], [26]. According to the International Energy Outlook 2016 [27], renewables are indicated as the fastest growing source of electrical energy, with their share predicted to increase by 2.9% per year from 22% in 2012 to 29% in 2040. Therefore, increased fluctuations can be expected for electricity generation in the near future.

On the demand side, the need for electrical energy varies daily and seasonally and is mostly uncontrollable [28]. In addition, energy consumed by both industrial and residential units steadily increases worldwide [29]. The United States Energy Information Administration differentiates between members and non-members of the Organization for Economic Cooperation and Development (OECD) in its reports. Among the member countries of the OECD, the residential sector plays a significant role in energy consumption since its high standard of living leads to an increased energy demand for heating, cooling and for other energy-consuming products [30]. On the other hand, industrial demand contributes to increased energy usage in the growing economies of the non-OECD member countries [27]. Non-OECD member countries have also been exhibiting faster rates of growth of electrical energy demand [27]. An additional, global contributing factor to the growing demand for energy is the progressive electrification of the transport sector, with the total electricity share of electrified light-duty vehicles expected to grow to 1% by 2040 [31].

At present, high lifecycle costs [32] and high energy and material requirements [33] make battery storage systems less attractive for grid balancing. However, a cost reduction can be achieved by using systems consisting of batteries, which do not exploit their full capacity at all times.

For this purpose, combined photovoltaic battery bank systems [34], mainly used for maximizing the self-consumption of locally produced energy [35] and smoothing the electricity feed-in to the grid [36], can be further used. Additionally, batteries on wind farms [37], [38], or EVs [39]–[43], can also be suitably adapted. Initial costs of battery storage systems to be used for grid balancing can also be reduced by using repurposed EV batteries [44]. This is because such batteries usually are replaced after their capacity falls below 70–80% of their initial capacity [45], [46], which means that they still have sufficient capacity for stationary applications. Therefore, using repurposed EV batteries as stationary storages is an interesting approach for grid balancing and is investigated in detail in the content of this thesis based on a theoretical and an experimental study.

1.1 Motivation

As Fig. 1 illustrates, the number of EVs in use worldwide has increased rapidly in recent years. This implies that a significant number of discarded EV-batteries for stationary applications will be available in the near future.

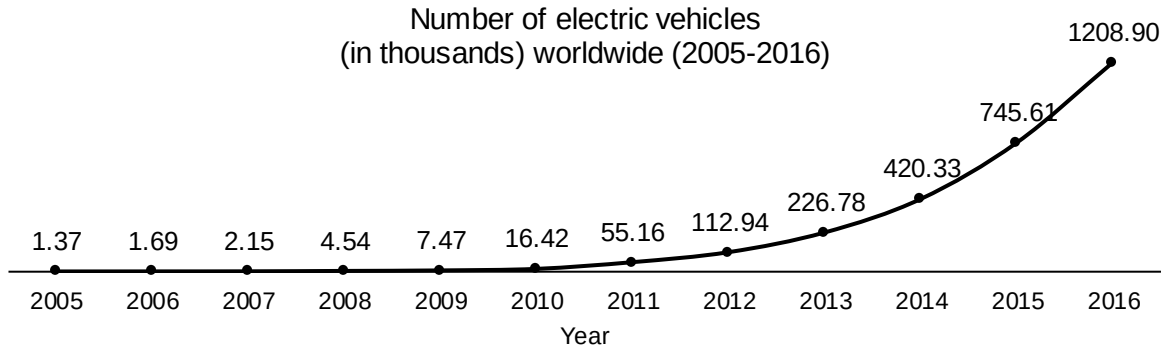

Fig. 1: Number of electric vehicles (in thousands) worldwide in use from 2005 to 2016 [47].

A second use of EV batteries reduces their ecological footprint [48] since discarding batteries will lead to a waste of remaining active bulk material [49]. Based on the calendar life of a battery, its lifetime could be almost doubled by a second use. The calendar life for lithium-ion (Li-ion) and high temperature sodium batteries is nearly 20 years [50]–[52] and the EV-use phase is just about 10 years [53]. The prerequisites for extending the lifetime of a battery are:

- The battery's cycle lifetime is not yet over.
- The battery has only been operated in the allowed temperature range to avoid thermal damaging.
- The battery has not experienced extraordinarily frequent overcharging or deep discharging.
- The battery has not been exposed to unsafe charging or discharging rates.

However, there are technical challenges associated with repurposing EV batteries for stationary applications. Since these batteries are designed as automotive batteries, they come with specific standards and safety measures. These measures vary across batteries and must occasionally be bypassed before they can be used as stationary storage. In addition, in order to repurpose these batteries, AC/DC charging/discharging converters may have to be installed.

Repurposed EV batteries may be used either for large, centralized battery storage systems made out of many individual batteries, or for many small, distributed storage systems. For large, aggregated, centralized storage systems, electrical grid integration of battery systems could be even more challenging due to a higher probability of diversity in the cell chemistry and different operational requirements of the individual battery types involved. Therefore, a "master" battery management system may have to be introduced to cover all different battery requirements. Whereas integrating one or several types of batteries into high-capacity storage installations may be done by large enterprises, single batteries may be adapted by households or small consumers for similar purposes. A vehicle manufacturer has already announced that it plans to reuse its old EV batteries to build a large stationary storage with a capacity of

13 MWh [54]. Reusing EV batteries as small, distributed, stationary storages, comprising of several kWh, for grid balancing has been discussed in numerous publications [48], [55], [56].

Grid balancing happens on different time scales, ranging from instantaneous to long-term measures. Traditionally, the generation of electrical energy follows the demand [19], [28] and is usually controlled through various markets:

- Forward markets represent the long-term, where trading is done for future power and energy deliveries. Trading can be centrally organized and regulated via exchanges, or involve unregulated, over-the-counter deals [57].
- Spot markets, more specifically day-ahead markets and intra-day markets, represent the medium-term, where the trades will be fulfilled within days. This markets can also be centrally organized and regulated via exchanges, or involve unregulated, over-the-counter deals [57].
- Tenders for short-term grid-balancing measures procure operating reserves for certain periods to ensure that fast reacting power plants compensate for generation and demand imbalances [58].

However, more recently, measures to adapt demand to generation have gained interest. Demand side management (DSM) is a portfolio of measures to balance the electrical grid on the consumption side [19]. In DSM, controllable, flexible loads and energy storage facilities reduce, increase or shift energy consumption in order to match electrical energy usage with generation [19]. Palensky et al. [19] classified DSM strategies according to the timing, and impact of the measures:

- Energy efficiency strategies, which are permanent measures, e.g. improving the efficiency of building sites;
- Time of use measures, which are medium-term measures aiming to shift demand to off peak hours, e.g. heating water using cheaper night tariff;
- Demand response measures, which are medium- to short-term measures and intend to cause a change in consumption patterns of end users;
- Strategies involving operating reserves, which are short-term measures and aim to control and to maintain the proper functionality of the electrical grid.

To operate battery storage systems as grid-balancing measures, an appropriate control strategy has to be developed based on the time scale of interest. With a repurposed battery storage, strategies are required to control demand during charging and regulate generation during discharging. Thus, an adaptive strategy combining demand side management and generation control is necessary for such an application. As for strategies in DSM, to motivate consumers to change their consumption according to the actual electrical energy generation, a specific tariff or program has to be provided [59]. To transmit such a specific tariff or program, different concepts have been proposed. While most grid-balancing concepts require two-way communication [60], local, autonomous control with unidirectional communication, as proposed by Kepplinger et al. [61], has been demonstrated to be an alternative grid-balancing solution for domestic hot water heaters. To the best of the author's knowledge, such a control approach has never been investigated for repurposing EV batteries as stationary storage for grid balancing. Neither theoretical considerations, nor a physical implementation, has been addressed in the literature.

1.2 Problem Statement

The available literature indicates that although the repurposing of electric vehicle batteries as stationary storage for grid balancing has attracted significant interest, aspects related to the technical and economic feasibility of such systems have not yet been investigated in the necessary scientific depth. Therefore, this study focuses on filling the knowledge gaps related to the following research questions:

- Is it technically feasible to repurpose these batteries as stationary storage for grid balancing?
- Which provisions have to be made for a physical implementation of repurposed electric vehicle batteries?
- What are the differences between the modeled and actual operation of such a repurposed battery?
- How can battery storages affect grid balancing in a low-voltage distribution grid?

The approach to answer these questions is discussed in detail in chapter 1.3. Chapter 2 provides a summary report of the scientific contributions published as a part of this thesis in PART II. A conclusion is given in chapter 3, which also discusses future research topics that have not yet been addressed within this work.

1.3 Approach

In this thesis, a theoretical and experimental investigation of a repurposed electric vehicle ZEBRA (Zero Emission Battery Research Activities) battery as stationary storage for autonomous grid balancing is presented. The battery is decommissioned from the electric vehicle THINK City [62]. As this type of EV ranks among the first commercial electric cars, these batteries are now available for second-use approaches.

The ZEBRA battery is a molten-salt, high-temperature battery operating efficiently and safely at an internal temperature between 270 and 350 °C [63]. Its operation is based on the reaction of sodium with nickel chloride. The redox reaction within a single battery cell is given by, c.f. [63], [64]:

$$2\mathrm{Na} + \mathrm{NiCl_2} \underset{\text{charge}}{\overset{\text{discharge}}{\rightleftarrows}} 2\mathrm{NaCl} + \mathrm{Ni} \qquad \text{Eq. 1}$$

The energy density of a ZEBRA battery is approximately 100 Wh/kg; the power density is approximately 150 W/kg [63], [65], [66]. The expected cycle lifetime is given to be about 3500 full charge and discharge cycles [66]. Therefore, ZEBRA batteries are interesting for stationary applications due to their long-term cyclic stability [51]. In addition, ZEBRA batteries are thermally insulated by a double-walled vacuum chamber, and hence can be operated between −40 to 70 °C ambient temperature [67]. The battery reused from the THINK City vehicle exhibits a capacity of 28.2 kWh.

The control strategy proposed to operate a stationary ZEBRA battery is close to strategies for DSM and is based on a unidirectionally communicated information flow—from a distributor to a participating device, cf. Fig. 2,. This only allows for indirect demand control. Via unidirectional communication, a pseudo-cost function (PCF) is transmitted to a locally implemented optimization routine. The PCF represents the intention of the operator to achieve a certain goal, e.g. grid balancing. However, the PCF can be any step-wise constant function [61]. In the remainder of this work, the PCF will also be referred as an “incentive”.

The optimization routine is driven by the PCF and determines the decision function, $u(t)$, reflecting the operation mode (charge, discharge, or idle) of the battery. Optimizing the battery operation locally allows for the modeling of device-specific properties, since data can be locally acquired for fast and continuous model adaptation. As a result, optimal operating decisions can be made due to high model accuracy. In addition, a high-level communication infrastructure to ensure safety and security is not necessary, as unidirectional communication protects user privacy since no locally obtained data are shared [61]. The battery control schematics are illustrated in Fig. 2, wherein P_{DC} and P_{AC} represents the direct and alternating powers.

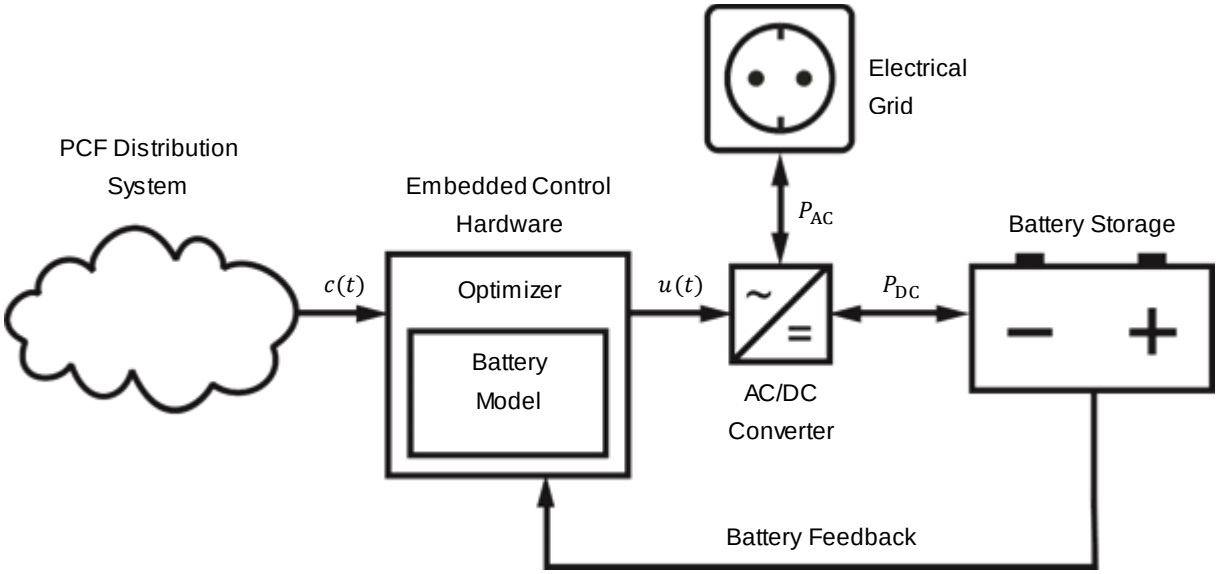

Fig. 2: Battery control schematics [68].

To achieve the above, as a first step, a mathematical model of the ZEBRA battery storage system is developed and used to simulate battery dynamics to estimate the grid-balancing potential of a repurposed battery storage system. Batteries can be modelled using electrochemical, statistical, or electrical models. As elaborated by Chen et al. [69], electrochemical models are often time-consuming and mainly used in order to investigate and improve the underlying electrochemical processes. Statistical models are often very abstract and used for system-level behavior prediction e.g. battery runtimes. Electrical models are equivalent circuits comprising electrical sources and components, like resistors. These models can be easily used in grid simulations, which is why, in this case, electrical models of the ZEBRA battery are developed. Historical Austrian day-ahead spot-market prices for electricity, provided by Energy Exchange Austria (EXAA) [70], are used as the PCF for the optimization, since real-time pricing has been discussed as an incentive for end-users to react to with their devices and corresponding demand [19], [71]–[73].

To validate the proposed battery model and the indicated potential for grid balancing, a ZEBRA battery is incorporated into a stationary setup and experiments are conducted. An embedded control hardware is developed and integrated into the battery storage setup. AC/DC charging/discharging converters enable the grid connection while an energy monitoring system logs the energy flows in and out of the system. The embedded control hardware fetches the PCF and enables the communication with all other hardware components. It performs the optimization and therefore decides if the battery gets charged, discharged, or stays idle. It also continuously records state data from the battery, evaluates it and adapts the battery model used in the optimization. In addition, the control hardware monitors safety-relevant aspects and in the event of a fault, is able to transfer the battery into a safe state.

Since the battery position in a low-voltage distribution grid, penetrated by distributed generation, may influence the balancing impact, a grid simulation study is conducted. Additionally, the consequences of different incentives, representing different intentions of the operators and used to find the operation mode of the battery (charge, discharge, or idle) by optimization, are evaluated. The simulation is based on a real, low-voltage distribution grid topology in combination with smart meter household load data and distributed photovoltaics

generation data. The study is intended to show the differences in balancing impacts based on the battery storage location and different incentives.

2. Summary Report

The following report summarizes the main achievements of the author's research, the results gained, and underlines scientific contributions made in the publications detailed in PART II. The research presented ranges from a feasibility study by simulation to validation via a field test. A local, autonomous battery control approach based on different optimization routines and battery model complexities is introduced. Combinations of optimization routines and battery models are simulated and the results are compared. Subsequently, to validate the proposed battery control approach, a repurposed electric vehicle battery is incorporated into a stationary storage setup and the performance is compared against simulations. Finally, a grid simulation study of a low-voltage distribution grid, penetrated by distributed generation, is used to show the impact of autonomous optimized batteries as a grid-balancing measure. To underline and to discuss the results achieved, key figures from the original publications in PART II have been used, in some cases with partial modifications.

2.1 Feasibility Study on Autonomous Battery Control

The content of this chapter has been adapted from the publication: B. Fäßler, P. Kepplinger, M. L. Kolhe, and J. Petrasch, "Decentralized on-site optimization of a battery storage system using one-way communication," presented at the International Conference on Renewable Power Generation, 2015, pp. 1–6.

In the first publication, the potential of a repurposed ZEBRA battery for balancing the electrical grid is investigated by simulation. Since the battery control is intended to run on a standalone, stationary storage, it is referred to as a local, autonomous battery control. The control strategy itself is based on an optimization routine minimizing an objective function calculated from a one-way communicated PCF, resulting in the operation mode (charge, discharge, or idle) of the battery, c.f. chapter 1.3. A similar control approach has already been proposed for domestic hot water heaters [61] but has never been investigated for batteries.

First, a battery model was developed based on a ZEBRA battery. Since this is a high-temperature battery, the battery has to maintain its temperature within a specified range in order to ensure proper functionality. Hence, the physical battery is equipped with auxiliary heating and cooling controlled by a built-in battery management system (BMS). The battery pack itself consists of several cells that are connected in series to form strings, resulting in a corresponding output voltage. The strings are connected in parallel to achieve a corresponding output current. The state of charge (SOC) is used as the normalized representation of the electrical energy content of the battery storage system.

To describe the state of the battery based on the SOC and the temperature, two nonlinear, coupled ordinary differential equations are necessary; one representing the electrical energy content, E_{el} and one representing the internal battery temperature, T. The two energy balances for the battery are:

$$\frac{\mathrm{d}E_{\mathrm{el}}}{\mathrm{d}t} = P_{\mathrm{DC}}(t) - P_{\mathrm{Ri}}\big(E_{\mathrm{el}}(t)\big) - P_{\mathrm{h}}(t) - P_{\mathrm{fan}}(t), \text{where} \qquad \text{Eq. 2}$$

$$P_{\mathrm{DC}}(t) = \begin{cases} \eta_{\mathrm{in}} \cdot P_{\mathrm{AC}}(t), & P_{\mathrm{AC}} \geq 0 \\ \eta_{\mathrm{out}}^{-1} \cdot P_{\mathrm{AC}}(t), & P_{\mathrm{AC}} < 0 \end{cases} \text{ and} \qquad \text{Eq. 3}$$

$$\frac{\mathrm{d}T}{\mathrm{d}t} = \frac{1}{C} \cdot \Big(P_{\mathrm{Ri}}\big(E_{\mathrm{el}}(t)\big) + P_{\mathrm{h}}(t) - \dot{Q}_{\mathrm{loss}}\big(T(t)\big) - \dot{Q}_{\mathrm{cool}}\big(T(t)\big)\Big) \qquad \text{Eq. 4}$$

In Eq. 2, P_{DC} represents the direct charging/discharging power, P_{Ri}, the heat dissipation across internal battery cell resistances, P_{h}, the auxiliary heating power, and P_{fan}, the cooling fan power. If the battery gets charged/stays idle, $P_{\mathrm{AC}} \geq 0$, and if it discharges, $P_{\mathrm{AC}} < 0$, cf. Eq. 3, which means there may be different charging/discharging converter efficiencies (η_{in} and η_{out}) that have to be taken into account. In Eq. 4, C represents the heat capacity, $\dot{Q}_{\mathrm{cool}}$, the heat transfer rate due to cooling, and $\dot{Q}_{\mathrm{loss}}$, the heat loss rate via the insulation of the battery pack. The proposed battery model is parameterized based on logged battery data provided by the battery's BMS. The data are based on charging and discharging cycles of a ZEBRA battery from a THINK City electric vehicle.

A comparison between simulated and measured SOC shows that below 80%, the SOCs coincide. Above 80%, the BMS balances the battery cells, which is followed by a reduction in charging power until the SOC reaches 100%. The cell balancing process and its duration highly depends on the state of each individual battery cell. Since the thermal energy balance depends

on the SOC, the modeled internal temperature also differs from the measured one. This makes these effects difficult to explicitly model and therefore these were not included in the model.

The model developed is used to simulate the dynamics of the battery storage. Additionally, it is used to constrain the control optimization to ensure that the battery's SOC and temperature is within the operational bounds. 20% ≤ SOC ≤ 100% are the bounds used, to ensure enough SOC for emergency temperature control. In the optimization, the permissible battery temperatures depend on the operation mode (charge, discharge, or idle) and the SOC. For a given time window, $[t_0, t_n]$, the optimization problem can be formulated as

$$\min_u \int_{t_0}^{t_n} \left(c(t) \cdot u(t) \cdot P_{\mathrm{AC,max}}\right) dt, \qquad \text{Eq. 5}$$

where $c(t)$ represents the PCF and $u(t)$, the decision function reflecting the operation mode of the battery. In this feasibility study, the battery operation is simulated using historic quarter-hour day-ahead prices for electricity provided by Energy Exchange Austria [70]. It is assumed that the price data is known 36 hours in advance. The continuous values of the resulting decision function are restricted from -1 to 1; -1 represents discharging at maximum power, 0 the idle state, and 1 charging at maximum power. To solve the optimization problem, MATLAB [74] with its built-in sequential quadratic programming (SQP) algorithm is used.

The optimization, which determines the battery operation, is performed every 24 hours at noon, taking the next 36 hours into account. This reflects the clearing of the day-ahead market at late morning for the next day. The simulation is conducted using price data from 4 September 2014 to 31 December 2014. The charging/discharging power is assumed constant at 1.5 kW. The capacity of the battery is 28.2 kWh.

The resulting optimal battery operation shows continuous charging and discharging mostly at maximum power; no idle state was detected. Continuous charging/discharging causes self-heating via the cell resistances, resulting in less energy needed for the auxiliary heating system. This in turn results in a high round-trip efficiency (converter-battery-converter) of about 80%. Additionally, it shows that the battery is operating close to the low end of the allowed temperature limit, causing minimal heat loss. The mean SOC is observed to be about 40% with a standard deviation of 15%. For the chosen battery setup (power, capacity), theoretical earnings of about 37 € are predicted over the four month simulation period, indicating feasible operation of a repurposed electric vehicle battery for grid balancing.

Since the battery model and the optimization routine need excessive computational costs, they need to be adapted for implementation on physical hardware with limited resources, for an experimental field test. Therefore, autonomous control algorithms featuring different model complexities and resulting control optimality have to be investigated for a physical control algorithm implementation on a stationary battery storage system. This study is considered in chapter 2.2.

2.2 Modification of Autonomous Battery Control

The content of this chapter has been adapted from the publication: B. Faessler, P. Kepplinger, and J. Petrasch, “Decentralized price-driven grid balancing via repurposed electric vehicle batteries,” *Energy*, vol. 118, pp. 446–455, Jan. 2017.

In this publication, steps are taken towards implementing the proposed battery control approach on a real, repurposed ZEBRA battery. Since embedded hardware with limited computational resources will be used to control the system, highly efficient simulation and optimization routines have to be developed. To this end, different nonlinear and linear optimization approaches are compared by simulation with respect to computational costs and resulting control optimality. The battery dynamics are simulated by the nonlinear battery model developed in chapter 2.1.

To investigate battery storage systems as grid balancing measures, the long-term behavior of such systems is of greater interest than the operational dynamics. Therefore, a linear battery model is developed, since the high dynamics during switching are not of interest. Additionally, a general loss term, P_{loss}, which incorporates the temperature model, is introduced instead of individual, nonlinear loss terms, resulting in a linear battery model for the electrical energy content

$$\frac{\mathrm{d}E_{\mathrm{el}}}{\mathrm{d}t} = P_{\mathrm{DC}}(t) - P_{\mathrm{loss}}. \qquad \text{Eq. 6}$$

P_{loss} is estimated by simulating 100 charge and discharge cycles of the nonlinear battery model at $P_{\mathrm{DC,max}}$ for 20% ≤ SOC ≤ 100%.

Along with the battery control approach based on a SQP routine, cf. chapter 2.1, a dynamic programming (DP) routine and an integer linear programming (ILP) routine have been developed and implemented. The SQP routine is used for nonlinear optimization whereas DP and ILP are considered for linear optimization.

The DP is based on the idea that the optimal solution of a problem can be composed by the solutions of many similar sub-problems [75], which are achieved using the linearized battery model. A self-implemented recursive routine is used to solve the optimization problem for discretized E_{el} values backward in time. In doing so, based on the PCF, costs for discretized decision states can be calculated. Finally, the cheapest path for each discretized E_{el} start state can be determined by calculating forward in time. The discretized decision states $u(t)$ are limited to maximum charging, discharging, and idle (1, −1, and 0). As indicated in chapter 2.1, the cost-optimal operation of the battery is achieved by continuously charging or discharging, and mostly at maximum power. The DP is constrained by an upper and lower bound for the SOC.

The concept of DP is graphically explained in Fig. 3. Starting at all discrete E_{el} end states, for a single time step backwards in time, charging is represented by a negative cell shift of two, discharging by a positive cell shift of three and the idle state by a positive cell shift of one. Based on the PCF, costs for each step can be determined; costs are accounted positive for discharging, negative for charging, and zero for idling. Finally, the decision states $u(t)$ can be determined by the cost-optimal solution of all sub-problems.

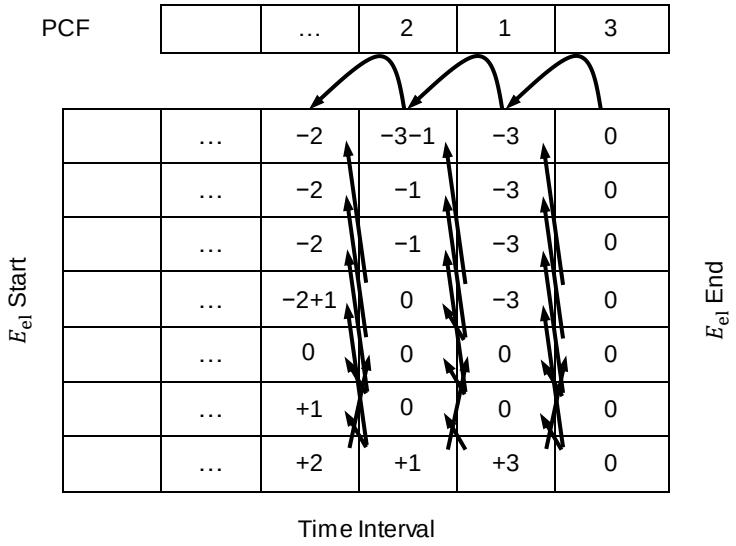

Fig. 3: Concept of self-implemented dynamic programming approach. The decision states are found backwards in time determined by the cost-optimal solution of all sub-problems [76].

In addition to SQP and DP, an ILP routine using the linear battery model is implemented. The decision states $u(t)$ are, as in the case of DP, discrete states for charging, discharging, and idling (1, −1, and 0). In doing so, the optimization approach has to be formulated using two decision variables (u^+ and u^-) for each time step indicating charging/idling and discharging separately. Thus, converter efficiencies can be included linearly in the objective function and the linear battery model can be used as a constraint independently of the converter efficiencies.

$$\min_u \int_{t_0}^{t_n} c(t) \cdot \left(u^+(t) \cdot \eta_{\mathrm{in}}^{-1} \cdot P_{\mathrm{DC,max}} - u^-(t) \cdot \eta_{\mathrm{out}} \cdot P_{\mathrm{DC,max}}\right) dt \qquad \text{Eq. 7}$$

Finally, the decision states are calculated by, $\boldsymbol{u}(t) = \boldsymbol{u}^+(t) - \boldsymbol{u}^-(t)$. To solve the minimization problem, MATLAB's *intlinprog* routine [74] is used.

To investigate the performance of these three optimization approaches with respect to runtime and control optimality, a simulation study is conducted. As PCF, hourly historic Austrian day-ahead stockmarket price data provided by EXAA [70] from 2015 are used. Again, it is assumed that the price data is known 36 hours in advance. The optimization is performed every 24 hours at noon, taking the next 36 hours into account. Table 1 summarizes the results. The SQP routine leads to the highest earnings per battery capacity and results in the best round-trip efficiency (converter-battery-converter) since the highest battery model complexity is used in the optimization. ILP shows the lowest runtime (approximately 50 times faster than SQP) and comparable results in terms of control optimality. DP performs marginally worse than ILP. However, DP would allow for a straightforward implementation since no library functions are needed.

Table 1: Performance comparison of SQP, DP and ILP using hourly based EXAA price data of 2015 [76].

Optimizer	Runtime relative to ILP (–)	Earnings/ Capacity (€/kWh)	Round-trip efficiency (%)
SQP	50.7	1.83	78.6
DP	1.29	1.74	77.5
ILP	1.00	1.75	77.4

Based on the results achieved, ILP is used to determine the economic potential of battery storage systems using the developed autonomous control approach in the period 2003–2015. As PCF, hourly historic day-ahead stock market price data is used. Fig. 4 shows the annual earnings per battery capacity, dependent on a mean value of the standard deviation in the day-ahead price for each day of the respective year.

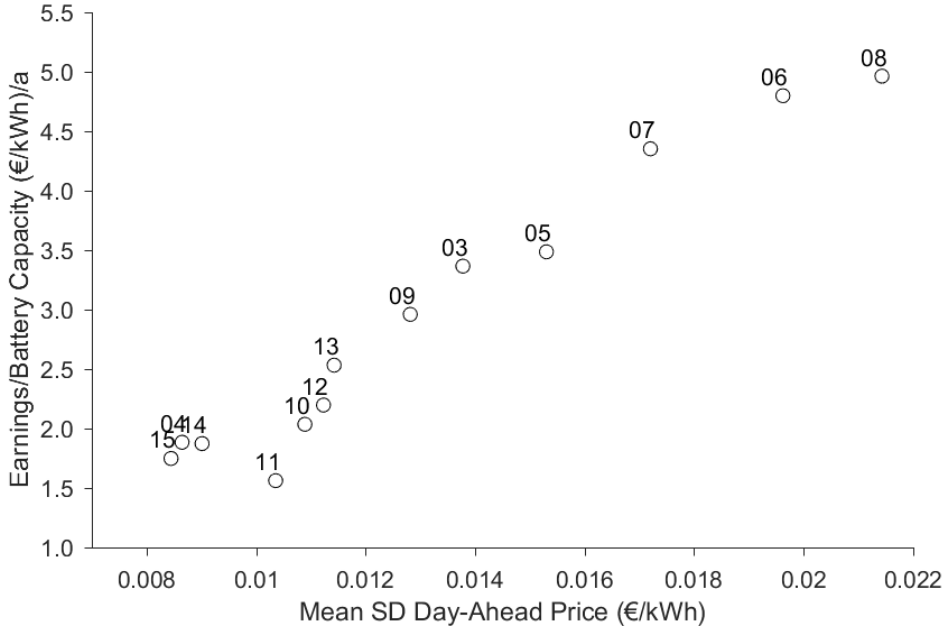

Fig. 4: Annual earnings per kWh battery capacity from 2003 to 2015 as a function of mean standard deviation of the day-ahead prices [76].

Two short-term products are typically traded on the Austrian electrical energy stock market: the hour- and 15-min-based day-ahead prices. Therefore, hour- and 15-min-based intervals are used in simulations to investigate the economic potential of the autonomously controlled, optimized battery storage. ILP is used to perform the study. Based on the results shown in Table 2, higher earnings per battery capacity and a better round-trip efficiency can be expected for 15-min-based products due to higher price dynamics leading to more dynamic battery operation. The simulations indicate that for current day-ahead stock market prices an economic operation is not possible since variations in price are currently too low. This indicates that such batteries must be operated on markets with higher volatility and/or a larger price range to increase the viable earnings.

Table 2: Performance comparison of ILP using hourly and quarter-hourly EXAA price data of 2015 [76].

Time product	Runtime relative to hourly based prices (–)	Earnings/ Capacity (€/kWh)	Round-trip efficiency (%)
Hour	1.00	1.75	77.4
15 min	3.86	2.86	78.3

A further investigation showed the impact of the capacity-to-power ratio of the battery on grid-balancing potential. To this end, the nonlinear battery model is scaled by changing the numbers of cells while keeping the cell properties the same. The capacity can be increased by adding battery cell-strings in parallel resulting in an unchanged terminal voltage. The maximum charging and discharging current changes proportional to the number of strings, resulting in an adjustable charging and discharging power. Assuming geometrical similarity, the auxiliary heating power and the thermal losses via the battery insulation are scaled by the battery pack surface to volume ratio. Since the heat generated via cell resistances is proportional to the square of the current, the heat transfer required for battery cooling and thus, fan power, is scaled by the current squared.

The battery operation is simulated using ILP driven by historic hour- and 15-min-based day-ahead prices of 2015. The earnings per battery capacity as a function of the capacity-to-power ratio always exhibit one distinct maximum. For low capacity-to-power ratios, the storage system does not have sufficient capacity to realize all optimal charging and discharging opportunities. For high capacity-to-power ratios, the full system capacity is never exploited. Generally, large systems are preferable since relative thermal losses are smaller as the surface to volume ratio decreases.

2.3 Field Testing of an Autonomously Controlled Battery

The content of this chapter has been adapted from the publication: B. Faessler, P. Kepplinger, and J. Petrasch, “Field testing of repurposed electric vehicle batteries for price-driven grid balancing,” (Submitted to Elsevier Energy Journal, Manuscript Number: EGY-D-17-05788)

Having demonstrated that a sufficient control objective can be obtained using linear optimization, the control approach for grid balancing is implemented on a decommissioned, high-temperature ZEBRA battery to validate the approach experimentally. Since these batteries have been used in early commercial electric vehicles, they are now available for second-use approaches. The presented control approach can also be applied to other types of batteries after adapting the linear battery model. The experimental setup uses the author’s self-developed software consisting of routines for communication, optimization and operation of the battery storage system. Additional hardware components had to be installed and were partly self-developed.

The schematics and the physical implementation of the repurposed ZEBRA EV battery storage system is shown in Fig. 5. It consists of an embedded control hardware (ECH), charging/ discharging converters, a ZEBRA battery including a BMS, and an energy monitoring system.

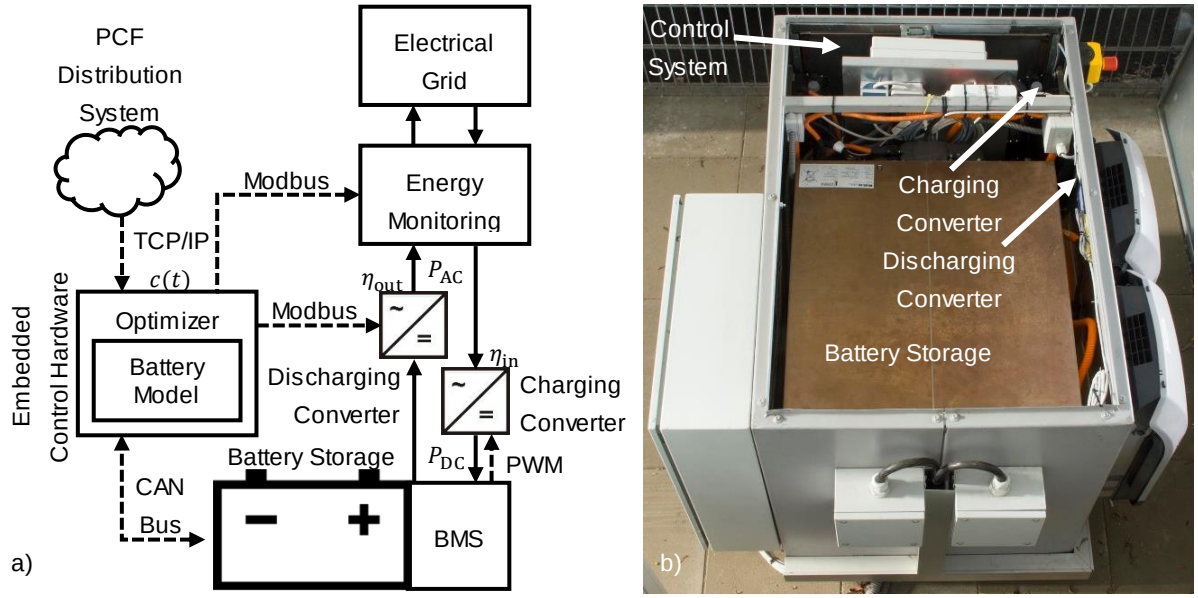

Fig. 5: Repurposed ZEBRA EV battery as stationary storage system:
a) schematics; b) physical implementation.

The ZEBRA battery used has a capacity of 28.2 kWh. The ECH consists of a BeagleBone Black – Rev C [77] and a serial cape [78]. Thus, the ECH is able to communicate with the BMS, the charging/discharging converters, the energy monitoring system, and the PCF distribution system via TCP/IP, CAN bus, and Modbus TCP. Furthermore, the control approach is implemented on the ECH. The PCF is fetched from a PCF distribution system. In case of this field test, the actual trading result of the Austrian 15-min-based stock market price for electricity is used to drive the optimization. This price data is published by EXAA [79] daily on weekdays at 12 noon for the next 36 hours. For charging and discharging, separate converters are used since the original EV single-phase charger [80] is not designed for discharging. The

charging converter efficiency ranges from 95% for 3.2 kW to 90% for 0.4 kW [80]. The average DC charging power measured during a charging process is 1.49 kW. For discharging, a three-phase converter from Fronius [81] is used since its discharging power can be controlled continuously from 0–100% of the maximum power. The efficiency ranges from about 90% to 97.5% depending on the output power [81]. Measurements showed that the average DC discharging power between 20% and 100% SOC is 8.64 kW, i.e. 5.8 times the DC charging power. All energy flows are measured and recorded by an energy monitoring system from Algodue [82] at a resolution of 15 minutes. The measured in- and output energy flows also include the powering of the energy counter and the BMS.

To control the battery, a mixed integer linear programming optimization routine (MILP) using a linear battery model is used to find the optimal operation mode by minimizing the objective function calculated from the PCF, based on the prevailing 15-min-based Austrian day-ahead stock market price for electricity. MILP is used since the presented optimization approach in chapter 2.2 has to be adapted to account for different charging and discharging power and converter efficiencies. Furthermore, since the converters perform inefficiently up to 20% of their maximum output power, the boundary conditions have to exclude charging or discharging for lower values. Additionally, boundary conditions have to ensure that the battery's SOC stay within the operational bounds (20%–100% SOC). P_{loss} used in the battery model is estimated by a least squares approach once a day by fitting the battery model on seven days of historic P_{DC} and SOC data. Battery state data are continuously monitored.

The performance of the storage system was investigated from 24 May 2017, 4:15 to 6 June 2017, 9:00. Furthermore, a preliminary lead-time of one week served to determine the initial battery loss term. During the experiment, the stationary storage system operated with a round-trip efficiency (converter-battery-converter) of 74.4%. In doing so, the system performed 9.43 full battery charge cycles with a median SOC of 65.2%. An accuracy analysis of the proposed linear battery model shows a root mean square error of 7.6% between the simulated and the measured SOC during the experiment. Reasons for the model error are indicated in Fig. 6, which shows a 36-hour time window during the experiment, depicting the day-ahead price, the decision function, the measured SOC, and the predicted SOC based on the executed decision states. In the case shown in Fig. 6, the optimization starts at midnight and predicts the battery operation for the next 24 hours since the available day-ahead price ends at midnight of the following day. Two major model deviations can be observed, one occurs at approximately 6:15, the other around 14:30. The first deviation can be explained by a battery cell balancing procedure always performed by the BMS during charging at 80% SOC. The second deviation can be explained by a battery balancing procedure followed by a SOC reset to 100%. This reset is caused by the fact that the BMS estimates the SOC by measuring the charging/discharging current. The end of charge, however, is determined by measuring the cell voltage leading to this SOC estimation error by the BMS.

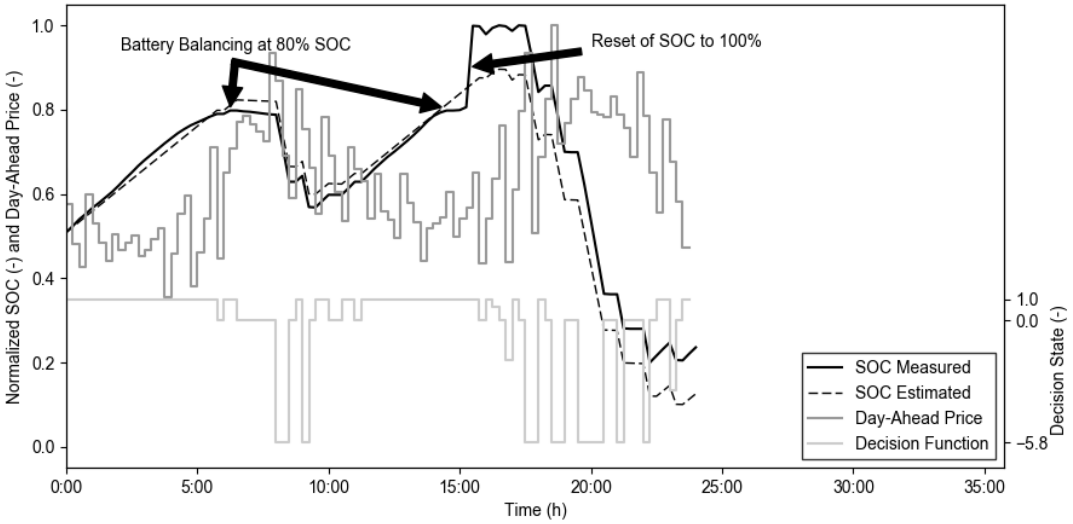

Fig. 6: Exemplary battery operation indicating estimated SOC (dashed black line) and measured SOC (black line) based on the 15 minutes Austrian day-ahead stock market price for electricity (dark grey line). All values on the left axis are normalized with respect to their maximum value. The light grey line indicates the decision states executed on the storage in a 15-minute time interval.

Additionally, the realized earnings have been compared to the potential earnings, which are investigated by simulation assuming linear battery behavior. To this end, the model is continually initialized at 12 noon, using the corresponding 36 hours day-ahead price and the battery losses estimated during the experiment. The new battery state is calculated and used as the initial state for the next day optimization. The resulting potential earnings during the experiment differs by 37.5% compared to the realized earnings. This discrepancy can be attributed to insufficiencies in representation of the BMS, battery behavior and converter characteristics. The significant economic deviation between model and experiment shows the urgent need for field tests of grid-balancing strategies to investigate their realizable potential. In addition, the results indicate that the earnings achieved must be significantly higher in order to operate the storage economically, even without considering the installation and equipment costs. Even accounting for seasonal price differences in the Austrian electricity price, battery operation based on the day-ahead price is not profitable from today's perspective. However, as a prospective application, the technical grid-balancing potential is investigated in a grid simulation study in chapter 2.4.

2.4 Grid Simulation Study of Batteries as Grid-Balancing Measure

The content of this chapter has been adapted from the publication: B. Faessler, M. Schuler, M. Preißinger, and P. Kepplinger, “Battery storage systems as grid-balancing measure in low-voltage distribution grids with distributed generation,” *Energies*, vol. 10, no. 12, pp. 1–14, Dec. 2017.

The fourth publication investigates the impact of autonomously optimized battery storage systems as a grid-balancing measure in a low-voltage distribution grid, penetrated by distributed generation, via grid simulation. The grid consists nodes representing households, each of which have a load profile and may or may not have an electrical generation profile through photovoltaics. The influence on the power quality in this grid, of a single, feed-in-tied battery storage system is compared to the influence of multiple, distributed storage systems attached to nodes in this grid where electrical generation occurs. It is assumed that the capacity and the maximum charging and discharging power of the single, central storage equals the sum of all distributed storages. Battery operation is determined via a linear optimization routine, which relies on minimizing an objective function calculated from a one-way communicated PCF.

In this grid simulation study, different PCFs, addressing either market conditions for electricity generation, grid balancing, optimal photovoltaic utilization, load shifting, or self-consumption (i.e. a load profile obtained by subtracting generated PV electricity at source) are used as incentives. Market conditions are incorporated in the model using the historic Austrian 15-min-based day-ahead stock market prices for electricity. For grid balancing, optimal PV utilization, and load shifting, the incentives are based on the assumption that we have perfect prior knowledge of either the grid feed-in power, the PV generation, or the household consumption at each node. A detailed description of all incentives is given in Table 3. The configuration indicates whether the given incentive is applicable to only a single, central storage (c) or only multiple, distributed storages (d), or both (c/d). In case of incentives based on load shifting and self-consumption, the individual household load profile is assigned to the corresponding household-tied storage.

Table 3: Incentives used to drive BESS optimization. The considered configurations for BESS are abbreviated by c for a single, central storage and d for multiple, distributed storages [83].

Abbreviation	Description	Incentive	Configuration
REF	Reference case	-	-
RTP	Real-time pricing	EXAA day-ahead market price	c/d
GRID	Grid balancing	Total future grid load	c/d
PV	Optimal PV utilization	Future PV generation	c/d
LOAD	Load shifting	Future household consumption	d
SELF	Self-consumption	Future household load (incl. PV)	d

To allow for results close to reality, real data are applied for the low-voltage distribution grid topology, the household loads, and the distributed generation from photovoltaics. Data of commercially available Li-ion battery energy storage systems (BESSs) are used to keep

simulations practical. A self-implemented grid simulation tool is used to run the simulation [84]. This tool is based on a direct numerical method proposed by Ghatak and Mukherjee [85]. The temporal resolution of the grid simulation is 15 min.

The weakly meshed low-voltage distribution grid is shown in Fig. 7. It comprises of 50 nodes; a central feed-in node (slack node, 50), a node (19) as placeholder for a central BESS, and 48 nodes for households. At the slack node, the voltage is kept constant at 230 V with zero phase shift.

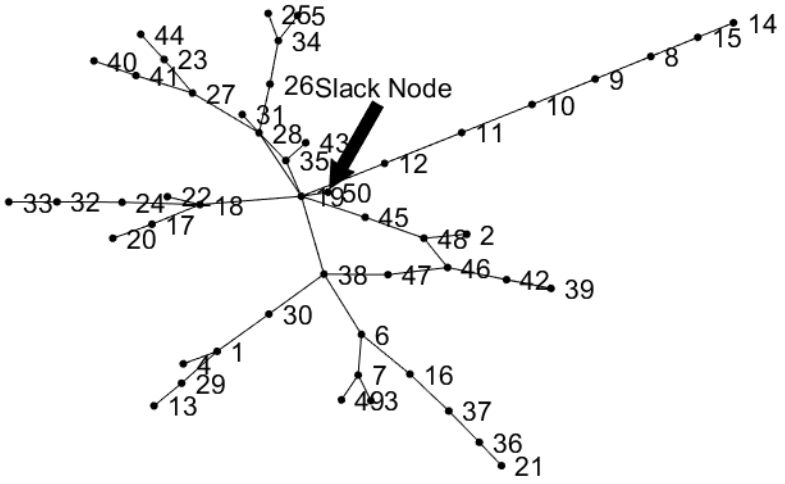

Fig. 7: Low-voltage distribution grid section with a central feed-in node (slack node) [83].

Smart meter household loads are assigned to the nodes. Three PV systems with different typically residential dimensions are allocated. Their location is chosen randomly. The photovoltaic peak power corresponds to approximately one quarter of the maximum load at the slack node. This is considered to be a feasible penetration rate for low-voltage distribution grids [86], [87]. Three different BESSs with different capacities and maximum charging and discharging power are assigned to the nodes with PV generation.

The resulting power quality is assessed by comparing the peak-to-average power ratio (PAPR) at the feed-in node, the maximum voltage drop/rise at all grid nodes, and the distribution losses. The voltage drop/rise describes the relation between the voltages of the individual nodes to the constant slack node voltage. The distribution losses are the cumulative losses of the investigated low-voltage distribution grid.

The grid simulation study is conducted from 8 June 2016, 12:00 to 15 June 2016, 12:00 since highly accurate time-resolved data for household loads and PV generation are available in this period. The assigned household loads, PV generation data, and parameterized batteries are unmodified throughout the simulations leading to comparable results regarding PAPR, voltage levels, and distribution losses.

In Fig. 8, the impact of a single, central storage and multiple, distributed storages on the power quality of the grid are compared to a reference case where no grid balancing exists, in the case of each of the aforementioned incentive functions. It can be seen that the PAPR is reduced with respect to the reference case, in all operation modes except for the RTP driven mode. Using RTP as the incentive results in additional peak loads. The voltage drop/rise shows that

a central storage does not deteriorate or significantly improve the power quality in terms of voltage deviation. Cumulative distribution losses remain the same as the reference case when using a central storage, whereas the use of distributed storages leads to higher distribution losses.

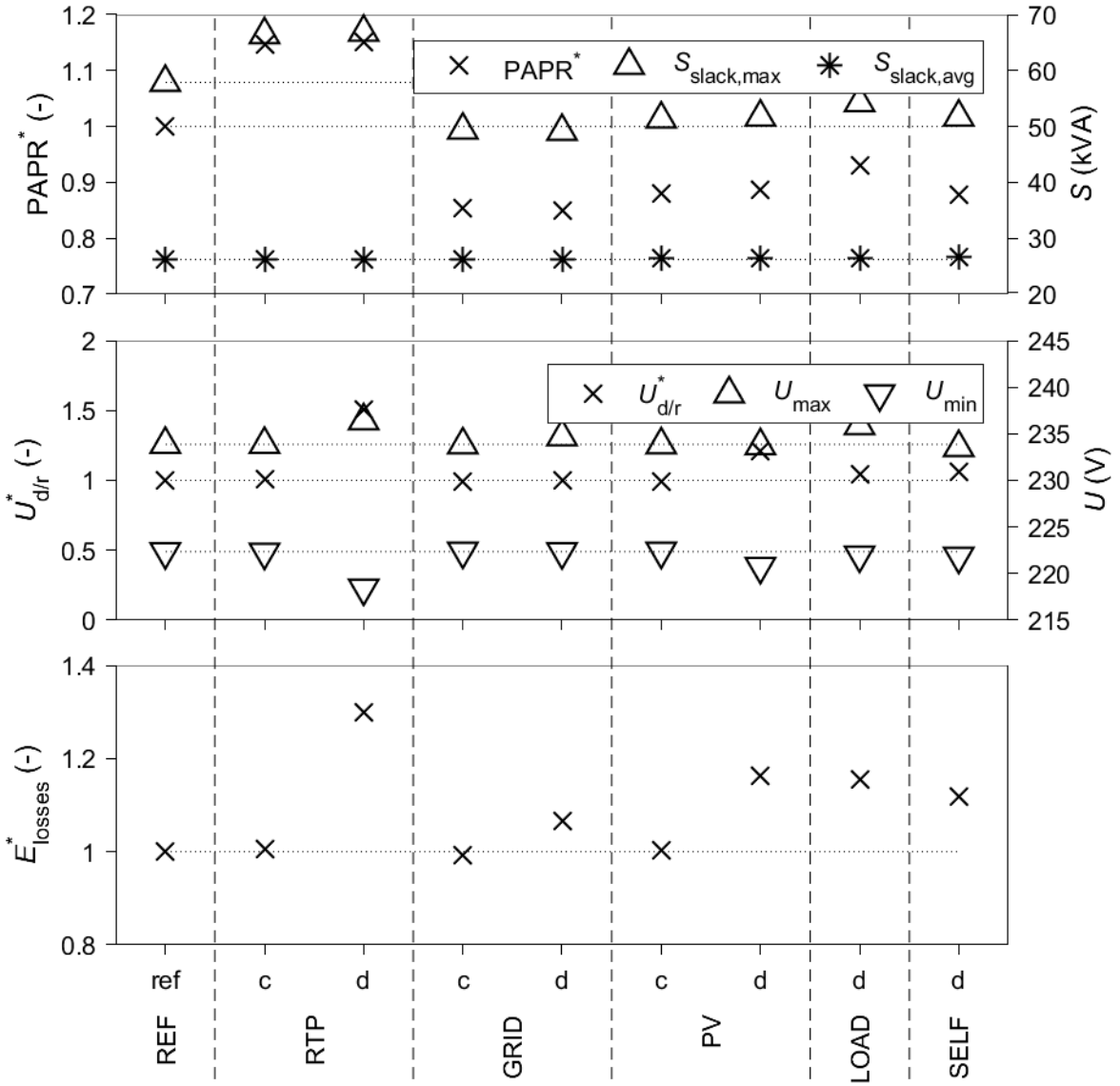

Fig. 8: PAPR, voltage drop/rise and cumulative distribution losses for all configurations for a single, central storage (c) and multiple, distributed storages (d). The superscript * refers to normed quantities with respect to the reference case [83].

The different cases show that incentives that reflect more general conditions, such as the RTP, may worsen power quality, since they are indicators for larger, non-local grids. This means that it is crucial to assess the impact of battery storage systems as a grid-balancing measure on all voltage levels of the electrical grid. For all other incentives, both a single, central storage as well as multiple, distributed storages have power quality related advantages in low-voltage distribution grids. A central storage shows lower voltage deviations and lower distribution losses. Distributed storages tend to improve the PAPR. Incentives that incorporate local grid characteristics should be used to ensure grid reliability.

2.5 Discussion

Research involves iterative efforts aimed at converging to an optimum solution. Such iterations were required during the course of this research, in order to address the unique modelling problems and implementation challenges that were encountered.

After showing that a battery storage system could be operated by an autonomous control approach, we were confronted with the fact that an embedded hardware would not be able to run the developed routine owing to its limited computational capacity. Hence, new control approaches had to be investigated.

Since we are interested in the long-term behavior of battery storages and not in dynamic effects such as those during switching, we attempted the use of linear optimization routines and linear battery models. We were able to prove that these newly developed routines showed similar control objectives as the initial, nonlinear control approach while needing less than 50 times the runtime.

The subsequent field test showed numerous challenges to the implementation. In this thesis, these challenges have not been detailed due to their implementation-specific nature. Effort was needed to repurpose an EV ZEBRA battery, both on the hardware and the software side. On the hardware side, additional to the original charging converter, a discharging converter had to be installed. In addition, an appropriate embedded hardware had to be found which is also able to communicate via various bus protocols. As a result, CAN bus could be used to communicate with the battery attached BMS and override in-built automotive safety features. It was also necessary to adapt the control approach to a form that was executable on the embedded hardware.

Finally, to investigate the grid-balancing capability of such storages, a grid simulation of a low-voltage distribution grid was executed. For this purpose, a grid simulation method, which is capable of handling autonomously controlled devices like battery storage systems, was needed. Such a method has been developed and implemented in-house by Schuler et al. [84]. This method allows the battery control routine to determine the operation mode of the battery (charge, discharge, or idle) and incorporates its outcome into the simulation study.

3. Conclusion

In this thesis, a theoretical and experimental investigation of a decommissioned and repurposed molten-salt, high-temperature ZEBRA (Zero Emission Battery Research Activities) battery as a small-scale, stationary storage for grid balancing has been investigated. The related questions as defined in the problem statement can be answered based on the presented scientific work.

Is it technically feasible to repurpose these batteries as stationary storage for grid balancing?

To show the technical feasibility of electric vehicle batteries repurposed as stationary storage, a ZEBRA battery model has been developed, fitted to experimental data, and used to simulate the battery dynamics. This type of battery ranks among the first commercial, electric vehicle batteries and these batteries are now available for second-use approaches. The operation mode of the battery (charge, discharge, or idle) is based on an autonomous, on-site optimization, minimizing an objective function calculated from a one-way communicated incentive, which represents the intention of the operator to achieve a certain goal, e.g. grid balancing. In this feasibility study, the historic Austrian day-ahead stock market price for electricity was used as incentive. The simulation of the proposed autonomous battery control algorithm indicated that a repurposed electric vehicle battery as stationary storage for grid balancing can be operated successfully based on the achieved earnings.

Which provisions have to be made for a physical implementation of repurposed electric vehicle batteries?

For a physical implementation of the battery control algorithm on an embedded hardware, steps towards developing highly efficient simulation and optimization routines have been taken. To this end, different nonlinear and linear optimization approaches were compared with respect to computational costs and the resulting control optimality. Again, the historic Austrian day-ahead stock market price for electricity served as the incentive. Results achieved by simulations showed that linear optimization routines based on linear models result in control objectives comparable to nonlinear ones, but run about 50 times faster. Hence, they are the best suited for a physical implementation on an embedded hardware with limited computational resources. Furthermore, the simulations showed a strong correlation between incentive-based earnings and the variation of the incentive during the same period. The resolution of the incentive defines the constraints on the grid-balancing measure; the shorter the time scale, the faster the reaction of the measure can be. In addition, the impact of changing the capacity-to-power ratio of the modelled battery was investigated to examine if there is an optimal combination of capacity and power resulting in maximum earnings for a given incentive. It showed that the capacity-to-power ratio always exhibits one distinct maximum.

What are the differences between the modeled and actual operation of such a repurposed battery?

A field test was conducted to show the practical feasibility of repurposed electric vehicle batteries for grid balancing. For the experimental setup, a software package has been developed and implemented. It comprises routines for communication, optimization and operation of the battery storage system. Additional hardware components were installed and partly self-developed. During a 14-day period, the system operated with a round-trip efficiency (converter-battery-converter) of about 74.4%. The accuracy of the proposed linear battery model showed a root mean squared error of 7.6% between the measured and estimated state of charge. For the simulation study, the prevailing Austrian day-ahead stock market price for electricity was used as the incentive. The realized earnings were 37.5% lower than the potential earnings indicated by simulation, assuming a linear battery behavior. This can be attributed to technical obstacles in the hardware implementation and model inaccuracies in the simulation. The resulting difference shows the urgent need for field tests to investigate the realizable potential of repurposed battery storage systems. Although the installation and equipment costs of the presented stationary battery storage cannot be determined, it can be stated that the earnings achieved must be significantly higher in order to operate the storage economically. This test implementation of a ZEBRA battery repurposed as stationary storage presented several unexpected challenges. We could expect similar but specific challenges (related to safety concerns, communication, etc.) for other battery storage types used in electric vehicles. This indicates that a second use of vehicle batteries for grid balancing has to be planned before the commissioning of such batteries.

How can battery storages affect grid balancing in a low-voltage distribution grid?

A grid simulation study of a low-voltage distribution grid penetrated by distributed generation was used to show how different battery storage locations affect the grid balancing. Additionally, different incentives addressing either market conditions for electricity generation, grid balancing, optimal photovoltaic utilization, load shifting, or self-consumption, have been used to determine the operation mode of the battery (charge, discharge, or idle). To this end, a simulation study was conducted using a real, low-voltage distribution grid topology, real smart meter household load profiles, and real photovoltaics load data. The impacts on power quality were measured in terms of the peak-to-average power ratio at the feed-in node and the maximum voltage drop/rise at all grid nodes. It was shown that incentives that reflect more general conditions, such as supraregional markets, might cause the deterioration of the power quality. Therefore, it is crucial to assess the impact of grid-balancing measures on all voltage levels of the electrical grid. Hence, to improve the power quality of a low-voltage distribution grid by the use of autonomously optimized devices, incentives reflecting load conditions are preferable. For these kinds of incentives, a single, feed-in-tied storage as well as multiple, distributed storages (which together have the same power and capacity as the central storage) attached to nodes exhibiting distributed generation, showed improvements on power quality. The former configuration performs better in terms of the voltage drop/rise, the latter in terms of the reduction of the peak-to-average power ratio. Hence, efforts should be made for grid and household load assessment, which include the contributions of distributed generation, in order to ensure grid reliability in the future.

Based on the main findings of this thesis, relevant future research is deduced.

As shown, earnings achieved by autonomously optimized battery storage systems driven by the day-ahead stock market price for electricity must be significantly higher in order to operate repurposed electric vehicle batteries as stationary storages economically. Simulation results for the investigated ZEBRA battery indicated that incentives with higher resolution and variation lead to more dynamic battery operation. This results in higher earnings, efficiencies, and shorter idle times and thus, better storage system utilization. This suggests that short-term and highly fluctuating markets such as the frequency response reserve market might be better suited for an economical operation. Since the presented physical setup is not capable of responding as fast as is necessary for the frequency response reserve market due to technical challenges such as delays due to grid synchronization, no further investigations have been conducted.

The nonlinear battery model used in the simulation studies to simulate the dynamics of the ZEBRA battery could be extended by a cyclic and calendric aging model. This can enable an investigation of the long-term behavior with higher accuracies. As a result, reasonable simulations lasting for several years could be executed.

A potential estimation of second-use electric vehicle batteries for different stationary storage applications, like large-scale (aggregated), centralized systems or small-scale, distributed systems, could be done. This may include an analysis of which technical conditions electric vehicle batteries must meet to be reusable as well as a corresponding estimation of the effort needed to repurpose such batteries as stationary storage. Additionally, a remaining battery lifetime assessment is of strong interest.

Furthermore, the premature exchange of electric vehicle batteries to maximize their total lifetime including a second use approach could also be explored. This could be of interest since the aging of a battery strongly depends on the operating conditions (applied charging/discharging power, temperature, etc.); using batteries for stationary applications rather than for mobile applications only, may extend their lifetime and thus reduce their ecological footprint.

The presented autonomous control approach can further be extended to other types of storages and loads. For this purpose, appropriate models must be developed and the used optimization routine must be adapted accordingly. This would offer the opportunity to simulate differently initialized grids with various autonomously optimized storages and loads and to evaluate their grid impacts.

References

[1] T. M. I. Mahlia, T. J. Saktisahdan, A. Jannifar, M. H. Hasan, and H. S. C. Matseelar, "A review of available methods and development on energy storage; technology update," *Renew. Sustain. Energy Rev.*, vol. 33, pp. 532–545, May 2014.

[2] K. C. Divya and J. Østergaard, "Battery energy storage technology for power systems—An overview," *Electr. Power Syst. Res.*, vol. 79, no. 4, pp. 511–520, Apr. 2009.

[3] A. R. Landgrebe and S. W. Donley, "Battery storage in residential applications of energy from photovoltaic sources," *Appl. Energy*, vol. 15, no. 2, pp. 127–137, Jan. 1983.

[4] M. A. Azam, N. S. A. Manaf, E. Talib, and M. S. A. Bistamam, "Aligned carbon nanotube from catalytic chemical vapor deposition technique for energy storage device: a review," *Ionics*, vol. 19, no. 11, pp. 1455–1476, Nov. 2013.

[5] P. Mercier, R. Cherkaoui, and A. Oudalov, "Optimizing a Battery Energy Storage System for Frequency Control Application in an Isolated Power System," *IEEE Trans. Power Syst.*, vol. 24, no. 3, pp. 1469–1477, Aug. 2009.

[6] P. J. Hall and E. J. Bain, "Energy-storage technologies and electricity generation," *Energy Policy*, vol. 36, no. 12, pp. 4352–4355, Dec. 2008.

[7] H. Chen, T. N. Cong, W. Yang, C. Tan, Y. Li, and Y. Ding, "Progress in electrical energy storage system: A critical review," *Prog. Nat. Sci.*, vol. 19, no. 3, pp. 291–312, Mar. 2009.

[8] E. Telaretti and L. Dusonchet, "Stationary battery systems in the main world markets: Part 2: Main trends and prospects," 2017, pp. 1–6.

[9] M. Müller *et al.*, "Evaluation of grid-level adaptability for stationary battery energy storage system applications in Europe," *J. Energy Storage*, vol. 9, pp. 1–11, Feb. 2017.

[10] D. Rastler, *Electricity energy storage technology options: a white paper primer on applications, costs and benefits*. Palo Alto, California: Electric Power Research Institute, 2010.

[11] R. Dufo-López and J. L. Bernal-Agustín, "Techno-economic analysis of grid-connected battery storage," *Energy Convers. Manag.*, vol. 91, pp. 394–404, Feb. 2015.

[12] J. M. Gurrero, L. G. De Vicuna, and J. Uceda, "Uninterruptible power supply systems provide protection," *IEEE Ind. Electron. Mag.*, vol. 1, no. 1, pp. 28–38, 2007.

[13] J. K. Kaldellis, D. Zafirakis, and K. Kavadias, "Techno-economic comparison of energy storage systems for island autonomous electrical networks," *Renew. Sustain. Energy Rev.*, vol. 13, no. 2, pp. 378–392, Feb. 2009.

[14] M. Singh and A. Chandra, "Control of PMSG based variable speed wind-battery hybrid system in an isolated network," 2009, pp. 1–6.

[15] J. Weniger, T. Tjaden, and V. Quaschning, "Sizing of Residential PV Battery Systems," *Energy Procedia*, vol. 46, pp. 78–87, 2014.

[16] D. Dong, P. Wang, W. Qin, and X. Han, "Investigation of a microgrid with vanadium redox flow battery storages as a black start source for power system restoration," 2014, pp. 140–145.

[17] C. Noce, S. Riva, G. Sapienza, and M. Brenna, "Electrical energy storage in Smart Grid: Black-start study using a real-time digital simulator," 2012, pp. 216–220.

[18] M. Beaudin, H. Zareipour, A. Schellenberglabe, and W. Rosehart, "Energy storage for mitigating the variability of renewable electricity sources: An updated review," *Energy Sustain. Dev.*, vol. 14, no. 4, pp. 302–314, Dec. 2010.

[19] P. Palensky and D. Dietrich, "Demand Side Management: Demand Response, Intelligent Energy Systems, and Smart Loads," *IEEE Trans. Ind. Inform.*, vol. 7, no. 3, pp. 381–388, Aug. 2011.

[20] A. Mohd, E. Ortjohann, A. Schmelter, N. Hamsic, and D. Morton, "Challenges in integrating distributed Energy storage systems into future smart grid," 2008, pp. 1627–1632.

[21] J. Leadbetter and L. Swan, “Battery storage system for residential electricity peak demand shaving,” *Energy Build.*, vol. 55, pp. 685–692, Dec. 2012.

[22] C. Pang, P. Dutta, and M. Kezunovic, “BEVs/PHEVs as Dispersed Energy Storage for V2B Uses in the Smart Grid,” *IEEE Trans. Smart Grid*, vol. 3, no. 1, pp. 473–482, Mar. 2012.

[23] M. Bragard, N. Soltau, S. Thomas, and R. W. De Doncker, “The Balance of Renewable Sources and User Demands in Grids: Power Electronics for Modular Battery Energy Storage Systems,” *IEEE Trans. Power Electron.*, vol. 25, no. 12, pp. 3049–3056, Dec. 2010.

[24] N. W. Miller, R. S. Zrebiec, R. W. Delmerico, and G. Hunt, “Battery energy storage systems for electric utility, industrial and commercial applications,” 1996, pp. 235–240.

[25] H. Qian, J. Zhang, J.-S. Lai, and W. Yu, “A high-efficiency grid-tie battery energy storage system,” *IEEE Trans. Power Electron.*, vol. 26, no. 3, pp. 886–896, Mar. 2011.

[26] A. Pina, C. Silva, and P. Ferrão, “The impact of demand side management strategies in the penetration of renewable electricity,” *Energy*, vol. 41, no. 1, pp. 128–137, May 2012.

[27] IEA, “Electricity,” in *World Energy Outlook 2016*, IEA, 2016, p. 684.

[28] G. Strbac, “Demand side management: Benefits and challenges,” *Energy Policy*, vol. 36, no. 12, pp. 4419–4426, Dec. 2008.

[29] P. Nejat, F. Jomehzadeh, M. M. Taheri, M. Gohari, and M. Z. Abd. Majid, “A global review of energy consumption, CO2 emissions and policy in the residential sector (with an overview of the top ten CO2 emitting countries),” *Renew. Sustain. Energy Rev.*, vol. 43, pp. 843–862, Mar. 2015.

[30] IEA, “Buildings sector energy consumption,” in *World Energy Outlook 2016*, IEA, 2016.

[31] IEA, “Transportation sector energy consumption,” in *World Energy Outlook 2016*, IEA, 2016.

[32] T. Ma, H. Yang, and L. Lu, “Feasibility study and economic analysis of pumped hydro storage and battery storage for a renewable energy powered island,” *Energy Convers. Manag.*, vol. 79, pp. 387–397, Mar. 2014.

[33] C. J. Barnhart and S. M. Benson, “On the importance of reducing the energetic and material demands of electrical energy storage,” *Energy Environ. Sci.*, vol. 6, no. 4, p. 1083, 2013.

[34] O. M. Toledo, D. Oliveira Filho, and A. S. A. C. Diniz, “Distributed photovoltaic generation and energy storage systems: A review,” *Renew. Sustain. Energy Rev.*, vol. 14, no. 1, pp. 506–511, Jan. 2010.

[35] C. Dötsch, A. Kanngießer, and D. Wolf, “Speicherung elektrischer Energie – Technologien zur Netzintegration erneuerbarer Energien,” *Uwf UmweltWirtschaftsForum*, vol. 17, no. 4, pp. 351–360, Dec. 2009.

[36] M. Meisel *et al.*, “Erfolgsversprechende Demand-Response-Empfehlungen im Energieversorgungssystem 2020,” *Inform.-Spektrum*, vol. 36, no. 1, pp. 17–26, Feb. 2013.

[37] S. Teleke, M. E. Baran, A. Q. Huang, S. Bhattacharya, and L. Anderson, “Control Strategies for Battery Energy Storage for Wind Farm Dispatching,” *IEEE Trans. Energy Convers.*, vol. 24, no. 3, pp. 725–732, Sep. 2009.

[38] J. Patten, N. Christensen, G. Nola, and S. Srivastava, “Electric vehicle battery — Wind storage system,” 2011, pp. 1–3.

[39] K. Clement-Nyns, E. Haesen, and J. Driesen, “The impact of vehicle-to-grid on the distribution grid,” *Electr. Power Syst. Res.*, vol. 81, no. 1, pp. 185–192, Jan. 2011.

[40] W. Kempton and J. Tomić, “Vehicle-to-grid power implementation: From stabilizing the grid to supporting large-scale renewable energy,” *J. Power Sources*, vol. 144, no. 1, pp. 280–294, Jun. 2005.

[41] T. Sousa, H. Morais, J. Soares, and Z. Vale, “Day-ahead resource scheduling in smart grids considering Vehicle-to-Grid and network constraints,” *Appl. Energy*, vol. 96, pp. 183–193, Aug. 2012.

[42] L. Wang, S. Sharkh, and A. Chipperfield, “Optimal coordination of vehicle-to-grid batteries and renewable generators in a distribution system,” *Energy*, vol. 113, pp. 1250–1264, Oct. 2016.

[43] B. Tarroja, L. Zhang, V. Wifvat, B. Shaffer, and S. Samuelsen, “Assessing the stationary energy storage equivalency of vehicle-to-grid charging battery electric vehicles,” *Energy*, vol. 106, pp. 673–690, Jul. 2016.

[44] S. Shokrzadeh and E. Bibeau, “Sustainable integration of intermittent renewable energy and electrified light-duty transportation through repurposing batteries of plug-in electric vehicles,” *Energy*, vol. 106, pp. 701–711, Jul. 2016.

[45] J. Neubauer and A. Pesaran, “The ability of battery second use strategies to impact plug-in electric vehicle prices and serve utility energy storage applications,” *J. Power Sources*, vol. 196, no. 23, pp. 10351–10358, Dec. 2011.

[46] V. V. Viswanathan and M. Kintner-Meyer, “Second Use of Transportation Batteries: Maximizing the Value of Batteries for Transportation and Grid Services,” *IEEE Trans. Veh. Technol.*, vol. 60, no. 7, pp. 2963–2970, Sep. 2011.

[47] IEA, *Global EV Outlook 2017*. IEA, 2017.

[48] C. Heymans, S. B. Walker, S. B. Young, and M. Fowler, “Economic analysis of second use electric vehicle batteries for residential energy storage and load-levelling,” *Energy Policy*, vol. 71, pp. 22–30, Aug. 2014.

[49] M. O. Ramoni and H.-C. Zhang, “End-of-life (EOL) issues and options for electric vehicle batteries,” *Clean Technol. Environ. Policy*, vol. 15, no. 6, pp. 881–891, Dec. 2013.

[50] G. Fuchs, B. Lunz, M. Leuthold, and D. U. Sauer, “Technology Overview on Electricity Storage: Overview on the potential and on the deployment perspectives of electricity storage technologies,” *RWTH Aachen*, Jun. 2012.

[51] J. Sudworth, “The sodium/nickel chloride (ZEBRA) battery,” *J. Power Sources*, vol. 100, no. 1–2, pp. 149–163, Nov. 2001.

[52] A. Saez-de-Ibarra *et al.*, “Analysis and comparison of battery energy storage technologies for grid applications,” 2013, pp. 1–6.

[53] K. Richa, C. W. Babbitt, G. Gaustad, and X. Wang, “A future perspective on lithium-ion battery waste flows from electric vehicles,” *Resour. Conserv. Recycl.*, vol. 83, pp. 63–76, Feb. 2014.

[54] Daimler AG, “World’s largest 2nd-use battery storage is starting up,” *http://media.daimler.com*, Lünen/Stuttgart, 13-Sep-2016.

[55] R. Hein, P. R. Kleindorfer, and S. Spinler, “Valuation of electric vehicle batteries in vehicle-to-grid and battery-to-grid systems,” *Technol. Forecast. Soc. Change*, vol. 79, no. 9, pp. 1654–1671, Nov. 2012.

[56] S. Shokrzadeh and E. Bibeau, “Repurposing Batteries of Plug-In Electric Vehicles to Support Renewable Energy Penetration in the Electric Grid,” 2012.

[57] A. Hujber, “Strukturen und Mechanismen des liberalisierten Strommarktes.” 15-Apr-2002.

[58] Austrian Power Grid AG, “Austrian Power Grid,” *APG - Strom bewegt*. [Online]. Available: www.apg.at. [Accessed: 08-Feb-2016].

[59] L. Gelazanskas and K. A. A. Gamage, “Demand side management in smart grid: A review and proposals for future direction,” *Sustain. Cities Soc.*, vol. 11, pp. 22–30, Feb. 2014.

[60] G. Deconinck, “An evaluation of two-way communication means for advanced metering in Flanders (Belgium),” 2008, pp. 900–905.

[61] P. Kepplinger, G. Huber, and J. Petrasch, “Demand Side Management via Autonomous Control-Optimization and Unidirectional Communication with Application to Resistive Hot Water Heaters,” *ENOVA 2014*, p. 8, Dec. 2014.

[62] THINK Global AS, “THINK City Bedienungsanleitung.” THINK Global AS, May-2010.

[63] C.-H. Dustmann, “Advances in ZEBRA batteries,” *J. Power Sources*, vol. 127, no. 1–2, pp. 85–92, Mar. 2004.

[64] K. Kronsbein, “Investigation and Modelling of the ZEBRA System to Optimise State of Charge Detection,” Thesis, Universität Karlsruhe (TH), Stabio, 2004.

[65] C. Daniel and J. O. Besenhard, Eds., *Handbook of battery materials*, 2., completely rev. and enl. ed., 1. Reprint. Weinheim: Wiley-VCH-Verl, 2012.

[66] T. M. O’Sullivan, C. M. Bingham, and R. E. Clark, “Zebra Battery Technologies for the All Electric Smart Car,” *SPEEDAM 2006 Int. Symp. Power Electron. Electr. Drives Autom. Motion*, 2006.

[67] C.-H. Dustmann, “ZEBRA battery meets USABC goals,” *J. Power Sources*, vol. 72, no. 1, pp. 27–31, Mar. 1998.
[68] B. Fäßler, P. Kepplinger, M. L. Kolhe, and J. Petrasch, “Decentralized on-site optimization of a battery storage system using one-way communication,” presented at the International Conference on Renewable Power Generation, 2015, pp. 1–6.
[69] M. Chen and G. A. Rincon-Mora, “Accurate Electrical Battery Model Capable of Predicting Runtime and I–V Performance,” *IEEE Trans. Energy Convers.*, vol. 21, no. 2, pp. 504–511, Jun. 2006.
[70] EXAA Abwicklungsstelle für Energieprodukte AG, “Historical Data - Spot Prices 2014.” EXAA Abwicklungsstelle für Energieprodukte AG, 13-Apr-2015.
[71] M. Doostizadeh and H. Ghasemi, “A day-ahead electricity pricing model based on smart metering and demand-side management,” *Energy*, vol. 46, no. 1, pp. 221–230, Oct. 2012.
[72] S. Gottwalt, W. Ketter, C. Block, J. Collins, and C. Weinhardt, “Demand side management—A simulation of household behavior under variable prices,” *Energy Policy*, vol. 39, no. 12, pp. 8163–8174, Dec. 2011.
[73] T. Logenthiran, D. Srinivasan, and T. Z. Shun, “Demand Side Management in Smart Grid Using Heuristic Optimization,” *IEEE Trans. Smart Grid*, vol. 3, no. 3, pp. 1244–1252, Sep. 2012.
[74] MATLAB, *MATLAB and Statistics Toolbox Release 2014a*. Natick, Massachusetts: The MathWorks Inc., 2014.
[75] S. P. Bradley, A. C. Hax, and T. L. Magnanti, “Dynamic Programming,” in *Applied mathematical programming*, Reading, Mass: Addison-Wesley Pub. Co, 1977, pp. 320–362.
[76] B. Faessler, P. Kepplinger, and J. Petrasch, “Decentralized price-driven grid balancing via repurposed electric vehicle batteries,” *Energy*, vol. 118, pp. 446–455, Jan. 2017.
[77] G. Coley, “BeagleBone Black System Reference Manual.” The BeagleBoard.org Foundation, 11-Apr-2013.
[78] Logic Supply, Inc., “BeagleBone Black Serial Cape Manual.” Logic Supply, Inc., 20-Feb-2015.
[79] EXAA Abwicklungsstelle für Energieprodukte AG, “Spotmarkt,” *EXAA Energy Exchange Austria*. [Online]. Available: www.exaa.at/de/marktdaten/handelsergebnisse. [Accessed: 18-Dec-2015].
[80] MES-DEA SA, “Battery Charger E.F.” MES-DEA SA, 02-Aug-2007.
[81] Fronius International GmbH, “Fronius Symo Datasheet.” Fronius International GmbH, 2011.
[82] Algodue Elettronica Srl, “UEM80.” Algodue Elettronica Srl, Mar-2016.
[83] B. Faessler, M. Schuler, M. Preißinger, and P. Kepplinger, “Battery Storage Systems as Grid-Balancing Measure in Low-Voltage Distribution Grids with Distributed Generation,” *Energies*, vol. 10, no. 12, pp. 1–14, Dec. 2017.
[84] M. Schuler, B. Faessler, M. Preißinger, and P. Kepplinger, “A Method for Grid Simulation Assessing Demand Side Management Strategies,” in *12. Forschungsforum der Österreichischen Fachhochschulen*, Salzburg, 2018, vol. 12, pp. 1–11.
[85] U. Ghatak and V. Mukherjee, “An improved load flow technique based on load current injection for modern distribution system,” *Int. J. Electr. Power Energy Syst.*, vol. 84, pp. 168–181, Jan. 2017.
[86] C. Bucher, “Analysis and Simulation of Distribution Grids with Photovoltaics,” ETH Zurich, 2014.
[87] C. Bucher, “Wie viel Solarstrom verträgt das Niederspannungsnetz?,” *Bulletin Electrosuisse*, no. 3/2014, pp. 37–40, Mar-2014.

PART II

Paper A: Decentralized On-Site Optimization of a Battery Storage System Using One-Way Communication

This chapter is based on the conference paper published as:

B. Fäßler, P. Kepplinger, M. L. Kolhe, and J. Petrasch, “Decentralized on-site optimization of a battery storage system using one-way communication,” presented at the International Conference on Renewable Power Generation, 2015, pp. 1–6.

The layout has been revised for better readability. Minor revisions have been made.

Abstract

Intermittent renewable energy sources (e.g. wind, solar energy systems) have been providing an exponentially growing share of electricity generation. Due to their highly transient and stochastic nature, they pose substantial challenges for power grid operation. Power dispatched from these sources are uncontrolled and do not necessarily coincide with demand; this in turn affects power quality. Hence, extensive demand side management (DSM) is required. DSM relies on flexible loads as well as energy storage facilities. Furthermore, renewable power generation is by its very nature highly distributed and consists of large numbers of small units. These have a substantial effect on traditional power grid operation and electricity pricing patterns.

In this paper, a concept of unidirectional, decentralized, on-site optimization of a battery storage system is presented. A mathematical model of the battery storage system is used to simulate battery dynamics. Battery operation is driven by an optimization procedure, which relies on a one-way communicated pseudo-cost function (PCF). Currently, day-ahead stock market electricity prices are used as the PCF. Optimal operation of the battery is carried out by finding a control function that minimizes the costs, or maximizes profits.

Keywords: Battery Storage System, Decentralized On-Site Optimization, One-Way Communication, Pseudo-Cost Function Driven, Demand Side Management

Nomenclature

A	Surface area of the battery pack (m²)	P_{h}	Auxiliary heating power (W)
C	Heat capacity (J/K)	P_{fan}	Cooling fan power (W)
c	Pseudo-cost function (€/MWh)	$\dot{Q}_{\mathrm{cool}}$	Heat transfer rate due to cooling (W)
c_{p}	Specific heat capacity (J/(kg·K))	$\dot{Q}_{\mathrm{loss}}$	Heat loss via the insulation (W)
d	Thickness of battery pack isolation (m)	R_{i}	Internal resistance (Ω)
E_{el}	Electrical energy content (J)	R_{l}	Internal resistance of single cell (Ω)
f	Heat removal proportionality constant (W/K)	SOC	State of charge (–)
h	Connective heat transfer coefficient (W/(m²·K))	T	Battery temperature (°C)
I_{DC}	Direct charging/discharging current (A)	T_{amb}	Ambient temperature (°C)
k	Thermal conductivity (W/(m·K))	t	Time (s)
m	Battery mass (kg)	u	Decision variable (–)
n_{c}	Number of battery cells per string (–)	U_{DC}	Direct terminal voltage (V)
n_{S}	Number of battery cells strings (–)	U_{T}	Thermal transmittance (W/(m²·K))
P_{AC}	Alternating power (W)	η	Charging/discharging efficiency (–)
P_{DC}	Direct power (W)	η_{in}	Charging converter efficiency (–)
P_{Ri}	Heat dissipation across internal resistance (W)	η_{out}	Discharging converter efficiency (–)

1 Introduction

The increasing share of renewable power generated from transient sources such as wind and solar poses a substantial challenge to power grid operation. Since the power generation from renewable sources cannot be controlled and does not necessarily coincide with the demand, power grids may be severely affected [1].

Currently, large, centrally operated pumped-storage hydroelectric power plants provide a means for managing short-term fluctuations due to the integrated renewable sources, such as the Sima hydroelectric power station in the west of Norway [2] or the Illwerke power plants in the Austrian Alps [3].

If the share of fluctuating renewable power generation further increases, alternative approaches are required; demand side management (DSM) provides one, which is extensively discussed in recent publications [4]. DSM relies on flexible loads as well as energy storage facilities [5]. Also, integration of distributed energy storage systems will most likely be necessary to provide additional capacity for short-term grid stabilization [6], [7].

Different concepts have been proposed for DSM of distributed flexible loads and distributed energy storage: 1) Centralized DSM with two-way communication, where the system state is communicated to one or more central entities, or restricted neighborhood communication [8], which directly controls the distributed systems [9], and 2) local autonomous DSM with unidirectional communication of incentive functions, where the distributed systems can act as independent agents. Local control intelligence of autonomous DSM only gives indirect demand control [8] to the energy supplier. This decentralized DSM concept has been implemented and tested successfully for the domestic hot water heaters [10], and is used in the current paper to manage decentralized battery systems.

Today, the main disadvantage of local energy storage systems is high initial capital investment (particularly for dedicated storage devices such as batteries). Using repurposed electric vehicle batteries may be an interesting alternative for decentralized energy storage. After several thousand of charge cycles, automotive batteries do not have sufficient capacity left for mobile applications, however, with 50% of the original capacity intact they may still be used for stationary energy storage applications. Furthermore, the ecological footprint of batteries can also be improved [11].

In this work, the potential of repurposed ZEBRA (Zero Emission Battery Research Activities) batteries for autonomous control, based on DSM, is investigated by simulation. Therefore, in section 2, a short discussion of the autonomous approach, the details of the ZEBRA battery, the modeling thereof, and the resulting optimization problem as well as details of the simulation are presented. Simulation results are given in section 3, followed by a conclusion in section 4.

2 Approach and Model

In the current work, the concept of unidirectional, decentralized, on-site optimization of electrochemical micro energy storage system is investigated. Fig. 1 illustrates the approach.

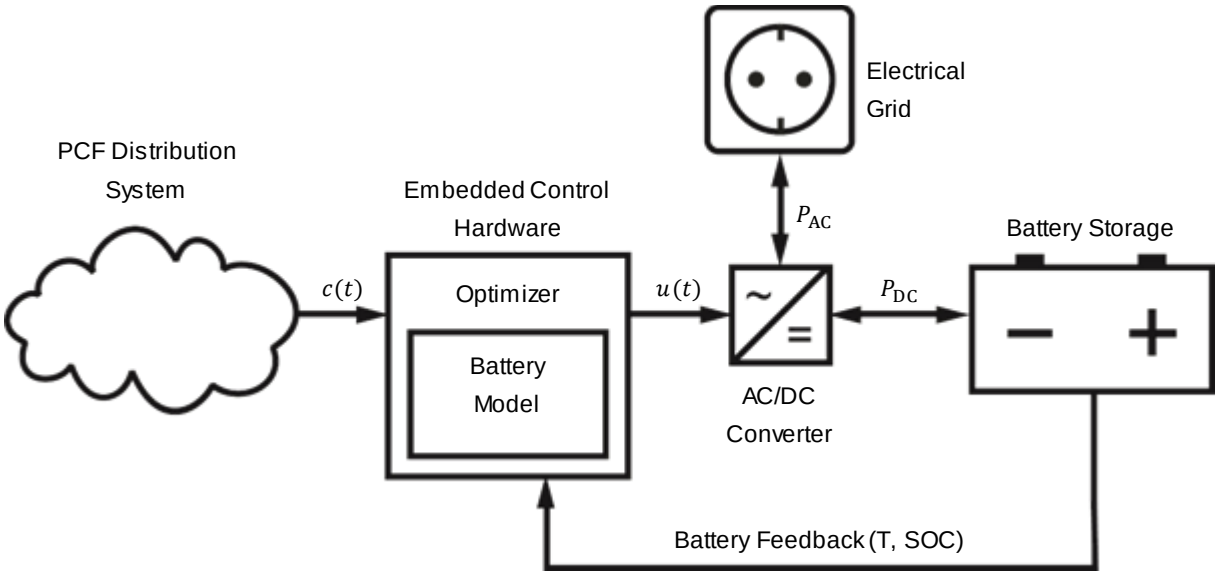

Fig. 1: Schematic of the battery operation.

The optimization relies on a pseudo-cost function, which can be interpreted as a measure for the expected gap between supply and demand at a given time in the future.

Unidirectional communication refers to one-directional transmission of information; from a central entity or marketplace to the participating device. Besides protecting user privacy, this approach allows for local data acquisition at high frequency for fast and continuous adaptation to disturbances and system inputs. Moreover, by local optimization, higher system robustness is expected [12].

A mathematical model of the battery is used for the optimization problem. Minimization of the objective function calculated from the pseudo-cost function is expected to reduce the peak demand on the network and allows operating the storage system in an economic way.

In the following, the details on the battery are discussed, followed by the development of a corresponding mathematical model in section 2.2. Afterwards, the parameterization of the model to reflect the real battery's behavior is discussed. In section 2.4, the optimization problem is formulated using the battery model and details on the conducted simulation are presented in section 2.5.

2.1 ZEBRA Battery

In this work, repurposed ZEBRA batteries are used. The ZEBRA batteries are efficient, compact, durable, and maintenance-free. Batteries with more than 14 years of operating time and over 2000 cycles are still in use [11].

The battery operates using a reaction of sodium with nickel chloride. The energy density is up to 120 Wh/kg and the power density is up to 180 W/kg [13]. A ZEBRA battery pack contains several cells. Cells are connected in series to form strings. Strings are connected in parallel to achieve the corresponding output voltage as well as the current.

The cell setup is shown in detail in Fig. 2. The outer cell case forms the negative electrode. It contains liquid sodium metal. The inner cell case forms the positive electrode, which contains a mixture of NaCl, Ni and Fe. These two electrodes are separated by a β''-alumina electrolyte. The ceramic electrolyte conducts sodium ions and serves as an insulator for electrons. The sodium ion conductivity exceeds 0.2 $\Omega^{-1}\mathrm{cm}^{-1}$ at 260 °C. The conductivity is temperature dependent with a positive gradient. The optimal temperature range of a ZEBRA battery lies between 270 and 350 °C [13].

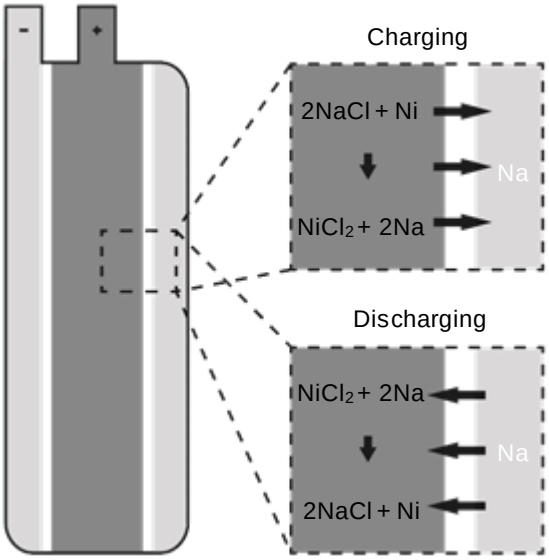

Fig. 2: Battery cell setup showing the chemical reaction for charging/discharging.

During discharge, cf. Fig. 2, Na^+ ions are conducted through the electrolyte and react with the chlorides of the positive electrode to form 2NaCl and Ni [14]. During charging, the reaction is reversed. The chemical process can be described by the following reaction [13]:

$$2\mathrm{Na} + \mathrm{NiCl_2} \underset{\text{charge}}{\overset{\text{discharge}}{\rightleftarrows}} 2\mathrm{NaCl} + \mathrm{Ni} \qquad \text{Eq. 1}$$

The ZEBRA battery is controlled by a battery management system (BMS). The BMS manages the terminal voltage and temperature of the battery cells and performs state of charge (SOC) detection [14].

To ensure functionality of the battery, the stored energy has to exceed 20% of the maximum capacity, i.e. $SOC_{\min} = 0.2$. By this, a backup of energy for the heating system is provided, and premature degeneration is avoided.

2.2 Battery Model

In this section, a simple dynamic model of the ZEBRA battery's state (SOC and temperature) is developed, assuming the battery consists of a voltage source and an internal resistance.

The battery's dynamics are described by a coupled system of two ordinary differential equations. The state of the battery is defined by its SOC and its internal temperature, T. Applying energy conservation the time derivative of SOC and temperature are given by

$$\frac{dSOC}{dt} = \frac{1}{E_{\mathrm{el}}}\Big(u(t)\cdot P_{\mathrm{AC,max}}\cdot\eta(t) - P_{\mathrm{Ri}}(SOC) - P_{\mathrm{h}}(t) - P_{\mathrm{fan}}(t)\Big), \quad \text{Eq. 2}$$

$$\text{where } \eta(t) = \begin{cases}\eta_{\mathrm{in}}, & u(t)\geq 0\\ {\eta_{\mathrm{out}}}^{-1}, & u(t)<0\end{cases} \text{ and} \quad \text{Eq. 3}$$

$$\frac{dT}{dt} = \frac{1}{C}\cdot\Big(P_{\mathrm{Ri}}(SOC) + P_{\mathrm{h}} - \dot{Q}_{\mathrm{cool}}(t) - \dot{Q}_{\mathrm{loss}}(t)\Big), \quad \text{Eq. 4}$$

$$\text{where } C = m\cdot c_{\mathrm{p}}. \quad \text{Eq. 5}$$

The charging/discharging power can be assumed to be constant, because power is held constant by a charge controller, resulting in a decision function of $-1 \leq u(t) \leq 1$. The efficiency of the charging/discharging converter ($\eta_{\mathrm{in}}, \eta_{out}$) is taken into account, since it reduces the maximum power input or output of the battery storage system. Thus, the input/output power, P_{AC}, cf. Fig. 1, is converted to the charging/discharging power, P_{DC}. In the following, individual energy flows are described.

2.2.1 Internal Resistance

The power converted to heat, P_{Ri}, in the battery by internal resistance can be described as

$$P_{\mathrm{Ri}}(SOC) = R_{\mathrm{i}}(SOC)\cdot I_{\mathrm{DC}}(SOC)^2, \quad \text{Eq. 6}$$

where R_{i} is the internal resistance and I_{DC} the charging/discharging current. As shown in Fig. 3, the internal resistance of a single battery cell depends on the SOC. If the cell is fully charged and a discharging process begins, Na ions pass through the β''-alumina and react with $NiCl_2$ that is closest to the ceramic. As discharging proceeds, the reaction front migrates inwards, causing the reaction area to decrease and the travel distance of the Na ions to increase, resulting in a higher resistance. For new cell designs, the relation between SOC and internal resistance is almost perfectly linear [14].

The ZEBRA battery used in the current study consists of $n_{\mathrm{s}} = 2$ parallel strings of $n_{\mathrm{c}} = 144$ cells each. Thereby, the internal resistance is the inverse of all string conductances that are connected in parallel, whereby the string conductance is the inverse of the sum of the serial connected cell resistances, R_{l}. This results in a total internal resistance, R_{i}, of

$$R_{\mathrm{i}} = \frac{\sum_{l=1}^{n_{\mathrm{c}}} R_{\mathrm{l}}}{n_{\mathrm{s}}}. \quad \text{Eq. 7}$$

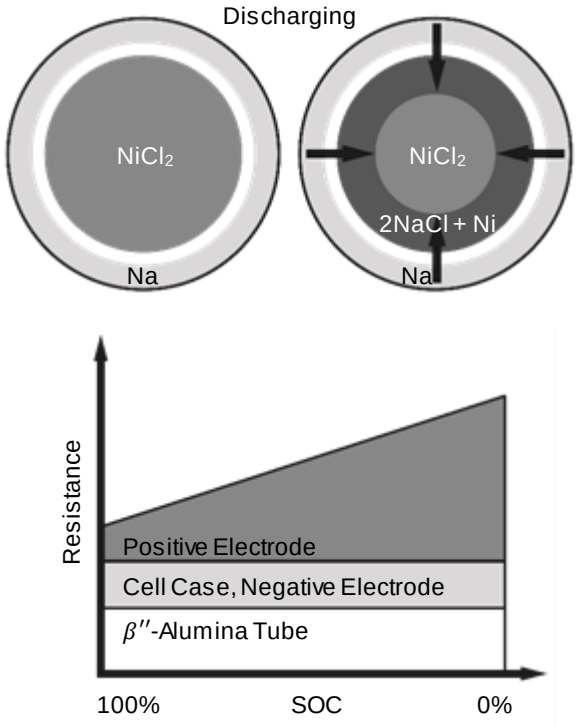

Fig. 3: Cell setup – internal resistance.

2.2.2 Heating

The auxiliary heating system with a heating power, P_{h}, is activated, if the battery temperature drops below a defined internal battery temperature limit to further ensure the functionality. In the ZEBRA battery, the auxiliary heating system is supplied by a resistance heater.

2.2.3 Heat Loss via the Insulation

In order to minimize the need for auxiliary heating, the battery is thermally insulated. A linear dependence between battery temperature, T, and ambient temperature, T_{amb}, is postulated.

$$\dot{Q}_{\mathrm{loss}}(t) = \left(T(t) - T_{\mathrm{amb}}(t)\right) \cdot U_{\mathrm{T}} \cdot A, \qquad \text{Eq. 8}$$

$$\text{where } U_{\mathrm{T}} = \frac{1}{\frac{d}{k} + \frac{1}{h}} \qquad \text{Eq. 9}$$

The thermal transmittance, U_{T}, through the outer surface area, A, of the battery pack is caused by conduction (d is the insulation thickness, k the thermal conductivity) and convection (h is the connective heat transfer coefficient).

2.2.4 Cooling

Again, to ensure the proper functionality of the battery, its temperature has to be in a certain range. If the upper internal temperature limit, which depends on the SOC, is exceeded, an internal cooling fan is activated with the power, P_{fan}. The cooling system induces an airflow inside the battery package. This enables a heat transfer between the cooling fins of each battery cell and the air flowing past to achieve better heat removal, $\dot{Q}_{\mathrm{cool}}$, from the system.

This can be formulated as

$$\dot{Q}_{\mathrm{cool}}(t) = f \cdot \big(T(t) - T_{\mathrm{amb}}(t)\big), \qquad \text{Eq. 10}$$

where f is the proportionality heat removal constant.

2.3 System Identification

Based on logged charge/discharge data provided by the BMS from a ZEBRA battery, the model is implemented in section 2.2 and parameterized, cf. Fig. 4 and Fig. 5. The data logging is performed using CAN bus communication, recording SOC and temperature of the battery every second. The battery system specifications are listed in Table 1 and the identified parameters in Table 2.

Table 1: Battery system specifications.

Direct charging voltage, U_{DC}	372.09 V
Direct charging current, I_{DC}	3.80 A
Direct discharging voltage, U_{DC}	349.20 V
Direct discharging current, I_{DC}	10.67 A
Heating power AC, P_{h}	<6.5 A at 240 V(AC)
Heating power DC, P_{h}	300 W
Cooling fan power, P_{fan}	62 W
Ambient temperature, T_{amb}	20 °C
Serial battery cells (two were damaged on the real system), n_{c}	142
Parallel strings of battery cells, n_{s}	2

Table 2: Identified battery system parameters.

Battery capacity, E_{el}	28.2 kWh
Lower temperature limit, T_{min}	245 °C
Upper temperature limit, T_{max}	280 °C
Thermal conductance, $U_{\mathrm{T}} \cdot A$	0.1519 W/K
Battery mass, m	243 kg
Specific heat capacity, cp	270 J/(kg·K)
Heat removal proportionality constant, f	9.5 W/K
Ambient temperature, T_{amb}	20 °C

For system identification, the heating power, P_{h}, during charging was set to be constant at 200 W, for discharging 300 W, for cooling the following behavior was identified with respect to the temperature and decision state:

$$P_{\mathrm{fan}}(t) = \begin{cases} 62\ \mathrm{W}, & T(t) \geq T_{\max} \\ 0.95\ \mathrm{W}, & T(\mathrm{t}) < T_{\max}\ \&\ u(t) \geq 0 \\ 1.77\ \mathrm{W}, & T(\mathrm{t}) < T_{\max}\ \&\ u(t) \geq 0, \text{after heating} \\ 0\ \mathrm{W}, & \text{else} \end{cases} \qquad \text{Eq. 11}$$

The listed parameters result in a root mean square error for the SOC of 3.36% for charging, and 0.46% for discharging. As shown in Fig. 4, the simulated SOC coincides with the measured SOC as long as the SOC remains below 0.8. Above 0.8, the BMS carries out a range of undocumented operations with no clearly identifiable pattern. However, it is not necessary to understand these operations to identify a useful and accurate model of battery dynamics.

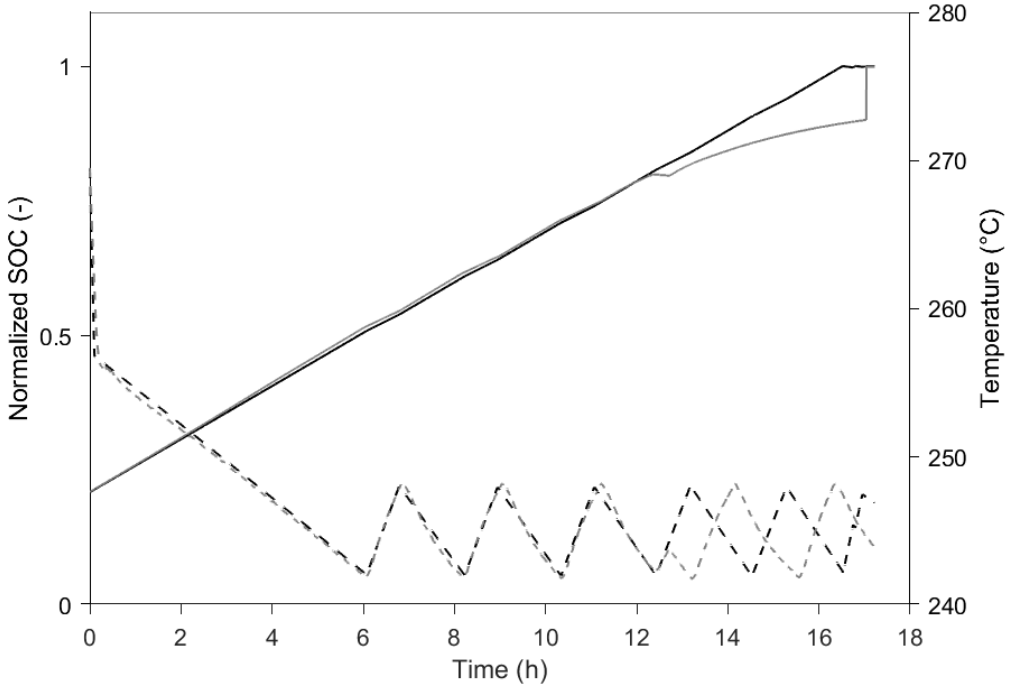

Fig. 4: System identification for charging. Solid lines: Normalized SOC, dashed lines: battery temperature. Black: model; Grey: BMS measurements.

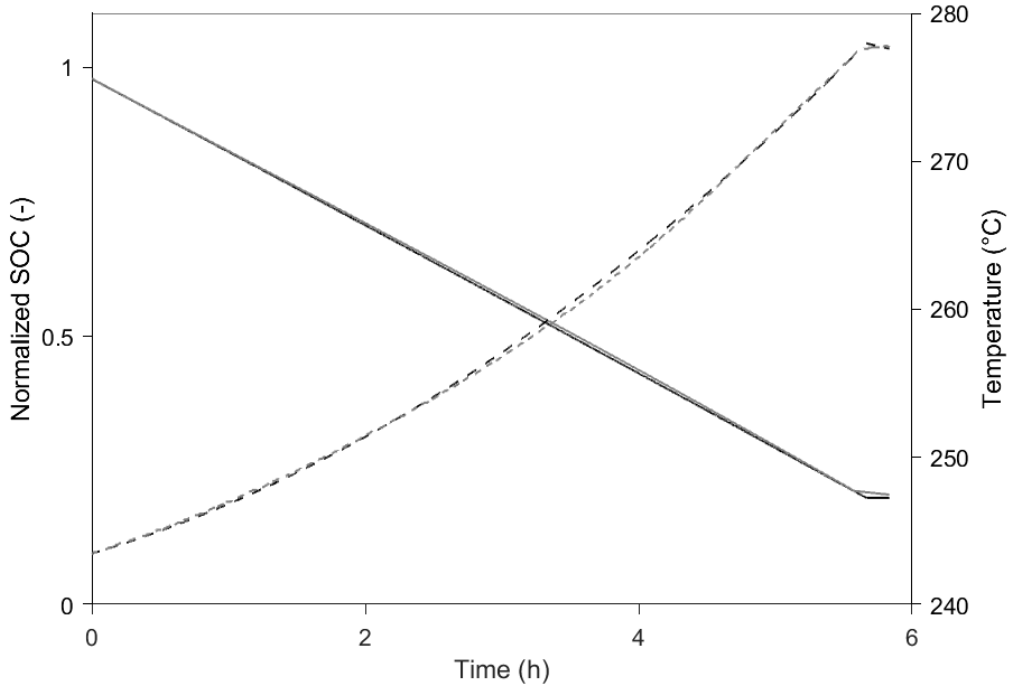

Fig. 5: System identification for discharging. Solid lines: Normalized SOC, the dashed lines: battery temperature. Black: model; Grey: BMS measurements.

2.4 Optimization

As discussed in section 2.1, the proposed approach is based on the on-site optimization of the battery with respect to unidirectionally communicated pseudo-costs. Optimization relies on the battery model as developed in section 2.2. Optimal control of a battery storage system means finding the optimal decision function, $u(t)$, that minimizes the costs. Given a time window, $[t_0, t_n]$, for the optimization, the minimization problem reads

$$\min_u \int_{t_0}^{t_n} \left(c(t) \cdot u(t) \cdot P_{\mathrm{AC,max}}\right) dt. \qquad \text{Eq. 12}$$

Additionally, the optimization problem is constrained by upper and lower bounds for the SOC and *T* at all times, i.e.

$$SOC_{\min} \leq SOC(t) \leq SOC_{\max}, T_{min} \leq T(t) \leq T_{max}, t_0 \leq t \leq t_n. \qquad \text{Eq. 13}$$

2.5 Simulation

MATLAB [15] is employed to solve the minimization problem, using the built-in sequential quadratic programming (SQP) algorithm provided by MATLAB's *fmincon* routine.

For the simulation, the battery is assumed to be charged/discharged with a constant voltage of $U_{\mathrm{DC,max}}$ = 370.34 V and a constant current of $I_{\mathrm{DC,max}}$ = 4.07 A. For charging and discharging, we assume an efficiency of η_{in} = 0.9 and η_{out} = 0.95, respectively, based on data provided by manufacturers of the converters BC-336-Z-3-A EF and Fronius Symo 8.2-3-M [16], [17]. The

initial battery SOC is set to 0.25 of the maximum SOC; the initial battery temperature is set to 269.5 °C.

The Energy Exchange Austria (EXAA) provide the day-ahead price for 2014, which is used as the PCF [18]. It integrates quarter hours on 3 September 2014 in the Austrian day-ahead market and provides price data for the upcoming 36 hours. For the simulation, the time-span ranges from 4 September 2014 to 31 December 2014. The optimization is performed every 24 hours at noon, taking the next 36 hours into account, reflecting the clearing of the day-ahead market at late morning for the next day.

3 Results

Table 3 summarizes the simulation results. The resulting optimal operation, cf. Fig. 6, shows continuous charging and discharging of the battery; no idle state was detected. Continuous charging/discharging causes self-heating due to the internal resistance and therefore less energy is used for the auxiliary heating system. This results also in a high efficiency.

Moreover, most of the times, only a portion of the battery capacity was utilized, resulting in a mean SOC of about 40% and a standard deviation of 15%.

Additionally, results show that the battery is operated close to the lower temperature limit, causing minimal heat loss.

Table 3: Simulation Results.

Runtime	118 days
Earnings	37.28 €
Mean SOC	41.18%
Standard deviation SOC	15.00%
Maximum SOC	94.32%
Round-trip efficiency	79.81%
Idling time during runtime	0.00%
Mean temperature	244.96 °C
Standard deviation temperature	1.65 °C

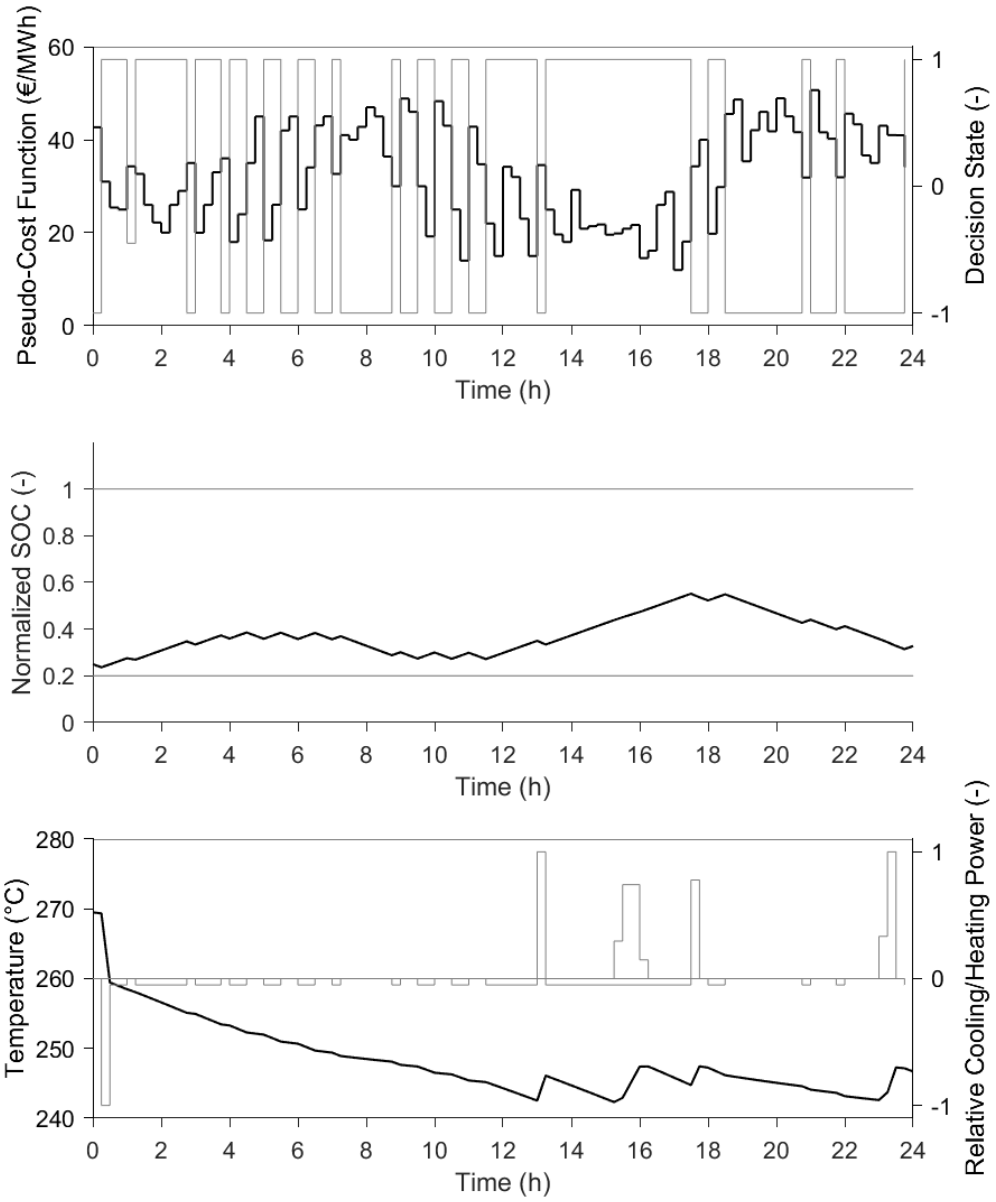

Fig. 6: Optimization results for a single day. Top: PCF (black) and decision function (grey). Middle: Normalized SOC (black), maximum and minimum SOC (grey). Bottom: Battery temperature (black), relative heating power, $P_{\mathrm{h,rel}}(t)$, (grey, positive), relative cooling power, $P_{\mathrm{fan,rel}}(t)$, (grey, negative), where $P_{\mathrm{h,rel}}(t) = \frac{P_{\mathrm{h}}(t)}{P_{\mathrm{h,max}}}$ and $P_{\mathrm{fan,rel}}(t) = \frac{P_{\mathrm{fan}}(t)}{P_{\mathrm{fan,max}}}$.

4 Conclusion

In this publication, a simulation was conducted to explore the potential of repurposed high-temperature ZEBRA batteries for grid balancing based on one-way communication. Therefore, a thermal-electrical model of the battery was developed and fitted to experimental data. Historic day-ahead prices from the Austrian electricity market were used to serve as pseudo-cost functions for the optimization procedure.

The simulation results show that the cost-optimal operation of the battery is achieved by permanent charging/discharging at maximum power; no idle state is detected.

The achieved results could be performed with a round-trip efficiency of about 80% including the charging and discharging converters.

For the investigated battery storage, the power to capacity ratio already allows us to successfully operate the device for grid balancing. This is reflected by the output of the optimizer. Earnings of about 37 € in four months can be achieved. With this, we show that it is possible to operate repurposed batteries using autonomous optimization as a means for demand side management.

Acknowledgements

We thank Dr. Steffen Finck at the Vorarlberg University of Applied Sciences for his help on developing the optimization routine. The financial support by the Austrian Federal Ministry of Science, Research and Economy and the National Foundation for Research, Technology and Development is gratefully acknowledged.

References

[1] C. Dötsch, A. Kanngießer, and D. Wolf, “Speicherung elektrischer Energie – Technologien zur Netzintegration erneuerbarer Energien,” *Uwf UmweltWirtschaftsForum*, vol. 17, no. 4, pp. 351–360, Dec. 2009.

[2] E. Solvang, A. Harby, and Å. Killingtveit, “Increasing balance power capacity in Norwegian hydroelectric power stations,” Technical Report, TR A7195, Feb. 2012.

[3] Vorarlberger Illwerke AG, “Kopswerk II.” *Kopswerk II*. [Online]. Available: www.kopswerk2.at. [Accessed: 15-Jan-2015].

[4] P. Siano, “Demand response and smart grids—A survey,” *Renew. Sustain. Energy Rev.*, vol. 30, pp. 461–478, Feb. 2014.

[5] D. Ohlhorst, M. Schreurs, and A. T. Gullberg, “Norway – ‘Battery’ for the German Energy Transition? Different National Interests in Energy Policies Norwegen – „Batterie“ der deutschen Energiewende? Unterschiedliche Länderinteressen in der Energiepolitik,” *GAIA - Ecol. Perspect. Sci. Soc.*, vol. 21, no. 4, pp. 319–320, Dec. 2012.

[6] M. Beaudin, H. Zareipour, A. Schellenberglabe, and W. Rosehart, “Energy storage for mitigating the variability of renewable electricity sources: An updated review,” *Energy Sustain. Dev.*, vol. 14, no. 4, pp. 302–314, Dec. 2010.

[7] P. Palensky and D. Dietrich, “Demand Side Management: Demand Response, Intelligent Energy Systems, and Smart Loads,” *IEEE Trans. Ind. Inform.*, vol. 7, no. 3, pp. 381–388, Aug. 2011.

[8] S. D. Ramchurn, P. Vytelingum, A. Rogers, and N. Jennings, “Agent-based control for decentralised demand side management in the smart grid,” in *The 10th International Conference on Autonomous Agents and Multiagent Systems-Volume 1*, 2011, pp. 5–12.

[9] P. Samadi, H. Mohsenian-Rad, R. Schober, and V. W. S. Wong, “Advanced Demand Side Management for the Future Smart Grid Using Mechanism Design,” *IEEE Trans. Smart Grid*, vol. 3, no. 3, pp. 1170–1180, Sep. 2012.

[10] P. Kepplinger, G. Huber, and J. Petrasch, “Autonomous optimal control for demand side management with resistive domestic hot water heaters using linear optimization,” *Energy Build.*, vol. 100, pp. 50–55, Aug. 2015.

[11] M. Meisel, T. Leber, K. Pollhammer, F. Kupzog, J. Haslinger, P. Wächter, J. Sterbik-Lamina, M. Ornetzeder, A. Schiffleitner, and M. Stachura, “Erfolgsversprechende Demand-Response-Empfehlungen im Energieversorgungssystem 2020,” *Inform.-Spektrum*, vol. 36, no. 1, pp. 17–26, Feb. 2013.

[12] P. Kepplinger, G. Huber, and J. Petrasch, “Demand Side Management via Autonomous Control - Optimization and Unidirectional Communication with Application to Resistive Hot Water Heaters,” *ENOVA 2014*, p. 8, Dec. 2014.

[13] C.-H. Dustmann, “Advances in ZEBRA batteries,” *J. Power Sources*, vol. 127, no. 1–2, pp. 85–92, Mar. 2004.

[14] K. Kronsbein, “Investigation and Modelling of the ZEBRA System to Optimise State of Charge Detection,” Thesis, Universität Karlsruhe (TH), Stabio, 2004.

[15] MATLAB, *MATLAB and Statistics Toolbox Release 2014a*. Natick, Massachusetts: The MathWorks Inc., 2014.

[16] MES-DEA SA, “Battery Charger E.F.” MES-DEA SA, 02-Aug-2007.

[17] Fronius International GmbH, “Fronius Symo Datasheet.” Fronius International GmbH, 2011.

[18] EXAA Abwicklungsstelle für Energieprodukte AG, “Historical Data - Spot Prices 2014.” EXAA Abwicklungsstelle für Energieprodukte AG, 13-Apr-2015.

Paper B: Decentralized Price-Driven Grid Balancing via Repurposed Electric Vehicle Batteries

This chapter is based on the journal paper published as:

B. Faessler, P. Kepplinger, and J. Petrasch, “Decentralized price-driven grid balancing via repurposed electric vehicle batteries,” *Energy*, vol. 118, pp. 446–455, Jan. 2017.

The layout has been revised for better readability. Minor revisions have been made.

Abstract

The share of electricity generated from intermittent renewable sources, e.g., wind and solar grows rapidly. This affects grid stability and power quality. If the share of renewable power generation is to be increased further, additional flexibilities must be introduced.

Aggregating small, distributed loads and energy storage facilities is a good medium-term option. In this paper, the suitability of decentralized and on-site optimized storage system consisting of repurposed electric vehicle batteries for grid balancing is investigated. Battery operation is controlled via an optimization procedure, which relies on a one-way communicated pseudo-cost function (PCF). Day-ahead electricity stock market prices are used as the PCF.

Based on one year simulations, a sequential quadratic programming (SQP) approach is compared to a dynamic programming (DP) and an integer linear programming (ILP) approach with respect to runtime and control objective. All approaches lead to very similar results, however ILP leads to the shortest runtimes. ILP is then used to investigate the grid-balancing potential using last decade's hourly day-ahead prices. Higher market data resolutions featuring quarter-hours introduced in 2014 lead to higher earnings. For hourly day-ahead prices the optimal capacity-to-power ratio of the battery is approximately 6 hours while for quarter-hourly prices it is about 3 hours.

Keywords: Grid Balancing, Vehicle Batteries, Repurposed, Battery Storage, Distributed Storage, Optimization

Nomenclature

A	Surface area of the battery pack (m²)	n	Total number of data points (–)
C	Path dependent costs in DP (€)	n_c	Number of battery cells per string (–)
c	Pseudo-cost function (€/MWh)	n_s	Number of battery cell strings (–)
c_p	Specific heat capacity (J/(kg·K))	P_AC	Alternating power (W)
d	Thickness of battery pack isolation (m)	P_DC	Direct power (W)
		$P_\mathrm{DC}^{(n_\mathrm{s})}$	Scaled direct power (W)
E_el	Electrical energy content (J)	P_fan	Cooling fan power (W)
$E_\mathrm{el}^{(n_\mathrm{s})}$	Scaled electrical energy content (J)	$P_\mathrm{fan}^{(n_\mathrm{s})}$	Scaled cooling fan power (W)
		P_h	Auxiliary heating power (W)
f	Heat removal proportionality constant (W/K)	$P_\mathrm{h}^{(n_\mathrm{s})}$	Scaled auxiliary heating power (W)
g_l, g_u	Constraints for lower and upper E_el in SQP (J)	P_loss	Linearized battery losses (W)
		P_Ri	Heat dissipation across internal resistance (W)
h	Connective heat transfer coefficient (W/(m²·K))	$P_\mathrm{Ri}^{(n_\mathrm{s})}$	Scaled heat dissipation across internal resistance (W)
I_DC	Direct charging/discharging current (A)	$\dot{Q}_\mathrm{cool}$	Heat loss via the insulation (W)
$I_\mathrm{DC}^{(n_\mathrm{s})}$	Scaled charging/discharging current (A)	$\dot{Q}_\mathrm{cool}^{(n_\mathrm{s})}$	Scaled heat transfer rate due to cooling (W)
k	Thermal conductivity (W/(m·K))	$\dot{Q}_\mathrm{loss}$	Heat loss via the insulation (W)
m	Battery mass (kg)	$\dot{Q}_\mathrm{loss}^{(n_\mathrm{s})}$	Scaled heat loss via insulation (W)
$m^{(ns)}$	Scaled battery mass (kg)		

R_c	Internal resistance of single cell (Ω)
R_i	Internal resistance (Ω)
SOC	State of charge (%)
s	Discrete states in dynamic programming (–)
T	Battery temperature (°C)
T_amb	Ambient temperature (°C)
t	Time (s)
U_DC	Direct terminal voltage (V)
U_T	Thermal transmittance (W/(m²·K))
u_AC	Decision variable on AC power side (–)
u_DC	Decision variable on DC power side (–)
u_hys	Boolean hysteresis variable (–)
η_in	Charging converter efficiency (–)
η_out	Discharging converter efficiency (–)
τ	Time interval for analytic solution (s)

1 Introduction

Global warming and dwindling fossil resources have sparked a strong growth in renewable power generation. Some industrialized countries have set very ambitious targets for increasing the proportion of renewables in electricity production [1]. For example, Germany plans to generate 80% of its electricity from renewable sources by 2050 [2]. However, fluctuating sources of renewable energy such as wind and solar severely affect grid operation [3], [4]. Supply and demand imbalances are traditionally compensated for by large-scale buffer storage systems, e.g. pumped storage hydro power plants. These grid-balancing strategies are limited by infrastructural considerations [5]. Therefore, developing additional, modular strategies for grid balancing are necessary [3], [6].

Aggregating small, distributed loads and energy storage facilities constitutes a promising approach. Such a strategy would reduce the need for new power plants [7]. In this context, demand side management (DSM), which is known as a portfolio of measures to balance the electrical grid on consumption side [6], has been extensively discussed [8]. In DSM, controllable, flexible loads and energy storage facilities reduce, increase or shift energy consumption in order to line up electrical energy usage with generation [6] The most important strategies used are peak clipping, valley filling, load shifting, strategic conservation, strategic load growth, and flexible load shaping [9]. To motivate consumers to change their consumption from the nominal pattern to respond according to the actual electrical energy generation, a specific tariff or program has to be provided [10]. Han et al. [11] distinguish between incentive- and time-based demand response (DR). In Ref. [10], they further divide incentive-based DR in classical and market-based DR. In case of classical DR, consumers agree to give-up the control of certain devices or react by limiting their consumption based on payments or preferential prices. Market-based DR allows consumers to bid with their loads and energy storage facilities on an appropriate marketplace. Time-based DR depend on received event signals e.g. price, which stimulates devices to react with their demand [11].

Contrary to DSM, distributed loads and energy storage facilities could be introduced to the power grid with the specific aim of balancing the grid.

In any case, these devices that are to be used for grid balancing have to be equipped with communication hardware. While most grid-balancing concepts require two-way communication [12]—as price signals, bid data, etc. have to be transmitted between utilities

and loads and energy storage facilities [10]—local, autonomous control with unidirectional communication proposed by Ref. [13] has been demonstrated as a robust and cost effective alternative.

With an increasing share of decentralized and fluctuating electricity generation due to sources such as wind and solar the voltage level in the power grid is affected [14], [15]. Such sources are often connected to the low voltage grid [16]–[18]. Active and reactive power control strategies have been discussed and applied to limit the voltage rise [14], [15], [19].

Battery storage systems are suitable for either large-scale applications or for aggregated approaches. They are practically maintenance-free [20], fast to respond [21] and highly efficient [22]. They have total round-trip efficiencies, including AC-DC converters, ranging from 65% to almost 90% [23]. Various types of battery storage systems have been investigated for balancing electrical grids [24]–[26]. A range of cell chemistry types have been considered, particularly lithium-ion (Li-ion), sodium sulfur (NaS), ZEBRA ($Na–NiCl_2$), nickel-cadmium (NiCd), nickel-metal hydride (NiMH), and lead acid (Pb-acid) type batteries [27], [28]. Divya et al. [29] state that the application timescales for future battery storage systems may range from seconds to days. Battery storage systems have been already investigated in large-scale applications for primary frequency control [30] and for secondary control [31]. Since lifecycle costs for such systems are higher than, for instance, pumped storage hydro power plants [32], numerous applications seek to aggregate already existing, small battery storage systems. Often, photovoltaic power systems are combined with small battery banks to increase the self-consumption [33]. Since the capacity of such batteries is not entirely used at all times, a DSM motivated approach would further increase the efficiency of usage. Such concepts have been extensively discussed in Ref. [34]. Guille et al. [35] state that on an average, electric vehicles (EV) stay idle for about 22 hours a day. Hence, in DSM, the idea of aggregating batteries of EVs for control strategies, a concept, which is known as vehicle-to-grid (V2G), seems to be promising and was proposed, among others, in Refs. [29], [36]–[40]. Daimler announced [41] that it plans to reuse their old EV batteries and connect them to the electrical grid, thus building the world's largest stationary storage facility with a capacity of 13 MWh. Using repurposed electric vehicle batteries may help to offset the costs associated with battery-based systems [42]. Batteries are generally not used in EVs once their capacity falls below 70–80% [43] of the initial capacity. However, they are still useful for stationary applications. This second-use approach also reduces the ecological footprint [44].

In the current paper, local, autonomous control with a unidirectionally communicated time-based event signal (pseudo-cost function) [45] (as is often used in DSM), which has been successfully tested for domestic hot water heaters [46], is applied to battery storage systems. In a previous paper [47], the potential of ZEBRA (Zero Emission Battery Research Activities) batteries for autonomous control has been investigated by simulation. In this paper, steps are taken towards implementing the approach on a physical battery system by developing an embedded control system with highly efficient simulation and optimization routines. To this end, different nonlinear and linear optimization approaches are compared with respect to computational costs and resulting control optimality. A sequential quadratic programming approach (SQP) is used for nonlinear optimization. Dynamic programming (DP) as well as integer linear programming (ILP) are approaches considered for linear optimization. The grid-balancing potential is estimated by simulating the battery system based on historic, Austrian, day-ahead market prices [48] for electricity in the period from 2003–2015. Voltage control

strategies of grid-connected converters is not discussed in the current paper since the scope of this work is on price-driven operation of battery storage systems. However, the pseudo-cost function could be made adaptable to the current grid situation to control the power feed-in and hence the voltage rise.

2 Approach and Model

A schematic representation of the physical battery storage system including all relevant components is shown in Fig. 1. The repurposed ZEBRA battery is connected to the electrical grid via an AC-DC converter. Alternating power, P_{AC}, is transformed through the converter to DC power, P_{DC}, which is used to charge the battery and vice versa. Conversion is carried out with an efficiency of η_{in} and η_{out}, respectively. The battery charge or discharge operation is controlled by a decision function, $u_{\mathrm{DC}}(t)$, indicating whether the battery is charged, discharged, or stays idle. The optimizer searches for an optimal $u_{\mathrm{DC}}(t)$ by minimizing costs based on an input function, called pseudo-cost function (PCF, $c(t)$) while keeping the battery's state of charge (SOC) within operational bounds, $E_{\mathrm{el,min}}$ and $E_{\mathrm{el,max}}$. The SOC represents the normalized electrical energy content, E_{el}, of a battery storage system. The pseudo-cost function is provided by the distribution system. This can be interpreted as a measure for the expected grid load [8]. For a given time window, $[t_0, t_n]$, the optimization problem can be formulated as:

$$\min_{u_{\mathrm{DC}}} \int_{t_0}^{t_n} c(t) \cdot P_{\mathrm{AC}}(u_{\mathrm{DC}}(t))\, dt, \mathrm{s.t.} \qquad \text{Eq. 1}$$

$$E_{\mathrm{el,min}} \leq E_{\mathrm{el}}(t) \leq E_{\mathrm{el,max}},\ t_0 \leq t \leq t_n \qquad \text{Eq. 2}$$

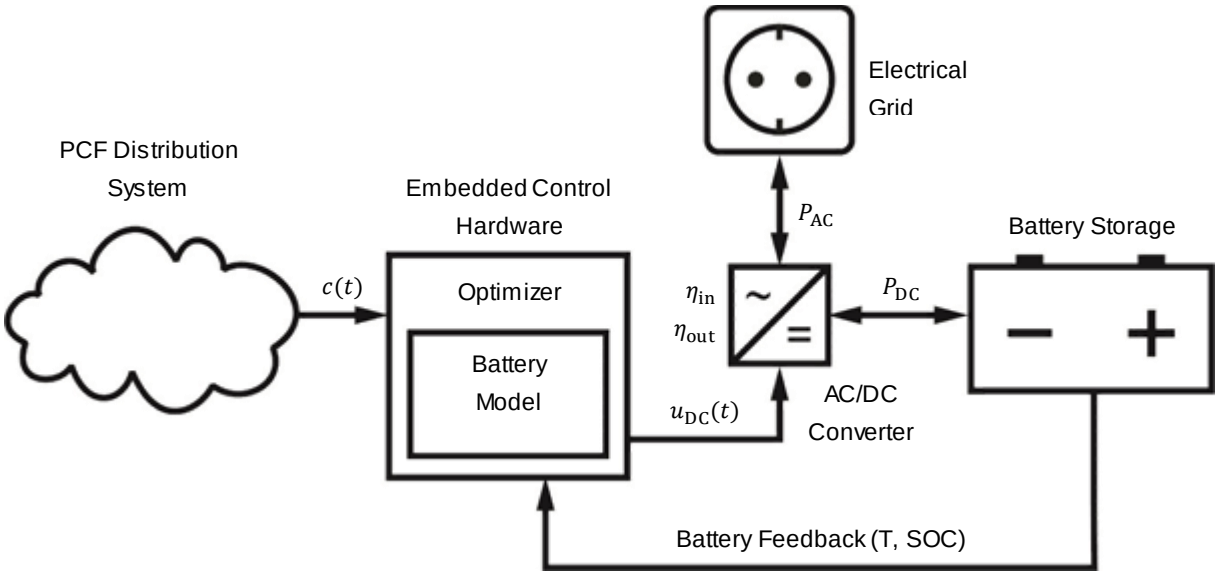

Fig. 1: Schematic of the battery operation.

2.1 Modeling and Simulation

A ZEBRA-type high temperature battery based on the reaction of sodium with nickel chloride is used. The optimal operational temperature range lies between 270 and 350 °C [49]. The redox reaction within the cell is given by, c.f. [49], [50]:

$$2\mathrm{Na} + \mathrm{NiCl_2} \underset{\text{charge}}{\overset{\text{discharge}}{\rightleftarrows}} 2\mathrm{NaCl} + \mathrm{Ni} \qquad \text{Eq. 3}$$

ZEBRA batteries are interesting for stationary applications due to their long-term cyclic stability [51]. Within a ZEBRA battery pack, battery cells are connected in series (strings) to achieve a desired output voltage. The desired output current is obtained by connecting strings in parallel. The energy density of a ZEBRA battery is about 90 Wh/kg; the power density about 150 W/kg [52].

The battery is equipped with an auxiliary heating and cooling system controlled by a built-in battery management system (BMS) to stabilize the operational temperature. It also limits currents at increased operating temperatures. A linear current reduction for discharging between 290 °C and 310 °C from a maximum current of 117 A/string to 20 A/string is imposed. Between 310 °C and 340 °C the discharging current is limited to 20 A/string. Above 340 °C no charge and discharge is allowed due to safety reasons. Furthermore, the BMS manages the total electrical power flow through the battery. This includes cell voltage control and the state of charge (SOC) detection [50]. The SOC is held above 20% to maintain an energy reserve to be used for temperature control. In addition, the BMS provides an interface for information about the battery state, namely SOC, temperature, voltage, and current.

2.1.1 Battery Model

As shown in Ref. [47], the battery dynamics can be described by a system of two nonlinear, coupled ordinary differential equations. The transient chemical (E_{el}) and thermal (T) energy balances are given by

$$\frac{\mathrm{d}E_{\mathrm{el}}}{\mathrm{d}t} = P_{\mathrm{DC}}(t) - P_{\mathrm{Ri}}\big(E_{\mathrm{el}}(t)\big) - P_{\mathrm{h}}(t) - P_{\mathrm{fan}}(t), \text{where} \qquad \text{Eq. 4}$$

$$P_{\mathrm{DC}}(t) = \begin{cases} \eta_{\mathrm{in}} \cdot P_{\mathrm{AC}}(t), & P_{\mathrm{AC}} \geq 0 \\ \eta_{\mathrm{out}}^{-1} \cdot P_{\mathrm{AC}}(t), & P_{\mathrm{AC}} < 0 \end{cases} \text{ and} \qquad \text{Eq. 5}$$

$$\frac{\mathrm{d}T}{\mathrm{d}t} = \frac{1}{m \cdot c_{\mathrm{p}}} \cdot \Big(P_{\mathrm{Ri}}\big(E_{\mathrm{el}}(t)\big) + P_{\mathrm{h}}(t) - \dot{Q}_{\mathrm{loss}}\big(T(t)\big) - \dot{Q}_{\mathrm{cool}}\big(T(t)\big)\Big). \qquad \text{Eq. 6}$$

P_{DC} is the input or output DC power. Losses inside the battery are modeled as an internal resistance. With decreasing SOC, the internal resistance increases due to chemical effects [50]. Thus, the internal resistance is E_{el} dependent. The relation between E_{el} and internal resistance is almost linear between a maximum resistance, $R_{\mathrm{c,max}}$, and a minimum resistance, $R_{\mathrm{c,min}}$, for a single battery cell [50]. The power converted to heat by internal resistance can be described by

$$P_{\mathrm{Ri}}(E_{\mathrm{el}}(t)) = R_{\mathrm{i}}(E_{\mathrm{el}}(t)) \cdot I_{\mathrm{DC}}\big(E_{\mathrm{el}}(t)\big)^2, \qquad \text{Eq. 7}$$

where I_{DC} is the direct charging or discharging current and R_{i} the total internal resistance. The presented battery consists of n_{s} parallel battery cell strings with n_{c} battery cells each. The total electrical energy content of the battery is given by $E_{\mathrm{el,max}}$.

Thus, the total internal resistance can be described as

$$R_{\mathrm{i}}(E_{\mathrm{el}}(t)) = \left(R_{\mathrm{c,max}} - \left(R_{\mathrm{c,max}} - R_{\mathrm{c,min}}\right) \cdot \frac{E_{\mathrm{el}}(t)}{E_{\mathrm{el,max}}}\right) \cdot \frac{n_{\mathrm{c}}}{n_{\mathrm{s}}}. \qquad \text{Eq. 8}$$

To keep the internal battery temperature within the prescribed range, an auxiliary resistive heating system with heating power, P_{h}, is activated, if the battery temperature drops below a the temperature limit, T_{min}. The battery pack is thermally insulated to minimize the energy necessary for auxiliary heating. A linear dependence between the battery temperature, T, the ambient temperature, T_{amb}, the thermal transmittance, U_{T}, and the outer surface area, A, of the battery pack is assumed. The ambient temperature is assumed to be constant as it is very small compared to the internal temperature of the battery and also has very small variation during operation. The heat losses via the insulation can be given by

$$\dot{Q}_{\mathrm{loss}}(T(t)) = (T(t) - T_{\mathrm{amb}}) \cdot U_{\mathrm{T}} \cdot A, \text{where} \qquad \text{Eq. 9}$$

$$U_{\mathrm{T}} = \frac{1}{\frac{d}{k} + \frac{1}{h}}. \qquad \text{Eq. 10}$$

The thermal transmittance of the battery pack is caused by conduction (where *d* is the insulation thickness and k the thermal conductivity) as well as convection (where h is the connective heat transfer coefficient).

A cooling fan with electrical input power, P_{fan}, is activated, if the upper temperature limit, T_{max}, is exceeded. Airflow across cooling fins is induced, which increases heat removal, $\dot{Q}_{\mathrm{cool}}$, from the system. A linear relation between fan power and heat removal is assumed

$$\dot{Q}_{\mathrm{cool}}(T(t)) = f \cdot \frac{P_{\mathrm{fan}}(t)}{P_{\mathrm{fan,max}}} \cdot (T(t) - T_{\mathrm{amb}}), \qquad \text{Eq. 11}$$

where the proportionality constant, f, has units of W/K.

Due to the typically long time constants of the battery system, the nonlinear terms in Eq. 4 and Eq. 6 can be approximated as constants during small time intervals ($\Delta\tau \leq 300$ s). The ensuing linear system can be solved analytically. For the transient electro-chemical energy balance the solution is given by

$$E_{\mathrm{el}}(t_0 + \Delta\tau) = E_{\mathrm{el}}(t_0) \cdot e^{c_2 \cdot \Delta\tau} + \frac{c_1}{c_2} \cdot \left(e^{c_2 \cdot \Delta\tau} - 1\right), \text{where} \qquad \text{Eq. 12}$$

$$c_1 = P_{\mathrm{DC}}(t_0) - P_{\mathrm{h}}(t_0) - P_{\mathrm{fan}}(t_0) - {I_{\mathrm{DC}}}^2 \cdot R_{\mathrm{c,max}} \cdot \frac{n_{\mathrm{c}}}{n_{\mathrm{s}}} \text{ and} \qquad \text{Eq. 13}$$

$$c_2 = {I_{\mathrm{DC}}}^2 \cdot \left(R_{\mathrm{c,max}} - R_{\mathrm{c,min}}\right) \cdot \frac{n_{\mathrm{c}}}{E_{\mathrm{el,max}} \cdot n_{\mathrm{s}}}. \qquad \text{Eq. 14}$$

In contrast for the case of $u_{\mathrm{DC}} = 0$, the solution reads

$$E_{\mathrm{el}}(t_0 + \Delta\tau) = E_{\mathrm{el}}(t_0) - \left(P_{\mathrm{h}}(t_0) + P_{\mathrm{fan}}(t_0)\right) \cdot \Delta\tau. \qquad \text{Eq. 15}$$

Similarly, the solution of the thermal energy balance is given by

$$T(t_0 + \Delta\tau) = T(t_0) \cdot e^{-c_4 \cdot \Delta\tau} + \frac{c_3}{c_4} \cdot \left(1 - e^{-c_4 \cdot \Delta\tau}\right), \text{where} \quad \text{Eq. 16}$$

$$c_3 = P_{\mathrm{Ri}}\left(E_{\mathrm{el}}(t_0)\right) + P_{\mathrm{h}}(t_0) + \left(U_{\mathrm{T}} \cdot A + f \cdot P_{\mathrm{fan}}(t_0)\right) \cdot \frac{T_{\mathrm{amb}}}{m \cdot c_{\mathrm{p}}} \text{ and} \quad \text{Eq. 17}$$

$$c_4 = \left(U_{\mathrm{T}} \cdot A + f \cdot P_{\mathrm{fan}}(t_0)\right) \cdot \frac{1}{m \cdot c_{\mathrm{p}}}. \quad \text{Eq. 18}$$

2.1.2 Parameter Identification

Model parameter identification of an experimental ZEBRA battery system for stationary applications has been presented in Ref. [47]. System identification was carried out based on logged charge/discharge data provided by the battery's BMS. These data include the SOC and the temperature of the battery. The voltage and current of each single battery cell is SOC dependent during charging and discharging. As this is managed internally by the BMS, the applied voltages and currents are modeled as independent of the current energy content, E_{el}, as already stated in Eq. 12. The corresponding battery system specifications are listed in Table 1; the identified model parameters are listed in Table 2.

Table 1: Battery system specifications.

Terminal voltage, U_{DC}	372 V
Charging/Discharging current, $I_{\mathrm{DC,nom}}$	4 A
Heating power charging, P_{h}	<6.5 A at 240 V(AC)
Heating power discharging, P_{h}	300 W
Maximum cooling fan power $P_{\mathrm{fan,max}}$	62 W
Ambient temperature, T_{amb}	20 °C
Serial battery cells, n_{c}	142
(two were damaged on the real system)	
Parallel strings of battery cells, n_{s}	2

Table 2: Identified battery system parameters.

Maximum energy content, $E_{\mathrm{el,max}}$	28.2 kWh
Minimum energy content, $E_{\mathrm{el,min}}$	5.64 kWh
Maximum resistance, $R_{\mathrm{c,max}}$	30^{-3} Ω
Minimum resistance, $R_{\mathrm{c,min}}$	10^{-3} Ω
Stage 1 temperature limit, T_1	280 °C
Stage 2 temperature limit, T_2	245 °C
Stage 3 temperature limit, T_3	260 °C
Stage 4 temperature limit, T_4	$(100 \cdot \frac{E_{\mathrm{el}}(t)}{E_{\mathrm{el,max}}} + 190)$ °C
Stage 5 temperature limit, T_5	270 °C
Overall heat transfer coefficient, $U_{\mathrm{T}} \cdot A$	0.15 W/K
Battery mass, m	243 kg
Specific heat capacity, c_{p}	270 J/(kg·K)
Heating power charging, $P_{\mathrm{h,1}}$	200 W
Heating power discharging, $P_{\mathrm{h,2}}$	300 W
Stage 1 cooling fan power, $P_{\mathrm{fan,1}}$	0.95 W
Stage 2 cooling fan power, $P_{\mathrm{fan,2}}$	1.77 W
Stage 3 cooling fan power, $P_{\mathrm{fan,3}}$	62 W
Heat removal constant, f_{max}	9.50 W/K
Ambient temperature, T_{amb}	20 °C

A hysteresis based control keeps the battery temperature within a defined band. To describe the observed dependencies of heating and fan power, a Boolean hysteresis variable, u_{hys}, is introduced as follows,

$$u_{\mathrm{hys}} = \begin{cases} 1, & \left(T(\mathrm{t}) < T_{\mathrm{max}} + T_{\mathrm{hys}}\right) \vee \left(u_{\mathrm{hys}} > 0 \wedge T(\mathrm{t}) \leq T_{\mathrm{min}} + T_{\mathrm{hys}}\right) \\ 0, & \text{else.} \end{cases} \quad \text{Eq. 19}$$

For the heating power, the following behavior was observed,

$$P_{\mathrm{h}}(t) = \begin{cases} P_{\mathrm{h,1}}, & u_{\mathrm{DC}}(t) > 0 \wedge u_{\mathrm{hys}} > 0, \\ P_{\mathrm{h,2}}, & u_{\mathrm{DC}}(t) \leq 0 \wedge u_{\mathrm{hys}} > 0. \end{cases} \quad \text{Eq. 20}$$

For the cooling fan power, the following behavior was observed,

$$P_{\mathrm{fan}}(t) = \begin{cases} P_{\mathrm{fan,1}}, & u_{\mathrm{DC}}(t) > 0 \wedge T(\mathrm{t}) < T_{\mathrm{max}} \wedge u_{\mathrm{hys}} > 0 \\ P_{\mathrm{fan,2}}, & u_{\mathrm{DC}}(t) > 0 \wedge T(\mathrm{t}) < T_{\mathrm{max}} \wedge u_{\mathrm{hys}} = 0 \\ P_{\mathrm{fan,3}}, & T(t) \geq T_{\mathrm{max}} \\ 0\ \mathrm{W}, & \text{else,} \end{cases} \quad \text{Eq.21}$$

where

$$f = \frac{P_{\mathrm{fan}}(t)}{P_{\mathrm{fan,max}}} \cdot f_{\mathrm{max}}. \quad \text{Eq. 22}$$

The maximum DC power is given by the terminal voltage times the nominal current:

$$P_{\mathrm{DC,max}} = U_{\mathrm{DC}} \cdot I_{\mathrm{DC,nom}} \quad \text{Eq. 23}$$

The upper temperature limit, T_{max}, and lower temperature limit, T_{min}, depend on the SOC. For charging, the limits are given by

$$T_{\mathrm{max}} = \begin{cases} T_3, & SOC \leq 70\% \\ T_4, & 70\% < SOC < 80\% \text{ and} \\ T_5, & SOC \geq 80\% \end{cases} \quad \text{Eq. 24}$$

$$T_{\mathrm{min}} = T_2 \quad \text{Eq. 25}$$

with a hysteresis of T_{hys} = ±3 °C.

The temperature limits during discharge are

$$T_{\mathrm{max}} = T_1 \text{ and} \quad \text{Eq. 26}$$

$$T_{\mathrm{min}} = T_2 \quad \text{Eq. 27}$$

with a hysteresis of T_{hys} = ±2.5 °C.

2.1.3 Scaling of the Battery Model

To investigate the impact of the capacity-to-power ratio on grid-balancing potential, the nonlinear battery model must be scaled. Scaling is carried out by changing the numbers of cells while keeping the cell properties the same. Hence, no assumptions regarding physical and chemical processes inside the cells are necessary.

Battery capacity is increased by connecting additional battery cell-strings in parallel. Thus, the terminal voltage remains unchanged. Further, we allow for higher charging and discharging current. This results in higher charging and discharging power. With the number of cell strings, $n_{\mathrm{s}} \in \mathbb{N}$, scaled battery capacity and mass are given by

$$E_{\mathrm{el,max}}^{(n_{\mathrm{s}})} = E_{\mathrm{el,max}} \cdot \frac{n_{\mathrm{s}}}{2} \text{ and} \quad \text{Eq. 28}$$

$$m^{(n_{\mathrm{s}})} = m \cdot \frac{n_{\mathrm{s}}}{2}. \quad \text{Eq. 29}$$

The reference battery has two strings. Assuming geometrical similarity and thermal losses proportional to the battery surface area, the rate of thermal losses and heating power are scaled according to

$$P_{\mathrm{h}}^{(n_{\mathrm{s}})} = \left(\frac{E_{\mathrm{el,max}}^{(n_{\mathrm{s}})}}{E_{\mathrm{el,max}}}\right)^{2/3} \cdot P_{\mathrm{h}}, \quad \text{Eq. 30}$$

$$\dot{Q}_{\mathrm{loss}}^{(n_{\mathrm{s}})} = \left(\frac{E_{\mathrm{el,max}}^{(n_{\mathrm{s}})}}{E_{\mathrm{el,max}}}\right)^{2/3} \cdot \dot{Q}_{\mathrm{loss}}. \quad \text{Eq. 31}$$

Varying the charging and discharging power due to a variation in current, $I_{\mathrm{DC}} \in \mathbb{R}^{+}$, or the number of cell strings, n_{s},

$$I_{\mathrm{DC}}^{(n_{\mathrm{s}})} = I_{\mathrm{DC}} \cdot \frac{n_{\mathrm{s}}}{2} \quad \text{Eq. 32}$$

$$P_{\mathrm{DC,max}}^{(n_{\mathrm{s}})} = U_{\mathrm{DC}} \cdot I_{\mathrm{DC}}^{(n_{\mathrm{s}})} \quad \text{Eq. 33}$$

leads to changes in the heat transfer rate due to cooling and the cooling power since the heat generation is increased by the internal resistance, which is increased by the current squared and decreased by adding cell strings. A proportional relation between them is assumed whereby they can be scaled according to

$$P_{\mathrm{Ri}}^{(n_{\mathrm{s}})}(E_{\mathrm{el}}(t)) = R_{\mathrm{i}}(E_{\mathrm{el}}(t)) \cdot {I_{\mathrm{DC}}^{(n_{\mathrm{s}})}}^{2} \quad \text{Eq. 34}$$

$$P_{\mathrm{fan}}^{(n_{\mathrm{s}})} = \left(\frac{I_{\mathrm{DC}}^{(n_{\mathrm{s}})}}{I_{\mathrm{DC,nom}}}\right)^{2} \cdot \frac{2}{n_{\mathrm{s}}} \cdot P_{\mathrm{fan}}, \quad \text{Eq. 35}$$

$$\dot{Q}_{\mathrm{cool}}^{(n_{\mathrm{s}})} = \left(\frac{I_{\mathrm{DC}}^{(n_{\mathrm{s}})}}{I_{\mathrm{DC,nom}}}\right)^{2} \cdot \frac{2}{n_{\mathrm{s}}} \cdot \dot{Q}_{\mathrm{cool}}. \quad \text{Eq. 36}$$

2.1.4 Linear Battery Model

Batteries have strong dynamics during switching [53]. In this study, the long-term behavior of battery systems is crucial, whereas fast dynamics are less important. Therefore, a simplified linear model that does not account for battery temperature is introduced. All losses, including thermal losses, are summarized as P_{loss}. The linear model is given by

$$\frac{\mathrm{d}E_{\mathrm{el}}}{\mathrm{d}t} = P_{\mathrm{DC}}(t) - P_{\mathrm{loss}}. \quad \text{Eq. 37}$$

The losses, P_{loss}, for different battery capacities and applied charging and discharging power are determined by parameter identification using MATLAB's built-in *fminsearch* routine [54]. Losses are estimated by performing 100 charge and discharge cycles by simulation of the full battery model at $P_{\mathrm{DC,max}}$ between the upper and lower SOC bound. For the battery system used the losses per battery capacity are found to be P_{loss} = 2.17 W/kWh.

2.2 Simulation

A range of optimization approaches are used to determine the decision variables. The resulting decision states are used as input for the nonlinear battery model. A time interval, $\Delta\tau$, of 60 seconds is used in the analytical solution of the nonlinear battery model shown in Eq. 12, Eq. 15 and Eq. 16.

Historical day-ahead prices for electricity, provided by the Energy Exchange Austria (EXAA), are used as PCF [48]. Price data is assumed to be known 36 hours in advance. The optimization is carried out daily at noon. Prices are available on an hourly and quarter-hourly basis [55]. Historical EXAA data on an hourly basis are available going back to 2003. Quarter-hourly products in day-ahead stock market have been available since 3 September 2014.

2.3 Optimization

The linear and the nonlinear model of the battery system lead to different formulations of the optimization problem, Eq. 1. As illustrated in Fig. 1 the battery storage system is fed by DC power. The DC power input or output can be mapped to a decision variable, u_{DC}.

$$-1 \leq u_{\mathrm{DC}} \leq 1, \quad \text{Eq. 38}$$

$$P_{\mathrm{DC}} = u_{\mathrm{DC}} \cdot P_{\mathrm{DC,max}} \quad \text{Eq. 39}$$

When considering the AC power side, converter losses have to be taken into account. Hence:

$$-\eta_{out} \leq u_{\mathrm{AC}} \leq {\eta_{in}}^{-1}, \quad \text{Eq. 40}$$

$$P_{\mathrm{AC}} = \begin{cases} P_{\mathrm{DC}} \cdot {\eta_{\mathrm{in}}}^{-1} & P_{\mathrm{DC}} > 0 \\ P_{\mathrm{DC}} \cdot \eta_{\mathrm{out}} & P_{\mathrm{DC}} \leq 0 \end{cases} \quad \text{Eq. 41}$$

2.3.1 Sequential Quadratic Programming (SQP)

In each iteration step, SQP approximates the nonlinear problem by a quadratic program. The constraint functions are replaced by linear approximations [56]. MATLAB's built-in *fmincon* routine [57] with its SQP algorithm is used to solve the minimization problem. The objective function is expressed by the decision variables, $\boldsymbol{u}_{\mathrm{AC}}$, the PCF, $\boldsymbol{c}$, and the maximum power, $P_{\mathrm{DC,max}}$, for a given time step, Δt, as follows,

$$\min_{\boldsymbol{u}_{\mathrm{AC}}} \sum_{i=1}^{n} c_i \cdot u_{\mathrm{AC},i} \cdot P_{\mathrm{DC,max}} \cdot \Delta t \text{, s. t.} \quad \text{Eq. 42}$$

the upper g_{u} and lower g_{l} bounds given by E_{el} are fulfilled by the decision variables, $\boldsymbol{u}_{\mathrm{DC}}$, i.e.

$$g_{\mathrm{u},i}(\boldsymbol{u}_{\mathrm{DC}}) = E_{\mathrm{el},i}(\boldsymbol{u}_{\mathrm{DC}}) - E_{\mathrm{el,max}} \leq 0 \text{ and} \quad \text{Eq. 43}$$

$$g_{\mathrm{l},i}(\boldsymbol{u}_{\mathrm{DC}}) = E_{\mathrm{el,min}} - E_{\mathrm{el},i}(\boldsymbol{u}_{\mathrm{DC}}) \leq 0 \quad \text{Eq. 44}$$

$$\text{for } 1 \leq i \leq n. \quad \text{Eq. 45}$$

Here, $E_{\mathrm{el},i}(\boldsymbol{u}_{\mathrm{DC}})$ signifies the energy content at time step i given the decision variables $\boldsymbol{u}_{\mathrm{DC}} = (u_{\mathrm{DC},1}, \ldots, u_{\mathrm{DC},n})$. The decision variables, $\boldsymbol{u}_{\mathrm{AC}}$ and $\boldsymbol{u}_{\mathrm{DC}}$, are constrained according to Eq. 40 and Eq. 38.

To reduce the computational time, the gradient of the objective function with respect to the decision variable is additionally provided to the optimization routine. For the objective function, the j^{th} component of the gradient is given by

$$\frac{\partial}{\partial \boldsymbol{u}_{\mathrm{AC},j}} \left(\sum_{i=1}^{n} c_i \cdot u_{\mathrm{AC},i} \cdot P_{\mathrm{DC,max}} \cdot \Delta t \right) = c_j \cdot P_{\mathrm{DC,max}} \cdot \Delta t. \quad \text{Eq. 46}$$

The initial decision variables for the SQP routine are calculated by the integer linear programming routine described in 2.3.3.

2.3.2 Dynamic Programming (DP)

Results in Ref. [47] show that the cost-optimal operation of the battery is achieved by continuously charging or discharging at maximum power. The values of the decision variable on the DC side can therefore be restricted to −1, 0, and 1, as required by discrete dynamic programming. Furthermore, dynamic programming requires that the optimal solution of the problem can be composed by the solutions of many similar sub-problems. Similarity in sub-problems is achieved using the linearized battery model (Eq. 37) [58]. A recursive routine, which solves the optimization problem for discretized E_{el} values backward in time, is

implemented. Depending on the PCF, the costs for each decision state, starting at all discretized E_{el} end values, are calculated to the E_{el} start values cf. Fig. 2. Subsequently, the cheapest path for each discretized E_{el} start state can be selected by calculating forward in time.

The smallest discretization step is defined by the smallest possible change per time interval, Δt, which in the current problem is given by P_{loss}. This allows for three possible paths leading to state transitions backwards in time reflecting charging, discharging, and idling, which change the state by steps of $-(\lfloor P_{\mathrm{DC,max}}/P_{\mathrm{loss}} \rfloor - 1)$, $\lceil P_{\mathrm{DC,max}}/P_{\mathrm{loss}} \rceil + 1$, and 1, respectively.

The total number of discrete states, s, is given by the usable battery capacity and the losses per optimized time interval, Δt:

$$s = \left\lfloor \frac{(E_{\mathrm{el,max}} - E_{\mathrm{el,min}})}{P_{\mathrm{loss}} \cdot \Delta t} \right\rfloor + 1 \qquad \text{Eq. 47}$$

Adding 1 ensures no null values for s are obtained. To compute the optimal path at a specific stage, the path leading to minimum total cost [58] is selected. The total costs, C, at each state i at step j is calculated according to

$$C_{i,j} = \min_{r \in \{i+\lfloor P_{\mathrm{DC,max}}/P_{\mathrm{loss}} \rfloor - 1, i-1, i-\lceil P_{\mathrm{DC,max}}/P_{\mathrm{loss}} \rceil - 1\}} \left(C(path_{r \to i}) + C_{r,j+1} \right), \text{where} \qquad \text{Eq. 48}$$

$$C(path_{r \to i}) = \begin{cases} \eta_{\mathrm{in}}^{-1} \cdot c_i, & \text{charging,} \\ 0, & \text{idling,} \\ -\eta_{\mathrm{out}} \cdot c_i, & \text{discharging.} \end{cases} \qquad \text{Eq. 49}$$

The basic idea is illustrated in Fig. 2. Backwards in time charging is represented by a negative cell shift of two, discharging by a positive cell shift of three and the idle state by a positive cell shift of one. Using the PCF, the optimal path for each time interval can be found. The optimal solution is given subsequently by the optimal solution of all sub-problems.

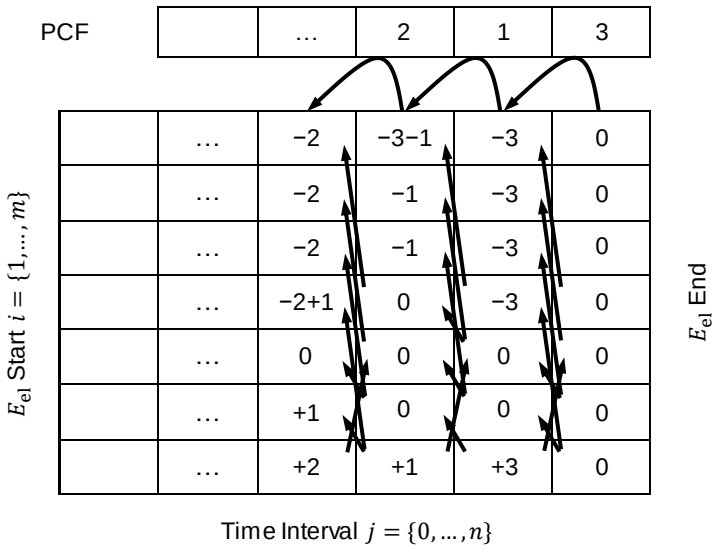

Fig. 2: Dynamic programming approach. The values inside the squares give the minimal pseudo-costs aggregated along the sub-path.

The DP optimization routine is constrained by an upper and lower bound for the E_{el} at each time interval, $E_{\mathrm{el,min}} \leq E_{\mathrm{el},i} \leq E_{\mathrm{el,max}}$. If the end state reached by a path violates the constraint, it is excluded from further analysis.

2.3.3 Integer Linear Programming (ILP)

The optimization problem Eq. 1 can be formulated as an integer linear programming (ILP) problem using the linear battery model and assuming only discrete switching (1, −1, and 0). The optimization approach is formulated introducing two decision variables, $u_{\mathrm{DC},i}^{+}$ and $u_{\mathrm{DC},i}^{-}$, for each time step indicating charging and discharging separately. Thus, converter efficiencies can be included linearly in the objective function and constraints can be formulated independently of converter efficiencies. $E_{\mathrm{el},0}$ represents the initial E_{el}.

$$\min_{u_{\mathrm{DC}}} \sum_{i=1}^{n} c_i(t) \cdot \left(u_{\mathrm{DC},i}^{+} \cdot \eta_{\mathrm{in}}^{-1} \cdot P_{\mathrm{DC,max}} - u_{\mathrm{DC},i}^{-} \cdot \eta_{\mathrm{out}} \cdot P_{\mathrm{DC,max}}\right) \cdot \Delta t, \text{s. t.} \quad \text{Eq. 50}$$

$$E_{\mathrm{el,min}} \leq E_{\mathrm{el},0} + \sum_{i=1}^{j} \left[u_{\mathrm{DC},i}^{+} \cdot P_{\mathrm{DC,max}} - u_{\mathrm{DC},i}^{-} \cdot P_{\mathrm{DC,max}} - P_{\mathrm{loss}}\right] \cdot \Delta t \leq E_{\mathrm{el,max}}, \forall j \in \{1, \cdots, n\}, \quad \text{Eq. 51}$$

$$u_{\mathrm{DC},i}^{+} + u_{\mathrm{DC},i}^{-} \leq 1, \quad \text{Eq. 52}$$

$$u_{\mathrm{DC},i}^{+}, u_{\mathrm{DC},i}^{-} \geq 0. \quad \text{Eq. 53}$$

The final decision variable can be calculated as $\boldsymbol{u}_{\mathrm{DC}} = \boldsymbol{u}_{\mathrm{DC}}^{+} - \boldsymbol{u}_{\mathrm{DC}}^{-}$. For simulation results, MATLAB's *intlinprog* routine [57] is used to solve the minimization problem.

3 Results

All results presented below are based on historic Austrian day-ahead stock market price data provided by EXAA [48]. The study consists of four parts: 1) The performance of the three optimization approaches is investigated with respect to runtime and optimality using historic price data from 2015. 2) Then, the best performing approach is used to determine the potential earnings using autonomous grid balancing in the period 2003–2015 based on hourly day-ahead stock market price data. 3) Differences in earnings and performance, using hour- and 15-min-based Austrian day-ahead stock market price data of 2015, are determined. 4) Finally, a battery capacity and charging/discharging power are scaled to find an optimal capacity-to-power ratio for hour- and 15-min-based stock market price data of 2015.

3.1 Optimizer Performance

Optimizers are compared with respect to runtime and optimality. Results achieved based on 2015 day-ahead data are shown in Table 3. The second column gives the relative runtime of the optimizers. Optimization was carried using out using MATLAB on a Lenovo T430u notebook equipped with an Intel Core i5-3317U and a main memory with 8 GB. The third column gives the annual earnings per battery capacity. Column four and five represent the standard deviation (SD) of the SOC in percent and the of the temperature in °C during optimal operation. The last two columns give the portion of idle states in percent and the round-trip efficiency of the battery storage system. For SQP optimization, a time interval, $\Delta\tau$, of 60 seconds is used in the analytical solution of the nonlinear battery model.

Table 3: Performance comparison of SQP, DP and ILP using hourly based EXAA price data of 2015.

Optimizer	Runtime relative to ILP (–)	Earnings/ Capacity (€/kWh)	SD SOC (%)	SD Temp (°C)	Portion of time in idle states (%)	Round-trip efficiency (%)
SQP	50.7	1.83	18.7	1.62	27.2	78.6
DP	1.29	1.74	18.5	1.61	27.5	77.5
ILP	1.00	1.75	18.7	1.60	27.2	77.4

The SQP routine leads to the highest earnings since a nonlinear battery model with high model accuracy is used in the optimization. The linear programming approach provides a good approximation and results in the lowest computing time and a small deviation to the SQP solved problem. The DP approach performs marginally worse than ILP, however, it allows for straightforward implementation on an embedded system since no library functions are needed. The deviation in results between the DB and ILP is due to the discretization of SOC states necessary for DP.

3.2 Potential for Autonomous Grid Balancing

Earnings based on ILP for the years from 2003 to 2015 are shown in Fig. 3 based on hourly day-ahead stock market price data. It shows the annual earnings per battery capacity as a function of the mean standard deviation within the 24 hours optimization period for the respective year.

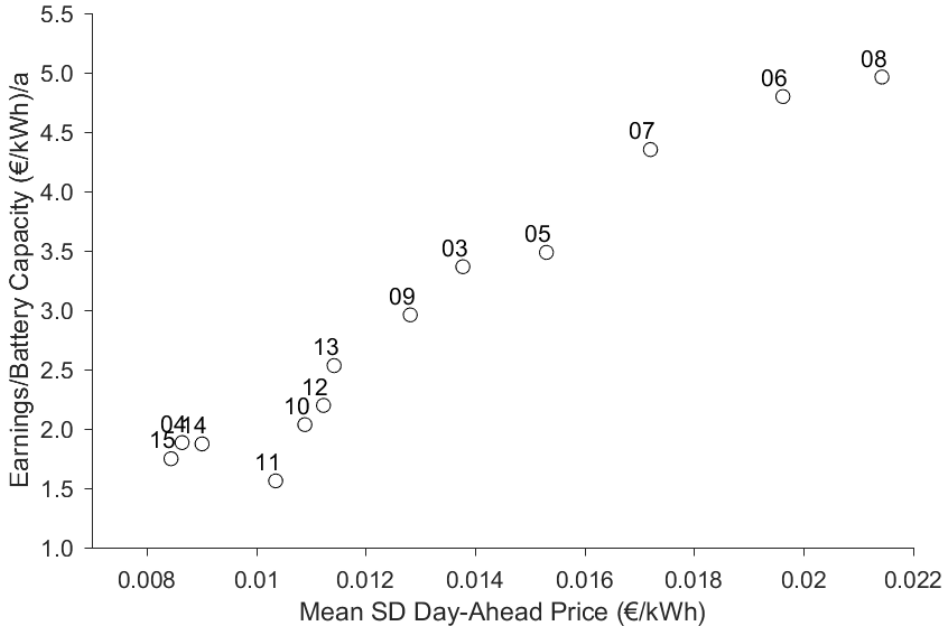

Fig. 3: Annual earnings per kWh from 2003 to 2015 as a function of mean standard deviation of the day-ahead prices.

3.3 Optimization based for Varying Day-Ahead Market Time Resolution

The results from section 3.2 suggest that higher earnings can be achieved by stronger market price fluctuations. Thus, the available hour and 15-min-based day-ahead price products are compared with each other. The integer linear programming algorithm is used to perform the analysis.

In Fig. 4, an optimization for both time products is done for 36 hours starting at 12:00 January 1 until 24:00 January 2 in 2015. Fig. 4(a) shows both time products and the corresponding decision variables. Fig. 4(b) shows the evolution of the SOC. Earnings of about 0.017 €/kWh of battery capacity can be gained for quarter-hourly day-ahead prices compared to only 0.0018 €/kWh of battery capacity for hourly PCFs. This is attributed to higher fluctuations in PCF. Also for 15-min-based time products the overall efficiency is 75% compared to 73% for hourly-based products. Finally, a lower total battery capacity is utilized for 15-min-based price products.

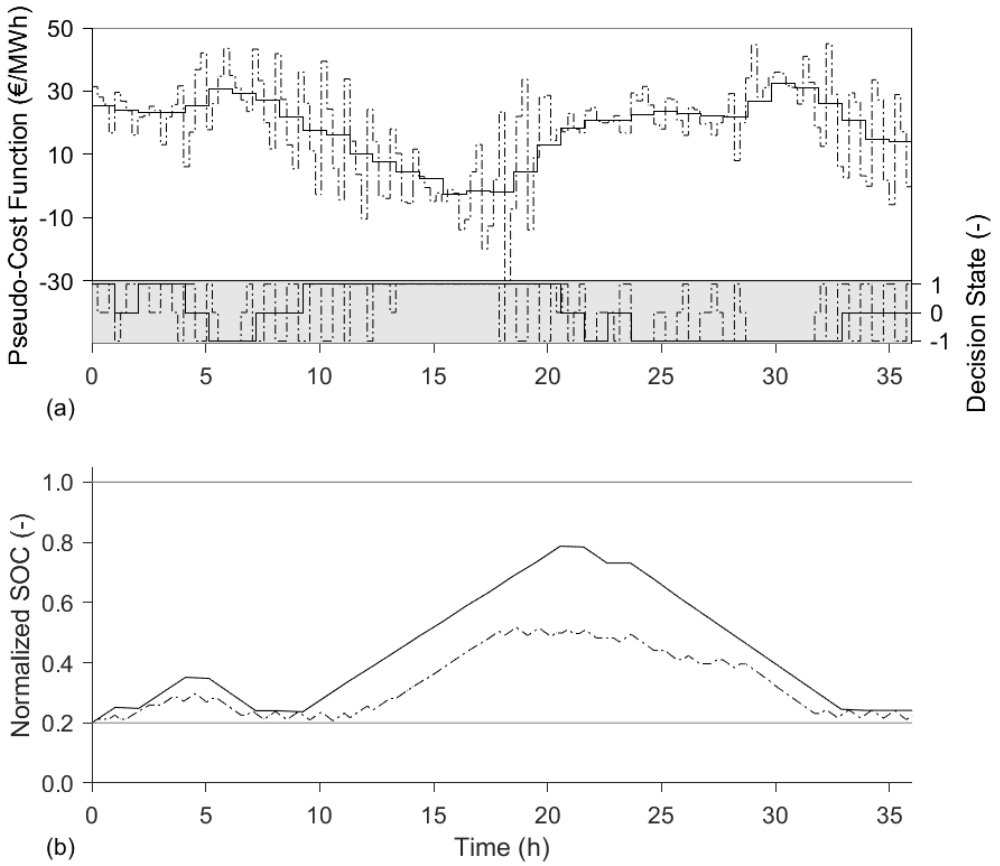

Fig. 4: Comparison between hour- and 15-min-based PCF for a period of 36 hours. Hourly-based results are represented by solid lines; 15-min-based results are represented by dashed lines. Results show higher fluctuations in PCF for 15-min-based PCF, which results in higher earnings and a better efficiency. In addition, a lower total battery capacity is necessary.

A one-year simulation of 2015 confirms the results of the first short-term simulation. It shows that substantially higher earnings can be achieved when price products exhibit more fluctuations. Additionally, fewer idle states indicate better battery system utilization. Detailed results are listed in Table 4. Results shown are evaluated according to Table 3.

Table 4: Performance comparison of ILP using hourly and quarter-hourly EXAA price data of 2015.

Time product	Runtime relative to hourly based prices (–)	Earnings/ Capacity (€/kWh)	SD SOC (%)	SD Temp (°C)	Portion of time in idle states (%)	Round-trip efficiency (%)
Hour	1.00	1.75	18.7	1.60	27.2	77.4
15 min	3.86	2.86	16.3	1.61	17.7	78.3

3.4 Variation of the Capacity-to-Power Ratio

Earnings with respect to scaling are investigated. Battery operation is simulated using hour- and 15-min-based day-ahead prices of 2015 for different battery capacities resulting from $n_s \in \{1, 2, 4, 8\}$ numbers of cell strings. Power scaling is done differently for both price products since shorter time products allow for the utilization of smaller capacity systems at a given charging/discharging power. Typically, capacities have to be 2–3 times the maximum charging/discharging power per interval (15 min or 1 h).

For hourly-based products the current is $I_{\mathrm{DC}} \in \{1, 1.5, 2, 2.5, 3, 4, 5, 6, 7\} \cdot I_{\mathrm{DC,nom}}$; for 15-min-based it is $I_{\mathrm{DC}} \in \{1, 1.5, 2, 2.5, 3, 4, 5, 6, 8, 10, 12, 14, 18\} \cdot I_{\mathrm{DC,nom}}$. Losses for the linear battery model are estimated due to the parameter identification described in section 2.1.4. Estimated losses per capacity for hourly-based products are presented in Fig. 5; for 15-min-based products in Fig. 6. Additionally, these figures show the earnings/capacity to capacity/power ratio achieved. In both cases, the earnings-to-capacity curve exhibits a maximum since at low capacity-to-power ratio the system does not have sufficient capacity to operate over the relevant timescales while at high capacities the full capacity of the system is never exploited. The optimal capacity/power ratio for maximum earnings is lower for quarter-hourly day-ahead prices. Generally, large storage systems are preferable since relative thermal losses decrease as the surface to volume ratio goes down. A sudden drop in capacity-to-power ratio is explained by the fact that the system loses the freedom to realize all optimal decision states.

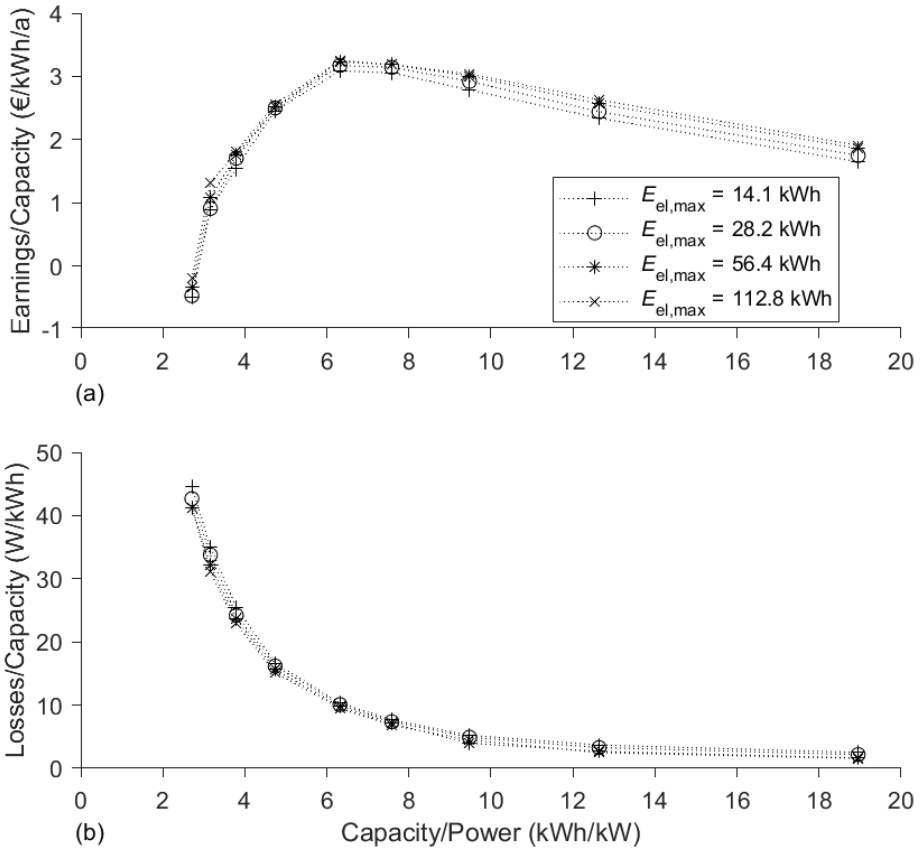

Fig. 5: Optimization based on variation of the battery capacity-to-power ratio for hourly-based time products. The upper graph a) illustrates the earnings/capacity to capacity/power ratio. The estimated losses-to-capacity for the ILP are shown in the lower graph b).

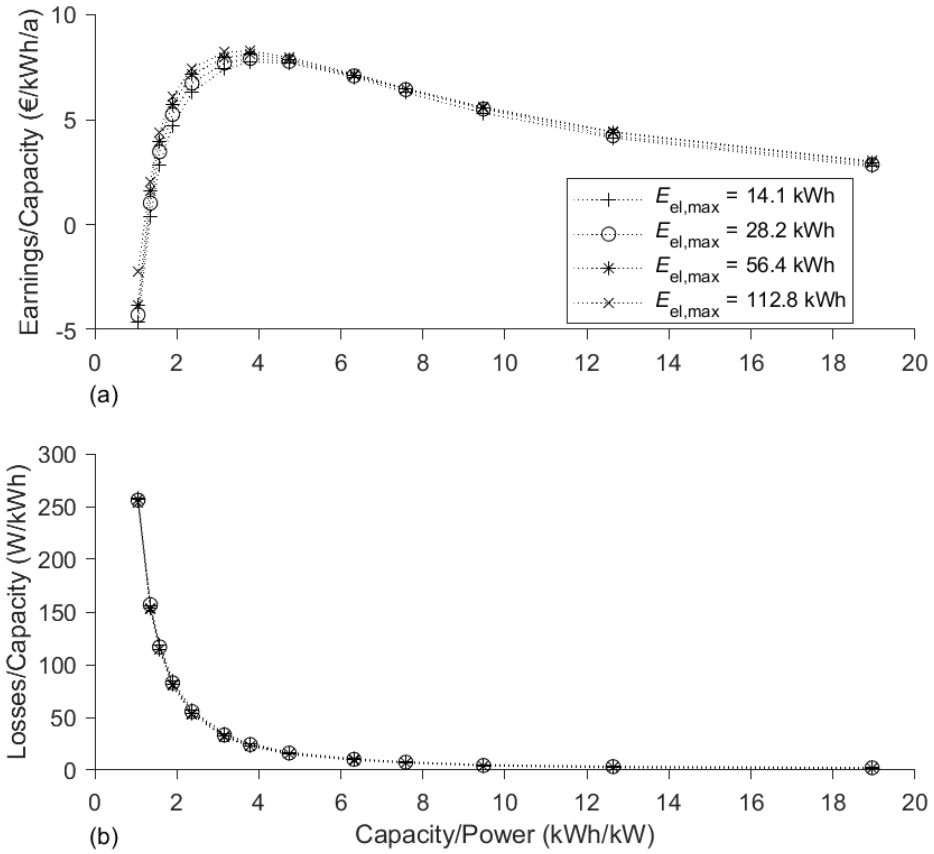

Fig. 6: Optimization based on variation of the battery capacity-to-power ratio for 15-min-based time products. The upper graph a) illustrates the earnings/capacity to capacity/power ratio. The estimated losses-to-capacity for the ILP are shown in the lower graph b).

4 Conclusion

In this paper, a modeled decentralized and on-site optimized high-temperature ZEBRA battery storage system was used for grid balancing. Optimal operation of this system is attained by minimizing an objective function calculated from a one-way communicated pseudo-cost function. Austrian day-ahead stock market prices for electricity were used as the pseudo-cost function.

Efficient and robust control and optimization algorithms are key to the implementation and operation based on embedded hardware. Hence, three optimization approaches are compared with respect to runtime and optimality: sequential quadratic programming (SQP), dynamic programming (DP), and integer linear programming (ILP). While SQP slightly outperforms ILP and DP based on the control objective, it does so at significantly higher computational costs, i.e. approximately 50 times the runtime of ILP. ILP results in the shortest runtime closely followed by DP. The slightly more optimal results from SQP do not justify the substantially increased model complexity and excessive computational costs. Therefore, in the current work ILP is used for long-term simulations.

Simulations reveal a strong correlation between pseudo-cost based earnings and the variation of the pseudo-costs during the same period. Simulations show that 15-min-based stock market

prices promise higher earnings than hourly-based prices. Higher price fluctuations lead to more dynamic battery operation, which results in higher earnings, efficiencies, and shorter idle times, which in turn indicate a better utilization of the storage system.

All simulations showed that at current day-ahead stock market prices and storage system costs profitable operation of the given battery system based on day-ahead prices is not possible since variations in price are currently too low. This indicates that short-term, highly fluctuating markets such as the primary frequency control market are better suited for battery systems.

Earnings per kWh of capacity as a function of the capacity-to-power ratio always exhibits one distinct maximum: At very low capacity-to-power ratios, the storage system is too small for efficient operation as it continuously threatens to violate boundary conditions, while at very high capacity-to-power ratios, the storage capacity is not fully used. For hourly day-ahead prices, the optimal capacity-to-power ratio was found with approximately 6 hours while for quarter-hourly day-ahead prices it is about 3 hours.

Acknowledgements

The financial support by the Austrian Federal Ministry of Science, Research and Economy and the National Foundation for Research, Technology and Development is gratefully acknowledged.

References

[1] R. Haas, G. Resch, C. Panzer, S. Busch, M. Ragwitz, and A. Held, “Efficiency and effectiveness of promotion systems for electricity generation from renewable energy sources – Lessons from EU countries,” *Energy*, vol. 36, no. 4, pp. 2186–2193, Apr. 2011.

[2] M. Kaltschmitt *et al.*, “VDI-Statusreport Regenerative Energien in Deutschland 2015,” 2015.

[3] M. Beaudin, H. Zareipour, A. Schellenberglabe, and W. Rosehart, “Energy storage for mitigating the variability of renewable electricity sources: An updated review,” *Energy Sustain. Dev.*, vol. 14, no. 4, pp. 302–314, Dec. 2010.

[4] A. Pina, C. Silva, and P. Ferrão, “The impact of demand side management strategies in the penetration of renewable electricity,” *Energy*, vol. 41, no. 1, pp. 128–137, May 2012.

[5] R. Madlener and J. M. Specht, “An Exploratory Economic Analysis of Underground Pumped-Storage Hydro Power Plants in Abandoned Coal Mines,” *FCN Work. Pap.*, vol. 2, p. 34, Feb. 2013.

[6] P. Palensky and D. Dietrich, “Demand Side Management: Demand Response, Intelligent Energy Systems, and Smart Loads,” *IEEE Trans. Ind. Inform.*, vol. 7, no. 3, pp. 381–388, Aug. 2011.

[7] G. Strbac, “Demand side management: Benefits and challenges,” *Energy Policy*, vol. 36, no. 12, pp. 4419–4426, Dec. 2008.

[8] P. Siano, “Demand response and smart grids—A survey,” *Renew. Sustain. Energy Rev.*, vol. 30, pp. 461–478, Feb. 2014.

[9] C. W. Gellings, “The concept of demand-side management for electric utilities,” *Proc. IEEE*, vol. 73, no. 10, pp. 1468–1470, 1985.

[10] L. Gelazanskas and K. A. A. Gamage, “Demand side management in smart grid: A review and proposals for future direction,” *Sustain. Cities Soc.*, vol. 11, pp. 22–30, Feb. 2014.

[11] J. Han and M. A. Piette, “Solutions for Summer Electric Power Shortages: Demand Response andits Applications in Air Conditioning and Refrigerating Systems,” *Refrig. Air Cond. Electr. Power Mach.*, vol. 29, no. 1, pp. 1–4, Jan. 2008.

[12] G. Deconinck, “An evaluation of two-way communication means for advanced metering in Flanders (Belgium),” 2008, pp. 900–905.

[13] T. Markel, M. Kuss, and P. Denholm, “Communication and control of electric drive vehicles supporting renewables,” 2009, pp. 27–34.

[14] T. Stetz, F. Marten, and M. Braun, “Improved Low Voltage Grid-Integration of Photovoltaic Systems in Germany,” *IEEE Trans. Sustain. Energy*, vol. 4, no. 2, pp. 534–542, Apr. 2013.

[15] X. Liu, A. Aichhorn, L. Liu, and H. Li, “Coordinated Control of Distributed Energy Storage System With Tap Changer Transformers for Voltage Rise Mitigation Under High Photovoltaic Penetration,” *IEEE Trans. Smart Grid*, vol. 3, no. 2, pp. 897–906, Jun. 2012.

[16] J. von Appen, M. Braun, T. Stetz, K. Diwold, and D. Geibel, “Time in the Sun: The Challenge of High PV Penetration in the German Electric Grid,” *IEEE Power Energy Mag.*, vol. 11, no. 2, pp. 55–64, Mar. 2013.

[17] A. A. Bayod-Rújula, “Future development of the electricity systems with distributed generation,” *Energy*, vol. 34, no. 3, pp. 377–383, Mar. 2009.

[18] P. M. S. Carvalho, P. F. Correia, and L. A. F. Ferreira, “Distributed Reactive Power Generation Control for Voltage Rise Mitigation in Distribution Networks,” *IEEE Trans. Power Syst.*, vol. 23, no. 2, pp. 766–772, May 2008.

[19] J. von Appen, T. Stetz, M. Braun, and A. Schmiegel, “Local Voltage Control Strategies for PV Storage Systems in Distribution Grids,” *IEEE Trans. Smart Grid*, vol. 5, no. 2, pp. 1002–1009, Mar. 2014.

[20] A. R. Landgrebe and S. W. Donley, “Battery storage in residential applications of energy from photovoltaic sources,” *Appl. Energy*, vol. 15, no. 2, pp. 127–137, Jan. 1983.

[21] A. Khaligh and Zhihao Li, “Battery, Ultracapacitor, Fuel Cell, and Hybrid Energy Storage Systems for Electric, Hybrid Electric, Fuel Cell, and Plug-In Hybrid Electric Vehicles: State of the Art,” *IEEE Trans. Veh. Technol.*, vol. 59, no. 6, pp. 2806–2814, Jul. 2010.

[22] B. Peng and J. Chen, “Functional materials with high-efficiency energy storage and conversion for batteries and fuel cells,” *Coord. Chem. Rev.*, vol. 253, no. 23–24, pp. 2805–2813, Dec. 2009.

[23] R. Dufo-López and J. L. Bernal-Agustín, “Techno-economic analysis of grid-connected battery storage,” *Energy Convers. Manag.*, vol. 91, pp. 394–404, Feb. 2015.

[24] J. Leadbetter and L. Swan, “Battery storage system for residential electricity peak demand shaving,” Energy Build., vol. 55, pp. 685–692, Dec. 2012.

[25] C. Pang, P. Dutta, and M. Kezunovic, “BEVs/PHEVs as Dispersed Energy Storage for V2B Uses in the Smart Grid,” *IEEE Trans. Smart Grid*, vol. 3, no. 1, pp. 473–482, Mar. 2012.

[26] N. W. Miller, R. S. Zrebiec, R. W. Delmerico, and G. Hunt, “Battery energy s torage systems for electric utility, industrial and commercial applications,” 1996, pp. 235–240.

[27] P. J. Hall and E. J. Bain, “Energy-storage technologies and electricity generation,” *Energy Policy*, vol. 36, no. 12, pp. 4352–4355, Dec. 2008.

[28] H. Chen, T. N. Cong, W. Yang, C. Tan, Y. Li, and Y. Ding, “Progress in electrical energy storage system: A critical review,” *Prog. Nat. Sci.*, vol. 19, no. 3, pp. 291–312, Mar. 2009.

[29] K. C. Divya and J. Østergaard, “Battery energy storage technology for power systems—An overview,” *Electr. Power Syst. Res.*, vol. 79, no. 4, pp. 511–520, Apr. 2009.

[30] T. Borsche, A. Ulbig, M. Koller, and G. Andersson, “Power and energy capacity requirements of storages providing frequency control reserves,” presented at the Power and Energy Society General Meeting, Vancouver, 2013, pp. 1–5.

[31] T. Pesch and P. Stenzel, “Analysis of the market conditions for storage in the German day-ahead and secondary control market,” 2013, pp. 1–8.

[32] T. Ma, H. Yang, and L. Lu, “Feasibility study and economic analysis of pumped hydro storage and battery storage for a renewable energy powered island,” *Energy Convers. Manag.*, vol. 79, pp. 387–397, Mar. 2014.

[33] M. Castillo-Cagigal, A. Gutiérrez, F. Monasterio-Huelin, E. Caamaño-Martín, D. Masa, and J. Jiménez-Leube, “A semi-distributed electric demand-side management system with PV generation for self-consumption enhancement,” *Energy Convers. Manag.*, vol. 52, no. 7, pp. 2659–2666, Jul. 2011.

[34] O. M. Toledo, D. Oliveira Filho, and A. S. A. C. Diniz, “Distributed photovoltaic generation and energy storage systems: A review,” *Renew. Sustain. Energy Rev.*, vol. 14, no. 1, pp. 506–511, Jan. 2010.

[35] C. Guille and G. Gross, “A conceptual framework for the vehicle-to-grid (V2G) implementation,” *Energy Policy*, vol. 37, no. 11, pp. 4379–4390, Nov. 2009.

[36] K. Clement-Nyns, E. Haesen, and J. Driesen, “The impact of vehicle-to-grid on the distribution grid,” *Electr. Power Syst. Res.*, vol. 81, no. 1, pp. 185–192, Jan. 2011.

[37] W. Kempton and J. Tomić, “Vehicle-to-grid power implementation: From stabilizing the grid to supporting large-scale renewable energy,” *J. Power Sources*, vol. 144, no. 1, pp. 280–294, Jun. 2005.

[38] T. Sousa, H. Morais, J. Soares, and Z. Vale, “Day-ahead resource scheduling in smart grids considering Vehicle-to-Grid and network constraints,” *Appl. Energy*, vol. 96, pp. 183–193, Aug. 2012.

[39] L. Wang, S. Sharkh, and A. Chipperfield, “Optimal coordination of vehicle-to-grid batteries and renewable generators in a distribution system,” *Energy*, vol. 113, pp. 1250–1264, Oct. 2016.

[40] B. Tarroja, L. Zhang, V. Wifvat, B. Shaffer, and S. Samuelsen, “Assessing the stationary energy storage equivalency of vehicle-to-grid charging battery electric vehicles,” *Energy*, vol. 106, pp. 673–690, Jul. 2016.

[41] Daimler AG, “World’s largest 2nd-use battery storage is starting up,” *http://media.daimler.com*, Lünen/Stuttgart, 13-Sep-2016.

[42] S. Shokrzadeh and E. Bibeau, “Sustainable integration of intermittent renewable energy and electrified light-duty transportation through repurposing batteries of plug-in electric vehicles,” *Energy*, vol. 106, pp. 701–711, Jul. 2016.

[43] J. Neubauer and A. Pesaran, “The ability of battery second use strategies to impact plug-in electric vehicle prices and serve utility energy storage applications,” *J. Power Sources*, vol. 196, no. 23, pp. 10351–10358, Dec. 2011.

[44] C. Heymans, S. B. Walker, S. B. Young, and M. Fowler, “Economic analysis of second use electric vehicle batteries for residential energy storage and load-levelling,” *Energy Policy*, vol. 71, pp. 22–30, Aug. 2014.

[45] P. Samadi, H. Mohsenian-Rad, R. Schober, and V. W. S. Wong, “Advanced Demand Side Management for the Future Smart Grid Using Mechanism Design,” *IEEE Trans. Smart Grid*, vol. 3, no. 3, pp. 1170–1180, Sep. 2012.

[46] P. Kepplinger, G. Huber, and J. Petrasch, “Autonomous optimal control for demand side management with resistive domestic hot water heaters using linear optimization,” Energy Build., vol. 100, pp. 50–55, Aug. 2015.

[47] B. Fäßler, P. Kepplinger, M. L. Kolhe, and J. Petrasch, “Decentralized on-site optimization of a battery storage system using one-way communication,” presented at the International Conference on Renewable Power Generation, 2015, pp. 1–6.

[48] EXAA Abwicklungsstelle für Energieprodukte AG, “Historical Data - Spot Prices 2014.” EXAA Abwicklungsstelle für Energieprodukte AG, 13-Apr-2015.

[49] C.-H. Dustmann, “Advances in ZEBRA batteries,” *J. Power Sources*, vol. 127, no. 1–2, pp. 85–92, Mar. 2004.

[50] K. Kronsbein, “Investigation and Modelling of the ZEBRA System to Optimise State of Charge Detection,” Thesis, Universität Karlsruhe (TH), Stabio, 2004.

[51] J. Sudworth, “The sodium/nickel chloride (ZEBRA) battery,” *J. Power Sources*, vol. 100, no. 1–2, pp. 149–163, Nov. 2001.

[52] H. Böhm and G. Beyermann, “ZEBRA batteries, enhanced power by doping,” *J. Power Sources*, vol. 84, no. 2, pp. 270–274, Dec. 1999.

[53] A. Jossen, “Fundamentals of battery dynamics,” *J. Power Sources*, vol. 154, no. 2, pp. 530–538, Mar. 2006.

[54] MATLAB, *MATLAB Function*. Natick, Massachusetts: The MathWorks Inc., 2014.

[55] EPEX SPOT SE, “EPEX SPOT SE,” *EPEX SPOT SE*. [Online]. Available: www.epexspot.com. [Accessed: 18-Dec-2015].

[56] K. Schittkowski and C. Zillober, “Nonlinear Programming: Algorithms, Software, and Applications,” in *System Modeling and Optimization*, vol. 166, J. Cagnol and J.-P. Zolésio, Eds. Boston: Kluwer Academic Publishers, 2005, pp. 73–107.

[57] MATLAB, *MATLAB and Statistics Toolbox Release 2014a*. Natick, Massachusetts: The MathWorks Inc., 2014.

[58] S. P. Bradley, A. C. Hax, and T. L. Magnanti, “Dynamic Programming,” in *Applied mathematical programming*, Reading, Mass: Addison-Wesley Pub. Co, 1977, pp. 320–362.

Paper C: Field Testing of Repurposed Electric Vehicle Batteries for Price-Driven Grid Balancing

This chapter is based on the journal paper submitted to Elsevier Energy Journal:

B. Faessler, P. Kepplinger, and J. Petrasch, "Field testing of repurposed electric vehicle batteries for price-driven grid balancing," (Manuscript Number: EGY-D-17-05788)

The layout has been revised for better readability.

Abstract

As electric cars become more widespread, the disposal and recycling of used batteries will become an important challenge. Typically, vehicle batteries are replaced if their capacity drops to 70–80% of their initial capacity. However, they may still be useful for stationary applications.

In this paper, results from a field test of an electric vehicle battery repurposed as stationary storage for grid balancing are presented. A molten salt high-temperature battery is used for price-driven grid balancing. The operation is based on a mixed integer linear programming control strategy driven by the Austrian electricity spot-market price.

A 14-day experiment resulted in a round-trip energy efficiency (converter-battery-converter) of about 74.4%. The earnings per battery capacity achieved in this period amounted to 0.10 €/kWh. This indicates that at current market volatilities and price ranges the suggested mode of operation is not economically feasible. An error analysis of the model underlying the optimization showed a root mean square error of 7.6% in state of charge estimation.

The field test implementation shows a substantial deviation between theoretical and physical potential of grid-balancing measures due to model inaccuracies and technical characteristics, thereby demonstrating the urgent need for field tests of stationary battery systems.

Keywords: Grid Balancing, Repurposed Vehicle ZEBRA Battery, Distributed Storage, One-Way Communication, Autonomous Optimization

Nomenclature

c	Pseudo-cost function (€/MWh)	R^2	Coefficient of determination (–)
$E_{\mathrm{AC,in}}$	Energy imported (Wh)	t	Time (s)
$E_{\mathrm{AC,out}}$	Energy exported (Wh)	t_{d}	Day-time function (s)
E_{el}	Electrical energy content (J)	x_{c}	Decision variable: charging (–)
n	Total number of data points (–)	x_{d}	Decision variable: discharging (–)
n_{cycle}	Battery charge cycles (–)	u_{DC}	Decision variable on DC power side (–)
n_{d}	Total amount of seconds per day (s)	η_{bat}	Battery efficiency (–)
P_{AC}	Alternating power (W)	η_{in}	Charging converter efficiency (–)
P_{DC}	Direct power (W)	η_{out}	Discharging converter efficiency (–)
P_{loss}	Constant battery loss (W)	η_{rt}	Round-trip efficiency (–)
s_{earn}	Achieved earnings (€)		
SOC	State of charge (%)		

1 Introduction

The electrical energy market is currently facing new challenges. Boßmann et al. [1] stated that load curves will substantially change due to evolving electricity demand.

Since renewable electricity generation, which is volatile by nature, adversely affects grid operation [2], [3], additional grid-balancing measures such as specific strategies and energy storage facilities will become necessary [4]–[6] in the foreseeable future.

Aggregation of small, distributed loads and storage systems for demand side management (DSM), along with the deployment of control strategies with the specific aim of balancing the grid, is considered a promising approach [4], [7], [8]. More specifically, battery storage systems have been proposed for distributed approaches [9], as:

- their time scales will soon range from seconds to days [10]
- they are practically maintenance-free [11]
- they are quick to respond [12]
- they are highly efficient [13], [14], exhibiting total round-trip efficiencies (converter-battery-converter) ranging from 65% to almost 90% [15]

Several types of battery technologies, using a range of cell chemistries [5], [14], have been investigated for grid-tied balancing approaches [16]–[20].

In order to reduce costs, systems that already include battery storage but do not entirely utilize the available capacity at all times, have been proposed. In this context, electric vehicles (EV) [23]–[27], battery bank systems combined with photovoltaics [21] or wind farms [22] have been discussed. Another option to help offset costs is to use repurposed EV batteries [28], [29]. Generally, EV batteries are exchanged if their capacity falls to 70–80% of their initial capacity [28]; at this point, they still have sufficient capacity for stationary applications. Second use of batteries will also reduce their ecological footprint [30], [31]. The German vehicle manufacturer Daimler has announced [32] plans to reuse old EV batteries in a large stationary storage facility with a capacity of 13 MWh. Reusing EV batteries as distributed stationary storage for grid-balancing measures on the kWh-scale has been discussed in previous publications [30], [33], [34]. However, no physical implementation for grid balancing is known to the authors.

This work presents a stationary grid balancing field test based on a retrofitted EV battery. A ZEBRA (Zero Emission Battery Research Activities) battery, decommissioned from a THINK City [35] vehicle, is incorporated into a stationary setup. An in-house controller software autonomously optimizes the operation based on the Austrian day-ahead electricity market as suggested by the authors in a previous work [9]. The economic performance and the battery efficiencies are evaluated through an energy monitoring system. We evaluated the error in the battery model by comparing it with the physical behavior of the ZEBRA battery. Moreover, we identify the difference in earnings between the physical implementation and theoretical simulation results.

2 Experimental Setup

The field test setup for the stationary battery storage system is shown in Fig. 1a. It comprises an embedded control hardware (ECH), two AC/DC converters, a repurposed EV battery including a battery management system (BMS), and an energy monitoring system.

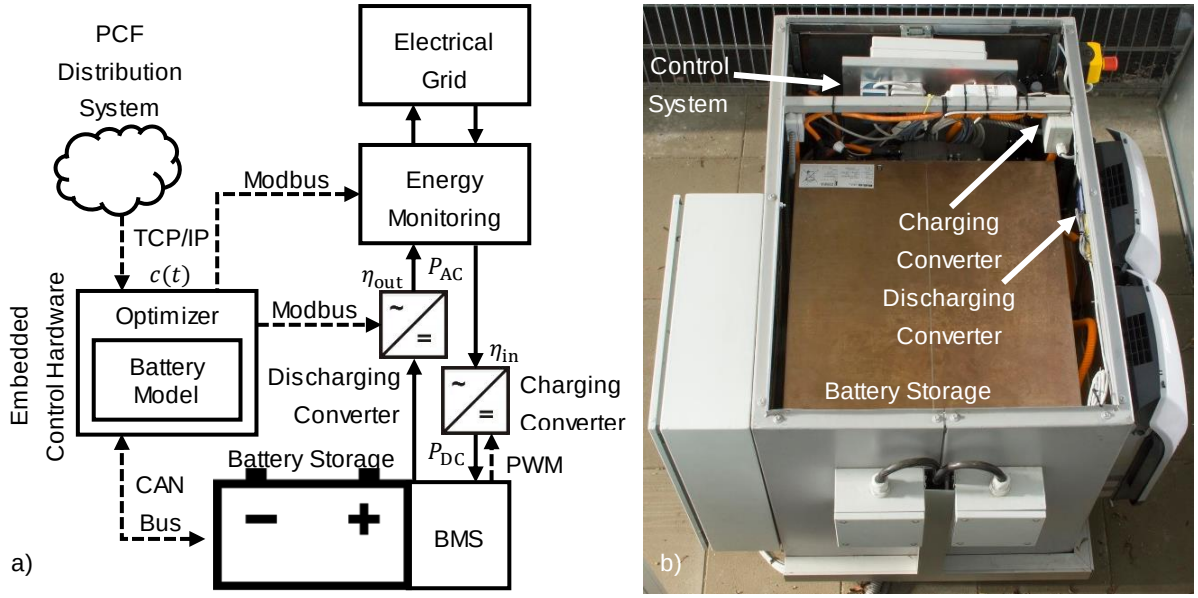

Fig. 1: Repurposed EV battery storage system including all hardware components: a) schematics; b) physical implementation.

For charging and discharging, separate converters are used. The converters have different conversion efficiencies, denoted by η_{in} and η_{out} for charging and discharging, respectively. The embedded control hardware is connected to a mobile-network-enabled router via TCP/IP, which establishes the connection to a pseudo-cost function (PCF) distribution system. The operation mode (charge, discharge, idle) is determined by optimization, minimizing an objective function calculated from the PCF, while keeping the battery's state of charge (SOC) within the given operational bounds. The communication between the ECH and the BMS is realized via CAN (Controller Area Network) bus [36]. It comprises the decision variable, cyclic alive messages, and the actual battery state.

Modbus TCP [37] is used to control the power of the discharging converter. The power through the charging converter is controlled by the BMS based on the battery state via a pulse-width modulation (PWM) signal. All energy flows through the converters are measured and recorded by an energy monitoring system. The physical battery storage setup is shown in Fig. 1b. The repurposed ZEBRA battery with its control system, converters and safety equipment is installed in a metal box.

2.1 ZEBRA Battery

The physical battery storage system is based on a repurposed ZEBRA vehicle battery. Cell chemistry relies on the reaction of sodium with nickel chloride [38]. The redox reaction [39] is:

$$2\text{Na} + \text{NiCl}_2 \underset{\text{charge}}{\overset{\text{discharge}}{\rightleftarrows}} 2\text{NaCl} + \text{Ni} \qquad \text{Eq. 1}$$

In this study, a repurposed ZEBRA battery of the type Z36-371-ML3X-76 is used. ZEBRA batteries reach energy densities of approximately 100 Wh/kg and power densities of about 150 W/kg [39]–[41]. The expected cycle lifetime is about 3500 full charge and discharge cycles [41]. The internal operational temperature is kept between 270 and 350 °C [39] for efficient

and safe operation. Therefore, the battery is equipped with a heating and cooling system controlled by the BMS. Additionally, the BMS performs state of charge detection and battery balancing. 20% of the initial battery capacity is used as a backup for the temperature control to avoid damage to the battery. The ZEBRA EV battery is thermally insulated by a double-walled vacuum chamber [42]. The battery has a capacity of 28.2 kWh. Battery parameters are listed in Table 1 of the Appendix.

2.2 Converters

As shown in Fig. 1, the battery storage setup comprises two AC/DC converters. The original BC-336-Z-3-A EF single-phase charger from MES-DEA [43] is used for charging. Charging power is controlled by the BMS based on the battery state. It is changed for the battery balancing process at 80% SOC and continuously reduced close to the end of the charging process, as shown in Fig. 2. Otherwise, full charging power is applied. The DC charging characteristics of a ZEBRA battery storage system, cf. Fig. 2, shows that charging is based on a constant current constant voltage (CCCV) strategy, i.e. the current is fixed until a certain end of charging voltage is reached. The three drops in current, voltage, and power, illustrated in Fig. 2, can be explained by the activation of the auxiliary temperature control systems. Subsequently, a battery balancing process is executed, during which the battery is also slightly discharged. Charging at a constant voltage follows. The charging current drops automatically with increasing SOC.

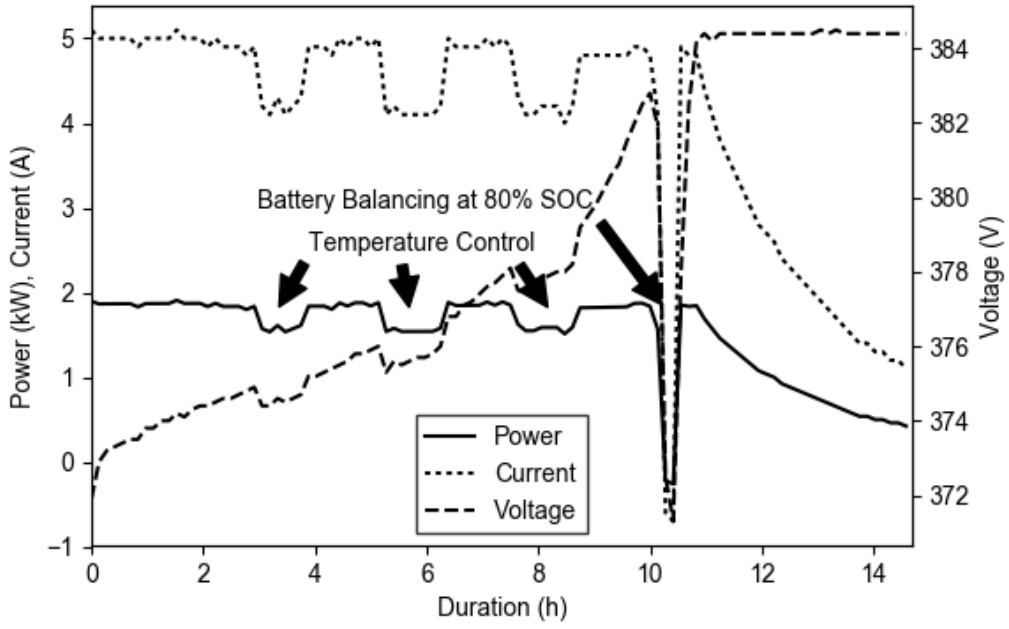

Fig. 2: DC charging characteristics of a ZEBRA battery storage system.

According to [43], the maximum DC charging power is 3.2 kW. The converter efficiency ranges from 95% for 3.2 kW to 90% for 0.4 kW [43]. Detailed information is given in Table 2 of the Appendix. The average DC charging power measured during a charging process is 1.49 kW.

Since the automotive charger BC-336-Z-3-A EF is not designed for discharging, a three-phase SYMO 8.2-3-M converter from Fronius [44], including a data manager module, is integrated.

The discharging power can be controlled continuously via Modbus TCP from 0–100% of the maximum power. The efficiency ranges from about 90% to 97.5% depending on the output power [44]. Detailed information is given in Table 3 of the Appendix. Preliminary measurements showed that the average DC discharging power between 20% and 100% SOC is 8.64 kW, i.e. 5.8 times the charging power.

2.3 Energy Monitoring

The three-phase energy counter Algodue UEM80-4D E [45] is used for energy monitoring and is connected between the converters and the electrical grid, cf. Fig. 1a. The ECH is able to fetch measured energy data via Ethernet (Modbus TCP). Technical details are given in Table 4 of the Appendix. The energy monitoring system measured in- and output energy, the powering of the energy counter, and the BMS. The energy flows are recorded at a resolution of 15 minutes.

2.4 Price-Driven Optimization

As shown by the authors in [9], a linear battery model approximates the dynamic behavior of the ZEBRA battery with reasonable accuracy. The linear battery model is described as follows,

$$\frac{\mathrm{d}E_{\mathrm{el}}}{\mathrm{d}t} = P_{\mathrm{DC}}(t) - P_{\mathrm{loss}}. \qquad \text{Eq. 2}$$

E_{el} reflects the electrical energy content of the battery, P_{DC} the DC charging/discharging power, and P_{loss} the constant losses. The losses include internal losses via battery cell resistance and the auxiliary heating and cooling power.

The approaches presented in [9], [46] are adapted to account for different charging and discharging power and converter efficiencies. For a given PCF, $c(t)$, at a resolution of Δt in the time window $[t_0, t_n]$, the optimization problem can be formulated as:

$$\min_{u_{\mathrm{DC}}} \int_{t_0}^{t_n} c(t) \cdot P_{\mathrm{AC}}(u_{\mathrm{DC}}(t))\, dt, \text{s. t.} \qquad \text{Eq. 3}$$

$$E_{\mathrm{el,min}} \leq E_{\mathrm{el}}(t) \leq E_{\mathrm{el,max}},\ t_0 \leq t \leq t_n \qquad \text{Eq. 4}$$

Here, P_{AC} denotes the power resulting at the electrical grid, accounting for power conversion.

To apply the optimization to the linear battery model, we formulate a mixed integer linear program (MILP) as

$$\min_{u_{\mathrm{DC}}} \sum_{i=1}^{n} c_i(t) \cdot \left(u_{\mathrm{DC},i}^{+} \cdot \eta_{\mathrm{in}}^{-1} \cdot P_{\mathrm{DC,max}} - u_{\mathrm{DC},i}^{-} \cdot \eta_{\mathrm{out}} \cdot P_{\mathrm{DC,max}}\right) \cdot \Delta t, \text{s. t.} \quad \text{Eq. 5}$$

$$E_{\mathrm{el,min}} \leq E_{\mathrm{el},0} + \sum_{i=1}^{j} \left[u_{\mathrm{DC},i}^{+} \cdot P_{\mathrm{DC,max}} - u_{\mathrm{DC},i}^{-} \cdot P_{\mathrm{DC,max}} - P_{\mathrm{loss}}\right] \cdot \Delta t \leq E_{\mathrm{el,max}}, \forall j \in \{1, \cdots, n\}, \quad \text{Eq. 6}$$

$$0 \leq x_{\mathrm{c},i} + x_{\mathrm{d},i} \leq 1, x_{\mathrm{c},i}, x_{\mathrm{d},i} \in \{0,1\}\ \forall i, \quad \text{Eq. 7}$$

$$u_{\mathrm{DC},i}^{+} \leq u_{\mathrm{DC,max}}^{+} \cdot \left(1 - x_{\mathrm{d},i}\right), \quad \text{Eq. 8}$$

$$u_{\mathrm{DC},i}^{+} \geq u_{\mathrm{DC,min}}^{+} \cdot x_{\mathrm{c},i}, \quad \text{Eq. 9}$$

$$u_{\mathrm{DC},i}^{-} \leq u_{\mathrm{DC,max}}^{-} \cdot \left(1 - x_{\mathrm{c},i}\right), \quad \text{Eq. 10}$$

$$u_{\mathrm{DC},i}^{-} \geq u_{\mathrm{DC,min}}^{-} \cdot x_{\mathrm{d},i}, \quad \text{Eq. 11}$$

$$u_{\mathrm{DC},i}^{+} \leq u_{\mathrm{DC,max}}^{+} \cdot \left(x_{\mathrm{c},i} + x_{\mathrm{d},i}\right), \quad \text{Eq. 12}$$

$$u_{\mathrm{DC},i}^{-} \leq u_{\mathrm{DC,max}}^{-} \cdot \left(x_{\mathrm{c},i} + x_{\mathrm{d},i}\right). \quad \text{Eq. 13}$$

To account for different charging and discharging power, we introduce two continuous decision variables, $u_{\mathrm{DC},i}^{+}$ and $u_{\mathrm{DC},i}^{-}$, for each time step, indicating charging and discharging separately. The composite decision variable is then given by $u_{\mathrm{DC}} = u_{\mathrm{DC}}^{+} + u_{\mathrm{DC}}^{-}$. Converter efficiencies, η_{in} and η_{out}, are included linearly in the objective function. Binary variables, $x_{\mathrm{c},i}$ and $x_{\mathrm{d},i}$, are used to exclude discharging during charging and vice versa. The maximum charging power, $u_{\mathrm{DC,max}}^{+}$, set to 1 and the maximum discharging power, $u_{\mathrm{DC,max}}^{-}$, set to 5.8, reflect the discharging to charging power ratio (cf. 2.2). Since the converters perform inefficiently up to 20% of their maximum output power, the boundary conditions exclude charging or discharging for lower values, reflected by Eq. 8 – Eq. 13. The charging efficiency, η_{in}, is set to 90% and the discharging efficiency, η_{out}, to 95%. The initial electrical energy content is denoted by $E_{\mathrm{el},0} = E_{\mathrm{el}}(t_0)$. The battery operation is bound by a minimum and maximum electrical energy content, $E_{\mathrm{el,min}}$ and $E_{\mathrm{el,max}}$, respectively.

2.4.1 Day-Ahead Market Based Control

Energy Exchange Austria (EXAA) offers daily block-based, hour-based and 15-min-based stock market prices for electricity, published daily on weekdays at 12 noon for the next 36 hours. Simulation results presented in a previous paper [9] reveal a strong correlation between the earnings and the variance of the PCF. The 15-min-based product was superior to the hour-based product and is therefore used as PCF [47].

2.4.2 Battery Loss Estimation

The constant loss term of the linear model is estimated by fitting the model using historic DC power and SOC data. More specifically, the integral form of Eq. 2 for a given time window, $[t_0, t_n]$, is evaluated, i.e.

$$E_{\mathrm{el}}(t_n) = E_{\mathrm{el}}(t_0) + \int_{t_0}^{t_n} P_{\mathrm{DC}}(t)\, dt - n \cdot P_{\mathrm{loss,est}}. \quad \text{Eq. 14}$$

The least squares problem can be formulated as

$$\min_x \|a \cdot x - b\|^2, \text{where} \quad \text{Eq. 15}$$

$$a_i = i \text{ and} \quad \text{Eq. 16}$$

$$b_i = \left(E_{\text{el}}(t_0) - E_{\text{el}}(t_i) + \int_{t_0}^{t_i} P_{\text{DC}}(t)\, dt \right), \forall i \in \{1, \cdots, n\}. \quad \text{Eq. 17}$$

E_{el} denotes the measured electrical energy content of the battery. To verify the quality of the fit, the coefficient of determination, R^2, is calculated. Losses are estimated once a day based on seven days of historic power and SOC data.

2.5 Implementation

The controller software is implemented in Python 3 [48] running on a BeagleBone Black – Rev C using a Debain Jessie 8.7. The BeagleBone [49] comes with an AM335x 1GHz ARM® Cortex™-A8 microprocessor, 512 MB DDR3 RAM, an internal CAN bus controller and a 16 GB Class 4 microSDHC card from SanDisk [50]. The BeagleBone CBB-Serial Cape with its integrated CAN bus transceiver [51] is used as interface between the physical CAN bus and the CAN bus controller. The Modbus connection is realized via TCP/IP. General-purpose input/output (GPIO) pins of the BeagleBone are used to actuate the relays connecting the converters to the battery.

Fig. 3 shows the interactions between the processes, the inputs and outputs, and the communication interfaces. The main routine is the central processing unit. Pseudo-cost function data, provided by a PCF fetcher, are used with battery state information to find the optimal decision values via an optimization routine. An execution process interprets the values and controls the battery charging/discharging process via CAN bus and/or Modbus TCP. The optimization routine is executed every 15 minutes, using GLPK (GNU Linear Programming Kit) [52] from the PyMathProg package [53] to solve the linear optimization problem. A time-based job scheduler (cronjob) starts all processes.

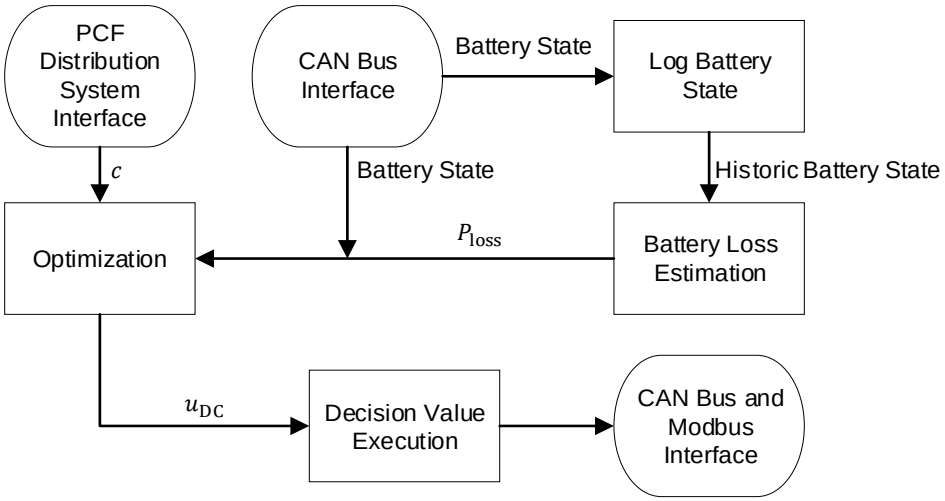

Fig. 3: In-house software implementation of battery control algorithm.

3 Results

The results obtained show the performance of the storage system during the experiment based on price-driven, on-site optimized operation and reveal the battery model accuracy used in the optimization in comparison to the physical behavior. Experimental results achieved were recorded from 24 May 2017, 4:15 to 6 June 2017, 9:00. Fig. 4 shows an exemplary 24 hours window of battery operation.

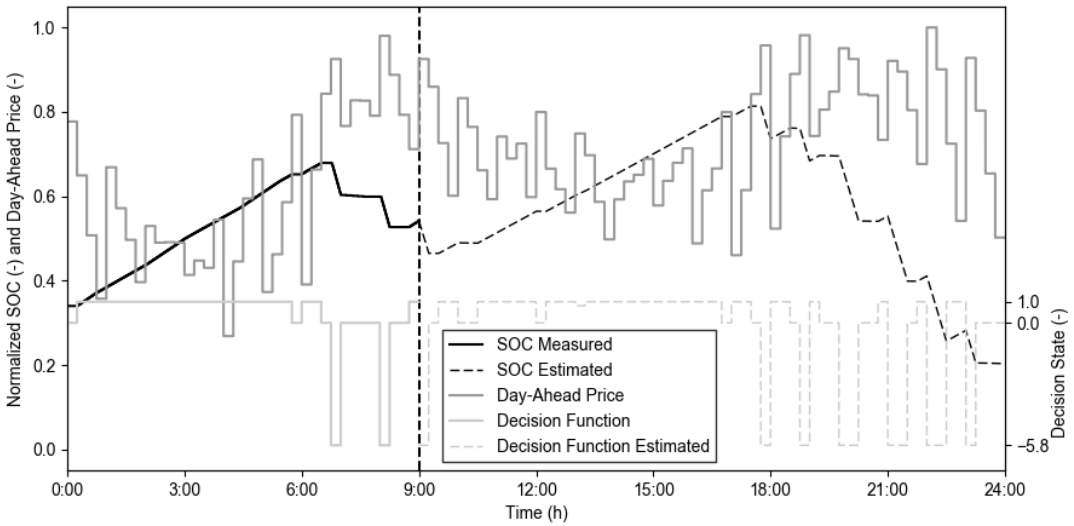

Fig. 4: Historic and future battery operation based on a 15 minutes Austrian day-ahead price optimization for 24 hours. The dashed horizontal line separates the historic execution and the future operation of the battery. The black solid line shows the historic change in SOC. The estimated future trend, based on the 15 minutes given day-ahead stock market price for electricity (grey line), is illustrated as a dashed black line. These values are normalized to their maximum occurring value. The light solid grey line indicates the decision states executed on the battery storage in a 15-minute time interval and the dashed line the estimated future decision states.

3.1 Model Accuracy

Daily battery losses are shown in Fig. 5. The minimum loss value observed is 1.93 W/kWh of battery capacity and the maximum value is 3.54 W/kWh of battery capacity. The median is 2.74 W/kWh of battery capacity, its first and third quartile are 2.42 W/kWh and 3.13 W/kWh of battery capacity, respectively. The coefficients of determination, R^2, for all loss estimations ranges from 0.86 to 0.96.

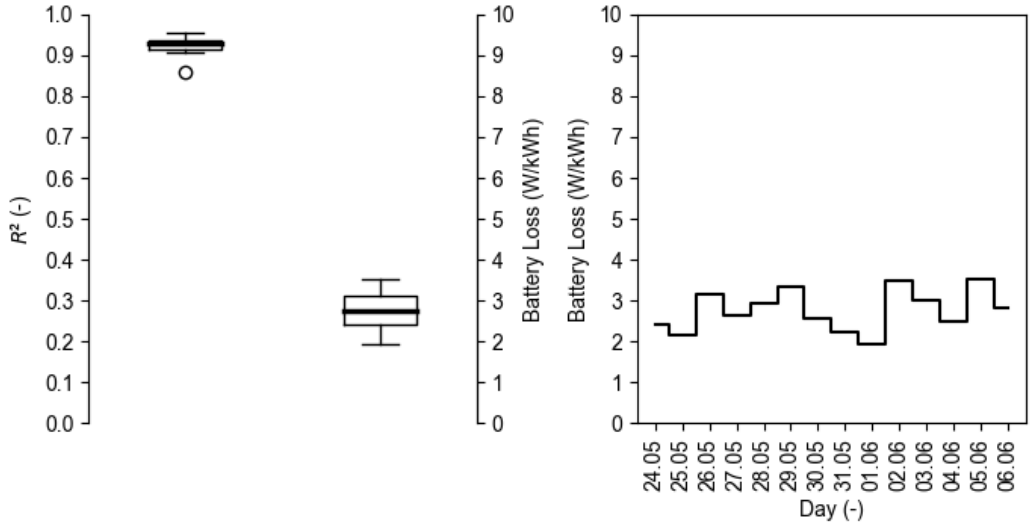

Fig. 5: Estimated constant battery loss and R^2 value for each day during the experiment. Boxplot (left) of R^2 values and estimated battery losses per capacity. Daily estimation of the battery loss per capacity (right).

To determine the quality of the linear battery model, the estimated SOC is compared to the SOC measured by the BMS. Fig. 6 shows a 36-hour time window out of the investigated 14-day period, depicting the day-ahead price (PCF), the corresponding decision function, the measured SOC, and the model prediction based on the decision states executed. The case shown represents optimization starting at midnight. It predicts the battery state for 24 hours since the currently available day-ahead price ends at midnight of the following day. Two major instances of model deviations are observed in Fig. 6. The first visible deviation occurs at approximately 6:15. According to the decision function, the battery should charge. Since the BMS balances the battery (cf. section 2.2), the charging process is interrupted. Another deviation occurs at approximately 14:30. Again, the charging process is interrupted by a battery balancing procedure followed by a short charging period. A sudden change in SOC to 100% is seen around 15:15, causing a second strong deviation. The BMS determines that the end of charge state is reached, by measuring cell voltages and hence resets its internal SOC estimation to 100%.

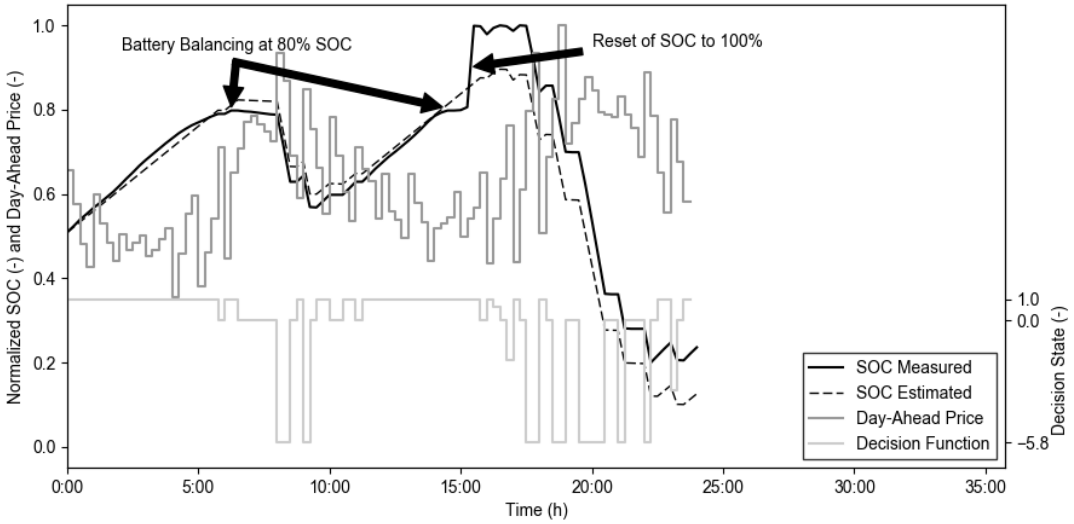

Fig. 6: Comparison of battery model estimation and the physical behavior of the battery storage system.

The estimated SOC is compared to the SOC provided by the BMS. The root mean square error (RMSE) is calculated from 24 May 2017, 12:00 to 5 June 2017, 00:00. To calculate the RMSE, every 15 minutes, i.e. Δt = 900 seconds, an estimation of the future SOC (SOC_{est}) for the available day-ahead price time window is calculated and compared to the historic SOC (SOC_{hist}). Introducing the day-time function, $t_{\mathrm{d}}(i)$, which returns the seconds passed for the current date-time since midnight for a given time step i, the calculation of the RMSE reflecting the model error can be formulated as

$$\mathrm{RMSE} = \sqrt{\sum_{j=i}^{i+k}\left(\frac{SOC_{\mathrm{est},j} - SOC_{\mathrm{hist},j}}{k}\right)^2}, i = \{1, \cdots, n\}, \text{where} \qquad \text{Eq. 18}$$

$$k = \begin{cases} \left\lceil \frac{n_{\mathrm{d}} - t_{\mathrm{d}}(i)}{\Delta t} \right\rceil, & 0 \le t_{\mathrm{d}}(i) < \frac{n_{\mathrm{d}}}{2} \\ \left\lceil \frac{n_{\mathrm{d}} - t_{\mathrm{d}}(i)}{\Delta t} + \frac{n_{\mathrm{d}}}{\Delta t} \right\rceil, & \text{else,} \end{cases} \qquad \text{Eq. 19}$$

where n_{d} is the total number of seconds per day. The resulting RMSE for the experiment yielded to 7.6%. Deviations of the estimated SOC are illustrated in Fig. 7.

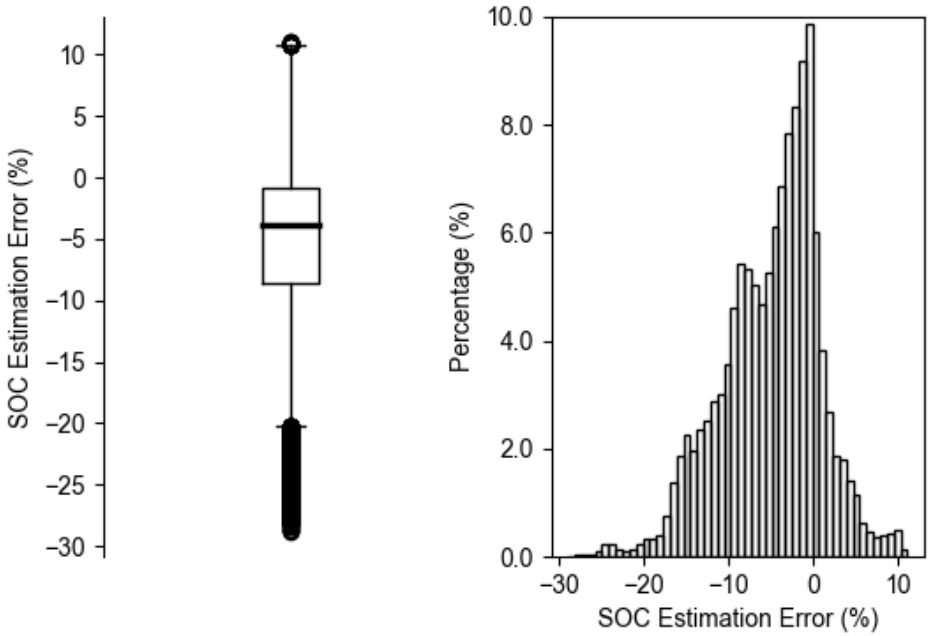

Fig. 7: Boxplot (left) and histogram (right) of the deviation of the estimated to the BMS measured SOC for the experiment conducted.

3.2 Battery Performance

Based on the energy monitoring measurements, the round-trip efficiency (converter-battery-converter), η_{rt}, is calculated as:

$$\eta_{\mathrm{rt}} = \frac{E_{\mathrm{AC,out}}}{E_{\mathrm{AC,in}}}, \qquad \text{Eq. 20}$$

where $E_{\mathrm{AC,in}}$ is the monitored input and $E_{\mathrm{AC,out}}$ the monitored output energy during the observed period. The battery efficiency, η_{bat}, is calculated as

$$\eta_{\mathrm{bat}} = \frac{\eta_{\mathrm{rt}}}{\eta_{\mathrm{in}} \cdot \eta_{\mathrm{out}}}. \qquad \text{Eq. 21}$$

A full battery charge cycle is defined as a complete turnover of twice the battery capacity. The number of cycles is hence estimated by the energy transferred in and out, $E_{\mathrm{AC,in}}$ and $E_{\mathrm{AC,out}}$, respectively:

$$n_{\mathrm{cycle}} = \frac{(E_{\mathrm{AC,in}} \cdot \eta_{\mathrm{in}} + E_{\mathrm{AC,out}} \cdot \eta_{\mathrm{out}}^{-1}) \cdot \eta_{\mathrm{bat}}}{2 \cdot E_{\mathrm{el,max}}} \qquad \text{Eq. 22}$$

For the 14-day duration of the experiment η_{rt} = 74.4%, η_{bat} = 87.0%, and n_{cycle} = 9.43.

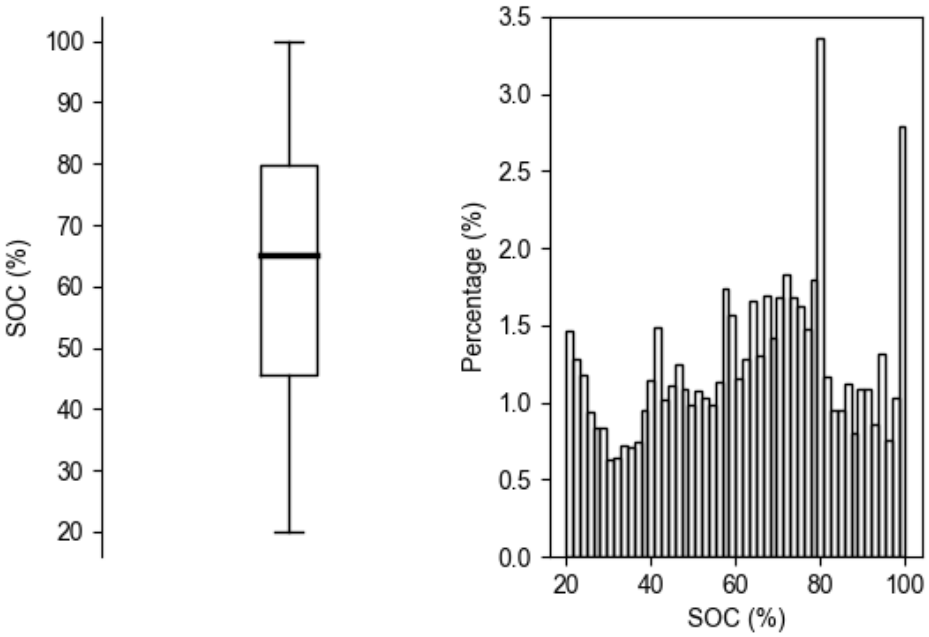

Fig. 8: Boxplot (left) and histogram (right) of the SOC for the experiment conducted.

Fig. 8 shows the SOC distribution during the experiment. The median is 65.2% SOC, the first quartile is 45.5%, and the third quartile is 79.8%. The peak at 80% SOC can be explained by the cell balancing since the battery holds this state until the process is completed. The peaks at 20% and 100% SOC can be explained by model inaccuracies e.g. the SOC reset during the charging process.

3.3 Cost Efficiency Analysis

The histogram of the day-ahead price for the period 24 May 2017, 4:15 until 6 June 2017, 9:00 is shown in Fig. 9. The minimum and maximum value of the day-ahead price observed are 0.45 €/MWh and 59.00 €/MWh, respectively. The median of the data is 30.20 €/MWh, the first and third quartile are 23.64 €/MWh and 37.54 €/MWh, respectively.

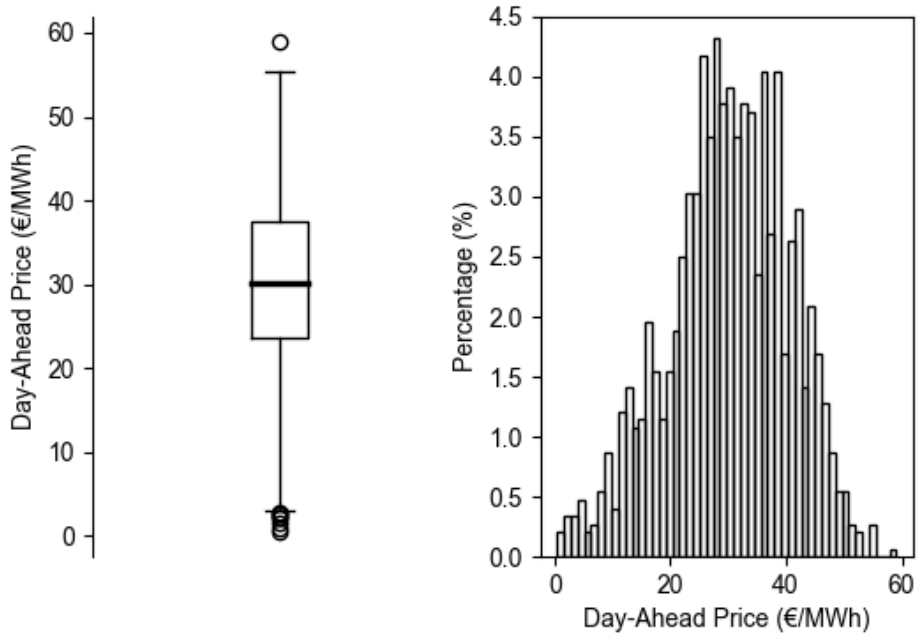

Fig. 9: Boxplot (left) and histogram (right) of the Austrian day-ahead stock market price for electricity for the period 24 May 2017, 4:15 until 6 June 2017, 9:00.

Fig. 10a shows the boxplot for the day-ahead price and the SOC separated according to the operation modes (charge, discharge, idle) for the same period from 24 May 2017, 4:15 until 6 June 2017, 9:00. For low prices, the predominant state is charging, for medium prices, the predominant state is idle, and for high prices, discharging is most common. However, this grouping is not clear-cut: all decision states can be found for almost all SOC states. Only charging at very high and discharging at very low SOC does not occur, when the remaining capacity is insufficient to execute this decision. The histograms in Fig. 10b reveals a strong correlation between price and decision states.

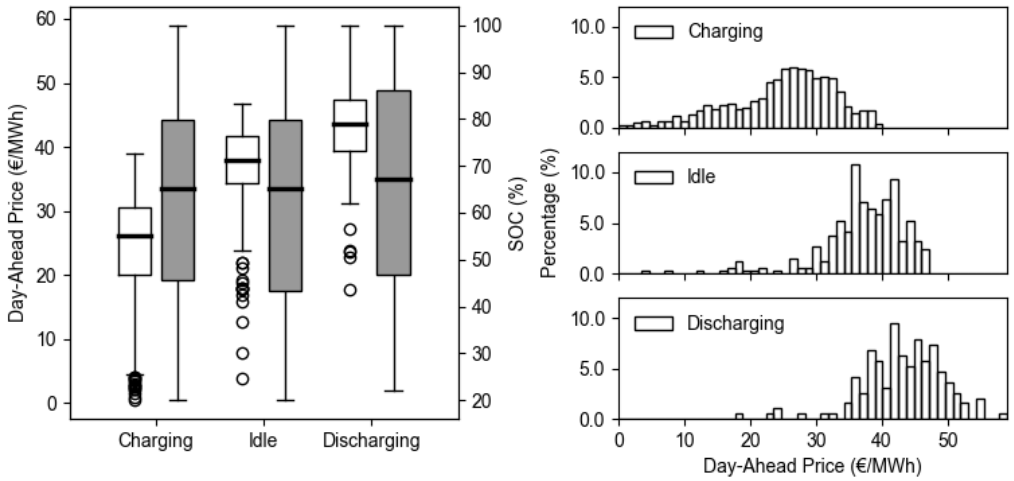

Fig. 10: a) Boxplot of the day-ahead stock market price for electricity and the SOC for the decision states.
b) Histogram of the day-ahead stock market price for electricity for the decision states.

The earnings achieved per kWh of battery capacity during the experiment are calculated as

$$s_{\text{earn}} = \frac{\sum_{i=1}^{n} c_i(t) \cdot \left(E_{\text{AC,in},i}(t) - E_{\text{AC,out},i}(t)\right)}{E_{\text{el,max}}}. \qquad \text{Eq. 23}$$

The potential earnings assuming linear battery behavior are investigated by simulation: the model is initialized at 12 noon, using the corresponding 36 hours day-ahead price and the estimated battery losses during the experiment. By simulation, the new battery state is calculated and used as the initial state for the next day optimization. The resulting potential earnings amount to 0.16 €/kWh of battery capacity. In comparison, the earnings realized during the experiment amount to 0.10 €/kWh of battery capacity.

4 Conclusion

In this paper, decentralized and on-site optimized grid balancing utilizing a repurposed high-temperature ZEBRA battery storage system is demonstrated experimentally in the field. The experimental setup uses in-house software comprising routines for communication, optimization and operation of the battery storage system. A mixed integer linear programming optimization routine using a linear battery model finds the optimal operation by minimizing an objective function calculated from one-way communicated Austrian quarter-hour day-ahead stock market electricity prices.

The field test shows that electrical vehicle batteries can indeed be reused as stationary storage for grid balancing. During a 14-day period from 24 May 2017, 4:15 to 6 June 2017, 9:00, the system operated with a round-trip efficiency (converter-battery-converter) of 74.4% and with a calculated battery efficiency of 87.0%. The estimated median of the daily battery loss amounted to 2.74 W/kWh of battery capacity. The battery storage system performed 9.43 full battery charge cycles with a median state of charge of 65.2%.

An accuracy analysis of the proposed linear battery model shows a root mean square error of 7.6% between the estimated and the measured state of charge during the experiment. In most cases, the state of charge is underestimated, cf. Fig. 7.

Earnings in the observed period amounted to 0.10 €/kWh of battery capacity, where the minimum and maximum day-ahead price were 0.45 €/MWh of battery capacity and 59.00 €/MWh of battery capacity, respectively. Although the installation and equipment costs of the presented stationary battery storage cannot be determined, it can be said that the earnings achieved must be significantly higher in order to operate the storage economically. We conclude that the battery must be operated on markets with higher volatility and/or a larger price range to increase the viable earnings.

The potential earnings, found by simulation assuming linear battery behavior, amounted to 0.16 €/kWh of battery capacity. The discrepancy to the experimental results is attributed to three main effects: 1) Insufficient representation of the battery management system and the battery behavior in the model (e.g., state dependent state of charge reset to 100%). 2) Delayed discharging due to a system check by the battery management system and a grid synchronizing processes of the converter. 3) Insufficient charging power estimation, since the battery is charged by a constant-current-constant-voltage strategy, which ends with a charging

power drop, cf. Fig. 2. The significant deviations between the model and the experiment due to technical obstacles and model inaccuracies show the urgent need for more field tests of grid-balancing strategies to investigate their potential.

The reuse of a ZEBRA battery for stationary application was time consuming and technically challenging, suggesting similar challenges if pursued for other battery storage types used in electric vehicles. This indicates that a second use of vehicle batteries for grid balancing has to be planned from the outset. Such planning efforts are highly recommended to electric vehicle manufacturers.

Acknowledgements

The financial support by the Austrian Federal Ministry of Science, Research and Economy and the National Foundation for Research, Technology and Development is gratefully acknowledged. We gratefully acknowledge financial support for parts of this work, as the stationary battery storage setup, by the FFG Austrian Research Promotion Agency within the framework of the SmartCity Rheintal project (FFG no. 836088).

References

[1] T. Boßmann and I. Staffell, "The shape of future electricity demand: Exploring load curves in 2050s Germany and Britain," *Energy*, vol. 90, pp. 1317–1333, Oct. 2015.

[2] M. Beaudin, H. Zareipour, A. Schellenberglabe, and W. Rosehart, "Energy storage for mitigating the variability of renewable electricity sources: An updated review," *Energy Sustain. Dev.*, vol. 14, no. 4, pp. 302–314, Dec. 2010.

[3] A. Pina, C. Silva, and P. Ferrão, "The impact of demand side management strategies in the penetration of renewable electricity," *Energy*, vol. 41, no. 1, pp. 128–137, May 2012.

[4] P. Palensky and D. Dietrich, "Demand Side Management: Demand Response, Intelligent Energy Systems, and Smart Loads," *IEEE Trans. Ind. Inform.*, vol. 7, no. 3, pp. 381–388, Aug. 2011.

[5] P. J. Hall and E. J. Bain, "Energy-storage technologies and electricity generation," *Energy Policy*, vol. 36, no. 12, pp. 4352–4355, Dec. 2008.

[6] A. T. Gullberg, D. Ohlhorst, and M. Schreurs, "Towards a low carbon energy future – Renewable energy cooperation between Germany and Norway," *Renew. Energy*, vol. 68, pp. 216–222, Aug. 2014.

[7] C. A. Hill, M. C. Such, D. Chen, J. Gonzalez, and W. M. Grady, "Battery Energy Storage for Enabling Integration of Distributed Solar Power Generation," *IEEE Trans. Smart Grid*, vol. 3, no. 2, pp. 850–857, Jun. 2012.

[8] P. Siano, "Demand response and smart grids—A survey," *Renew. Sustain. Energy Rev.*, vol. 30, pp. 461–478, Feb. 2014.

[9] B. Faessler, P. Kepplinger, and J. Petrasch, "Decentralized price-driven grid balancing via repurposed electric vehicle batteries," *Energy*, vol. 118, pp. 446–455, Jan. 2017.

[10] K. C. Divya and J. Østergaard, "Battery energy storage technology for power systems —An overview," *Electr. Power Syst. Res.*, vol. 79, no. 4, pp. 511–520, Apr. 2009.

[11] A. R. Landgrebe and S. W. Donley, "Battery storage in residential applications of energy from photovoltaic sources," *Appl. Energy*, vol. 15, no. 2, pp. 127–137, Jan. 1983.

[12] P. Mercier, R. Cherkaoui, and A. Oudalov, “Optimizing a Battery Energy Storage System for Frequency Control Application in an Isolated Power System,” *IEEE Trans. Power Syst.*, vol. 24, no. 3, pp. 1469–1477, Aug. 2009.

[13] B. Peng and J. Chen, “Functional materials with high-efficiency energy storage and conversion for batteries and fuel cells,” *Coord. Chem. Rev.*, vol. 253, no. 23–24, pp. 2805–2813, Dec. 2009.

[14] H. Chen, T. N. Cong, W. Yang, C. Tan, Y. Li, and Y. Ding, “Progress in electrical energy storage system: A critical review,” *Prog. Nat. Sci.*, vol. 19, no. 3, pp. 291–312, Mar. 2009.

[15] R. Dufo-López and J. L. Bernal-Agustín, “Techno-economic analysis of grid-connected battery storage,” *Energy Convers. Manag.*, vol. 91, pp. 394–404, Feb. 2015.

[16] J. Leadbetter and L. Swan, “Battery storage system for residential electricity peak demand shaving,” *Energy Build.*, vol. 55, pp. 685–692, Dec. 2012.

[17] C. Pang, P. Dutta, and M. Kezunovic, “BEVs/PHEVs as Dispersed Energy Storage for V2B Uses in the Smart Grid,” *IEEE Trans. Smart Grid*, vol. 3, no. 1, pp. 473–482, Mar. 2012.

[18] M. Bragard, N. Soltau, S. Thomas, and R. W. De Doncker, “The Balance of Renewable Sources and User Demands in Grids: Power Electronics for Modular Battery Energy Storage Systems,” *IEEE Trans. Power Electron.*, vol. 25, no. 12, pp. 3049–3056, Dec. 2010.

[19] N. W. Miller, R. S. Zrebiec, R. W. Delmerico, and G. Hunt, “Battery energy storage systems for electric utility, industrial and commercial applications,” 1996, pp. 235–240.

[20] H. Qian, J. Zhang, J.-S. Lai, and W. Yu, “A high-efficiency grid-tie battery energy storage system,” *IEEE Trans. Power Electron.*, vol. 26, no. 3, pp. 886–896, Mar. 2011.

[21] O. M. Toledo, D. Oliveira Filho, and A. S. A. C. Diniz, “Distributed photovoltaic generation and energy storage systems: A review,” *Renew. Sustain. Energy Rev.*, vol. 14, no. 1, pp. 506–511, Jan. 2010.

[22] J. Patten, N. Christensen, G. Nola, and S. Srivastava, “Electric vehicle battery — Wind storage system,” 2011, pp. 1–3.

[23] K. Clement-Nyns, E. Haesen, and J. Driesen, “The impact of vehicle-to-grid on the distribution grid,” *Electr. Power Syst. Res.*, vol. 81, no. 1, pp. 185–192, Jan. 2011.

[24] W. Kempton and J. Tomić, “Vehicle-to-grid power implementation: From stabilizing the grid to supporting large-scale renewable energy,” *J. Power Sources*, vol. 144, no. 1, pp. 280–294, Jun. 2005.

[25] T. Sousa, H. Morais, J. Soares, and Z. Vale, “Day-ahead resource scheduling in smart grids considering Vehicle-to-Grid and network constraints,” *Appl. Energy*, vol. 96, pp. 183–193, Aug. 2012.

[26] L. Wang, S. Sharkh, and A. Chipperfield, “Optimal coordination of vehicle-to-grid batteries and renewable generators in a distribution system,” *Energy*, vol. 113, pp. 1250–1264, Oct. 2016.

[27] B. Tarroja, L. Zhang, V. Wifvat, B. Shaffer, and S. Samuelsen, “Assessing the stationary energy storage equivalency of vehicle-to-grid charging battery electric vehicles,” *Energy*, vol. 106, pp. 673–690, Jul. 2016.

[28] J. Neubauer and A. Pesaran, “The ability of battery second use strategies to impact plug-in electric vehicle prices and serve utility energy storage applications,” *J. Power Sources*, vol. 196, no. 23, pp. 10351–10358, Dec. 2011.

[29] S. Shokrzadeh and E. Bibeau, “Sustainable integration of intermittent renewable energy and electrified light-duty transportation through repurposing batteries of plug-in electric vehicles,” *Energy*, vol. 106, pp. 701–711, Jul. 2016.

[30] C. Heymans, S. B. Walker, S. B. Young, and M. Fowler, “Economic analysis of second use electric vehicle batteries for residential energy storage and load-levelling,” *Energy Policy*, vol. 71, pp. 22–30, Aug. 2014.

[31] M. O. Ramoni and H.-C. Zhang, “End-of-life (EOL) issues and options for electric vehicle batteries,” *Clean Technol. Environ. Policy*, vol. 15, no. 6, pp. 881–891, Dec. 2013.

[32] Daimler AG, “World’s largest 2nd-use battery storage is starting up,” *http://media.daimler.com*, Lünen/Stuttgart, 13-Sep-2016.

[33] R. Hein, P. R. Kleindorfer, and S. Spinler, “Valuation of electric vehicle batteries in vehicle-to-grid and battery-to-grid systems,” *Technol. Forecast. Soc. Change*, vol. 79, no. 9, pp. 1654–1671, Nov. 2012.

[34] S. Shokrzadeh and E. Bibeau, “Repurposing Batteries of Plug-In Electric Vehicles to Support Renewable Energy Penetration in the Electric Grid,” 2012.
[35] THINK Global AS, “THINK City Bedienungsanleitung.” THINK Global AS, May-2010.
[36] I. Standard, “ISO 11898, 1993,” *Road Veh. Digit. Information–Controller Area Netw. CAN High-Speed Commun.*, 1993.
[37] I. Standard, “IEC 61158, 2014,” *Ind. Commun. Netw. - Profiles - Part 2 Addit. Fieldbus Profiles Real-Time Netw. Based ISOIEC 8802-3*, 2014.
[38] J. Sudworth, “The sodium/nickel chloride (ZEBRA) battery,” *J. Power Sources*, vol. 100, no. 1–2, pp. 149–163, Nov. 2001.
[39] C.-H. Dustmann, “Advances in ZEBRA batteries,” *J. Power Sources*, vol. 127, no. 1–2, pp. 85–92, Mar. 2004.
[40] C. Daniel and J. O. Besenhard, Eds., *Handbook of battery materials*, 2., Completely rev. and enl. ed., 1. Reprint. Weinheim: Wiley-VCH-Verl, 2012.
[41] T. M. O’Sullivan, C. M. Bingham, and R. E. Clark, “Zebra Battery Technologies for the All Electric Smart Car,” *SPEEDAM 2006 Int. Symp. Power Electron. Electr. Drives Autom. Motion*, 2006.
[42] C.-H. Dustmann, “ZEBRA battery meets USABC goals,” *J. Power Sources*, vol. 72, no. 1, pp. 27–31, Mar. 1998.
[43] MES-DEA SA, “Battery Charger E.F.” MES-DEA SA, 02-Aug-2007.
[44] Fronius International GmbH, “Fronius Symo Datasheet.” Fronius International GmbH, 2011.
[45] Algodue Elettronica Srl, “UEM80.” Algodue Elettronica Srl, Mar-2016.
[46] B. Fäßler, P. Kepplinger, M. L. Kolhe, and J. Petrasch, “Decentralized on-site optimization of a battery storage system using one-way communication,” presented at the International Conference on Renewable Power Generation, 2015, pp. 1–6.
[47] EXAA Abwicklungsstelle für Energieprodukte AG, “Spotmarkt,” *EXAA Energy Exchange Austria*. [Online]. Available: www.exaa.at/de/marktdaten/handelsergebnisse. [Accessed: 18-Dec-2015].
[48] Python Software Foundation, *Python 3.5.1*. Beaverton, USA: Python Software Foundation, 2015.
[49] G. Coley, “BeagleBone Black System Reference Manual.” The BeagleBoard.org Foundation, 11-Apr-2013.
[50] Western Digital Technologies, Inc., “SanDisk,” *SanDisk*, 2017. [Online]. Available: www.sandisk.de. [Accessed: 06-Nov-2017].
[51] Logic Supply, Inc., “BeagleBone Black Serial Cape Manual.” Logic Supply, Inc., 20-Feb-2015.
[52] A. Makhorin, *GLPK*. Boston, USA: Free Software Foundation, Inc., 2012.
[53] Y. Lan, *PyMathProg*. 2016.
[54] MES-DEA SA, “ZEBRA Battery.” MES-DEA SA, 25-Mar-2008.

Appendix

Table 1: ZEBRA battery parameters [54].

Maximum energy content, $E_{\mathrm{el,max}}$	28.2 kWh
Maximum degree of discharge	80%
Open circuit voltage (DC) (100–85% SOC)	371 V
Minimum operation voltage (DC)	248 V
Maximum discharging current (AC)	224 A
Cell type/Number of cells	ML3X/288
Weight with BMS	243 kg
Specific energy	118 Wh/kg
Specific power	168 W/kg
Operating temperature range	−40 to 50 °C
Thermal loss	< 130 W
Minimum discharge time	120 min

Table 2: MES-DEA battery charger parameters [43].

Maximum input current (AC)	15.5 A
Input voltage (AC)	110–253 V
Mains frequency	47–63 Hz
Operating temperature range	−20 to 40 °C
Output power (DC)	3.2 kW or max 26 A
Weight	7 kg

Table 3: Fronius SYMO 8.2-3-M converter parameters [44].

Maximum input current (DC)	16 A
Input voltage (DC)	200–1000 V
Operating temperature range	−25 to 60 °C
Output power (AC)	8.2 kW
Maximum output current (AC)	13.1 A
Weight	21.9 kg

Table 4: Algodue UEM80-4D E parameters [45].

Maximum consumption (each phase)	7.5 VA–0.5 W
Minimum current (AC)	250 mA
Maximum current (AC)	80 A
Voltage range (AC)	3x230/400 V
Mains frequency	50/60 Hz
Accuracy	Active energy class B according to EN 50470-3 Reactive energy class 2 according to IEC/EN 62053-23
Operating temperature range	−25 to 55 °C

Paper D: Battery Storage Systems as Grid-Balancing Measure in Low-Voltage Distribution Grids with Distributed Generation

This chapter is based on the journal paper published as:

B. Faessler, M. Schuler, M. Preißinger, and P. Kepplinger, “Battery storage systems as grid-balancing measure in low-voltage distribution grids with distributed generation,” *Energies*, vol. 10, no. 12, pp. 1–14, Dec. 2017.

The layout has been revised for better readability. Minor revisions have been made.

Abstract

Due to the promoted integration of renewable sources, a further growth of strongly transient, distributed generation is expected. Thus, the existing electrical grid may reach its physical limits. To counteract this, and to fully exploit the viable potential of renewables, grid-balancing measures are crucial.

In this work, battery storage systems are embedded in a grid simulation to evaluate their potential for grid balancing. The overall setup is based on a real, low-voltage distribution grid topology, real smart meter household load profiles, and real photovoltaics load data. An autonomous optimization routine, driven by a one-way communicated incentive, determines the prospective battery operation mode. Different battery positions and incentives are compared to evaluate their impact. The configurations incorporate a baseline simulation without storage, a single, central battery storage or multiple, distributed battery storages, which together have the same power and capacity. The incentives address either market conditions, grid balancing, optimal photovoltaic utilization, load shifting, or self-consumption.

Simulations show that grid-balancing incentives result in lowest peak-to-average power ratios, while maintaining negligible voltage changes in comparison to a reference case. Incentives reflecting market conditions for electricity generation, such as real-time pricing, negatively influence the power quality, especially with respect to the peak-to-average power ratio. A central, feed-in-tied storage performs better in terms of minimizing the voltage drop/rise and shows lower distribution losses, while distributed storages attached at nodes with electricity generation by photovoltaics achieve lower peak-to-average power ratios.

Keywords: Grid Balancing, Grid Simulation, Autonomously Optimized Battery Storage, Distributed Generation, Central and Distributed Energy Storage

Nomenclature

C	Set of neighboring nodes (–)	S_{slack}	Power at the slack node (VA)
c	Incentive (–)	SOC	State of charge (%)
DOD	Depth of discharge (%)	t	Time (s)
E_{el}	Electrical energy content (J)	U	Alternating voltage (V)
E_{losses}	Cumulative distribution losses (Wh)	$U_{\mathrm{d/r}}$	Alternating voltage drop/rise (V)
I	Alternating current (A)	U_{node}	Alternating voltage at the individual grid nodes (V)
I_{slack}	Alternating current at the slack node (A)		
N	Total set of nodes (–)	U_{slack}	Alternating voltage at the slack node (V)
n	Total number of data points (–)	u_{DC}	Decision variable on DC power side (–)
PAPR	Peak-to-average power ratio (–)	$\mathcal{Z}$	Impedance matrix (Ω)
P_{AC}	Alternating power (W)	η_{bat}	Battery efficiency (–)
P_{DC}	Direct power (W)	η_{con}	Converter efficiency (–)
P_{loss}	Linearized battery losses (W)	n_{load}	Amount of loads (–)

1 Introduction

Transition from traditional, large-scale and centralized electricity generation by fossil fuels to more distributed renewable generation by photovoltaics (PV) and wind power is being pushed forward by many countries [1]. The strong volatility of renewables means that generation does not always coincide with electricity demand. Hence, balancing measures need to be deployed in the power system to counteract the strong effect of renewables on grid operation [2], [3] and, thereby, exploit their full potential.

In particular, low-voltage distribution grids face three technical challenges due to the penetration by small-scale distributed generation (DG) like PV: 1) voltage rise during feed-in (which also limits the amount of DG capacity introduced); 2) possible harmonic distortion caused by feed-in controllers [4]; 3) creation of new power peaks [5]. Researchers already have investigated the impacts of DG on the distribution grid [6]–[10]. Besides feed-in control strategies for DG [11], grid-balancing measures have also been investigated. Demand side management (DSM) is being discussed as a promising approach for grid balancing [12], [13], as it changes electricity demand of consumers with respect to the time pattern of consumption and/or load magnitude [14]. In this context, many publications consider the special case of electric vehicles as usable buffer capacities [15]–[17].

The integration of additional stationary storage into the distribution grid has been considered [18]. In particular, battery energy storage systems (BESSs) have been proposed [19]–[24], different sizes and battery technologies have been discussed and their corresponding suitability demonstrated. BESSs are able to react practically instantaneously, and, based on their flexibility in capacity and location, last longer. Therefore, they can serve different purposes such as [25], [26]: 1) matching peak power demand; 2) improving power quality and reliability of the grid by providing balancing energy; 3) reducing supply interruption by bridging power; 4) load following to increase generation utilization.

Currently, BESSs for grid balancing face the obstacles of high lifecycle costs [27] and high energy and material requirements [28]. Used electric vehicle batteries have been proposed for a second use in stationary applications. As less active bulk material is wasted [29], costs are reduced [30], and the ecological footprint is improved [31].

In our previous work [30], [32], we proposed BESSs based on repurposed electric vehicle batteries for grid balancing. The prospective operation mode (charge, discharge, or idle) is determined based on an autonomous optimization routine driven by a one-way communicated incentive. The incentive represents the intention of the operator to achieve a certain goal [33], e.g. grid balancing, and can thus vary significantly. To the best of our knowledge, impacts of incentive-driven BESSs on low-voltage distributing grids have not been investigated so far. Therefore, the present work compares a single, central BESS and multiple, distributed BESSs driven by different incentives to evaluate their impact on grid load and power quality. With this, we want to discuss the following question: “Which incentives facilitate the integration of volatile, distributed electricity generation?” To this end, we investigate incentives that reflect different purposes, like real-time pricing, grid balancing, optimal PV utilization, DSM, or self-consumption.

In section 2, the detailed approach is discussed. First, the battery model, the incentive-driven optimization, and different incentives are presented. Then, the simulation setup is described in detail. Section 3 shows the achieved results based on our approach, followed by a brief discussion in section 4 and a conclusion in section 5.

2 Approach

Influences of integrated BESS on a low-voltage distribution grid with high PV penetration are investigated. A real, low-voltage distribution grid topology, real smart meter household load profiles, and real PV data are used. Additionally, simulated batteries are attached either to the feed-in node (central) or to the nodes comprising distributed PV penetration. Operation of the batteries relies on an autonomous optimization approach, which is driven by an incentive.

First, we discuss the battery model and optimization routine, followed by a detailed description of the different incentives used for battery operation. Then, we describe the simulation setup in detail, regarding the applied grid topology, load and PV data, as well as the simulated battery configurations and parameters. Finally, we define criteria to evaluate the impact on load, voltage levels and distribution losses.

2.1 Autonomously Optimized Storages

A BESS is operated autonomously based on a unidirectionally communicated incentive. This autonomous, on-site optimization approach allows for indirect load control. Different incentives enable the operator to pursue different measures. These measures reflect different intentions: 1) increase self-consumption; 2) facilitate grid balancing; 3) react to the electricity market.

2.1.1 Battery Model and Optimization

As shown in a previous study [32], linear models describe the battery behavior with accuracy comparable to nonlinear formulations in long-term simulations. Since only the long-term behavior of BESSs is of interest in this study, the simulations and optimizations are based on the linear battery model,

$$\frac{\mathrm{d}E_{\mathrm{el}}}{\mathrm{d}t} = P_{\mathrm{DC}}(t) - P_{\mathrm{loss}}, \qquad \text{Eq. 1}$$

where E_{el} describes the electrical energy content, P_{DC} the DC charging or discharging power rate, and P_{loss} all battery related losses. The operation mode of the battery is controlled via the decision function, $u_{\mathrm{DC}}(t)$, reflecting charging (> 0), discharging (< 0), and idle (= 0) modes, i.e. $P_{\mathrm{DC}}(t) = u_{\mathrm{DC}}(t) \cdot P_{\mathrm{DC,max}}$. The decision function is calculated by optimizing with respect to minimum costs for charging based on the incentive, $c(t)$. Constraints guarantee that the battery's state of charge (SOC) remains within the operational bounds, $E_{\mathrm{el,min}}$ and $E_{\mathrm{el,max}}$. For a given time span, $[t_0, t_n]$, the optimization problem is then formulated as

$$\min_{u_{\mathrm{DC}}} \int_{t_0}^{t_n} c(t) \cdot P_{\mathrm{AC}}(u_{\mathrm{DC}}(t))\, dt, \qquad \text{Eq. 2}$$

such that

$$E_{\mathrm{el,min}} \leq E_{\mathrm{el}}(t) \leq E_{\mathrm{el,max}},\ t_0 \leq t \leq t_n. \qquad \text{Eq. 3}$$

We assume continuous operation states ($-1 \leq u_{\mathrm{DC}}(t) \leq 1$) and introduce two decision variables, $u^{+}_{\mathrm{DC},i}$ and $u^{-}_{\mathrm{DC},i}$, for each time step specifying charging and discharging separately. The battery is connected to the electrical grid via an AC/DC converter. The conversion of AC to DC power and vice versa is assumed to exhibit a constant efficiency, i.e. $P_{\mathrm{AC}} = \eta_{\mathrm{con}} \cdot P_{\mathrm{DC}}$. By including the converter efficiency linearly in the objective, the optimization can be formulated as a linear program:

$$\min_{u_{\mathrm{DC}}} \sum_{i=1}^{n} c_i(t) \cdot \left(u^{+}_{\mathrm{DC},i} \cdot \eta_{\mathrm{con}}^{-1} \cdot P_{\mathrm{DC,max}} - u^{-}_{\mathrm{DC},i} \cdot \eta_{\mathrm{con}} \cdot P_{\mathrm{DC,max}}\right) \cdot \Delta t \qquad \text{Eq. 4}$$

Here, four boundary conditions must be fulfilled:

$$E_{\mathrm{el,min}} \leq E_{\mathrm{el,t}} \leq E_{\mathrm{el,max}} \qquad \text{Eq. 5}$$

$$E_{\mathrm{el,t}} = E_{\mathrm{el,0}} + \sum_{i=1}^{j} \left[u^{+}_{\mathrm{DC},i} \cdot P_{\mathrm{DC,max}} - u^{-}_{\mathrm{DC},i} \cdot P_{\mathrm{DC,max}} - P_{\mathrm{loss}}\right] \cdot \Delta t, 1 \leq j \leq n \qquad \text{Eq. 6}$$

$$u^{+}_{\mathrm{DC},i} + u^{-}_{\mathrm{DC},i} \leq 1 \qquad \text{Eq. 7}$$

$$u^{+}_{\mathrm{DC},i}, u^{-}_{\mathrm{DC},i} \geq 0 \qquad \text{Eq. 8}$$

$E_{\mathrm{el,0}}$ denotes the initial electrical energy content of the battery. The final operation state is calculated by $\boldsymbol{u}_{\mathrm{DC}} = \boldsymbol{u}^{+}_{\mathrm{DC}} - \boldsymbol{u}^{-}_{\mathrm{DC}}$.

2.1.2 Incentives

Reflecting alternative operation strategies for BESSs, we propose different incentives to drive the optimization routine, cf. section 2.1.1. The operation strategy addresses either market conditions, grid balancing, optimal PV utilization, load shifting, or self-consumption (see Table 1).

Real-time pricing (RTP) is often discussed to control loads and storage systems [34]–[37], reflecting the real cost of electricity generation [37]. The Austrian Energy Stock Market (EXAA) offers daily block-based, hour-based and 15-min-based day-ahead stock market prices for electricity [38]. They are available on weekdays at 12 noon for the next 36 hours. We use 15-min-based data as it was shown that balancing measures are improved by RTP based on shorter time intervals [32]. To compensate for peak loads, the future total load at the feed-in node defines another incentive, assuming perfect a priori knowledge of the total grid load. To support self-consumption of households with an integrated BESS through an incentive-driven approach, the incentive should reflect the future PV generation as well as the household load. However, to investigate the effects of consumption and generation separately, PV generation and total household consumption are used to define additional incentives. Again, we assume perfect prior knowledge of the loads and feed-in power. We classify GRID central/distributed and PV central as grid-motivated incentives and PV distributed, LOAD distributed, and SELF distributed as consumer-motivated incentives.

Table 1: Incentives used to drive BESS optimization. The considered configurations for BESS are abbreviated by c for a single, central storage and d for multiple, distributed storages.

Abbreviation	Description	Incentive	Configuration
REF	Reference case	-	-
RTP	Real-time pricing	EXAA day-ahead market price	c/d
GRID	Grid balancing	Total future grid load	c/d
PV	Optimal PV utilization	Future PV generation	c/d
LOAD	Load shifting	Future household consumption	d
SELF	Self-consumption	Future household load (incl. PV)	d

2.2 Simulation Setup

Most studies in literature are based on artificial grid topologies [39], characteristic household loads [40], and simulated PV generation [41]. Instead, we apply real data for the low-voltage distribution grid topology, the household loads, and the distributed generation from photovoltaics to allow for results close to reality. Commercially available Li-ion BESSs are chosen as buffers for grid balancing to keep simulations practical. The grid simulation is based on a direct numerical method, as proposed by Ghatak and Mukherjee [42], which allows us to calculate the load flow for both, line grids as well as weakly meshed grids. The method has already been applied successfully in various forms [42]–[45], and used to setup a simulation tool in MATLAB [46]. The tool provides interfaces to include loads reacting on incentives for the purpose of testing load management strategies [47]. The grid is simulated at a temporal resolution of 15 min.

2.2.1 Grid Topology

We investigate a rural distribution grid, for which all information is available from the local system operator, Vorarlberger Energienetze GmbH, Bregenz, Austria [48]. The weakly meshed low-voltage distribution grid (Fig. 1) comprises of 50 nodes, with the slack node, i.e. central feed-in node (50), and an additional node (19) as placeholder for a central BESS. At the slack node, the voltage, U_{slack}, is set to 230 V and no phase shift is assumed. The termination condition for the iterative calculation procedure in the grid simulation is set to $\Delta U < 1$ mV at all nodes.

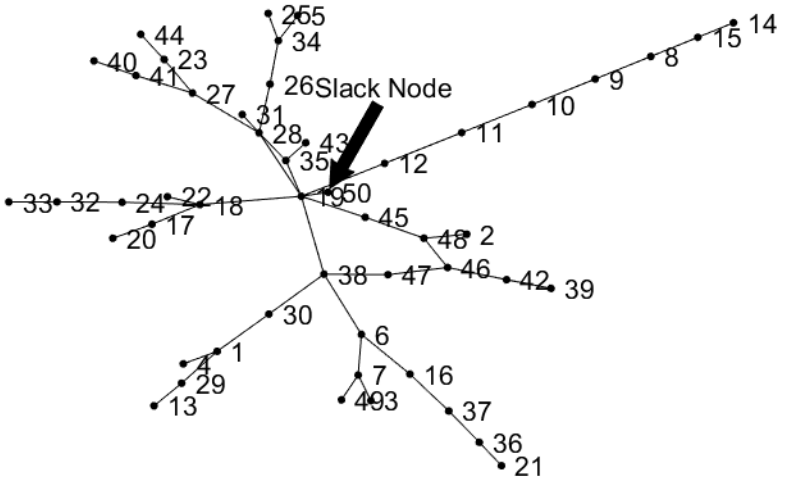

Fig. 1: Low-voltage distribution grid from local system operator.

2.2.2 Load and Photovoltaics Data

Smart meter household loads provided by Vorarlberger Kraftwerke AG (VKW), Bregenz, Austria [49], are assigned to the 48 load nodes. The temporal resolution of the load data is 15 min. In addition, electrical energy supply data of solar panels are required in the same resolution, the same period, and the same geographic area as the household load data. The data has been recorded at a photovoltaic power plant owned by VKW [49]. It consists of 270 modules with a total module surface area of about 460 m² and a nominal output power of 62.1 kWp [50]. For the simulations, the PV systems at the load nodes are scaled to typically residential dimensions of 3, 5, and 6 kWp [51]. The location in the grid is chosen randomly, attaching a PV system of 3 kWp at node 37, of 5 kWp at node 21, and of 6 kWp at node 24. The total photovoltaic peak power accounts for 14 kWp. This corresponds to approximately one quarter of the maximum load noted at the slack node over the course of the simulation period, and in the absence of photovoltaics, which is a feasible penetration rate for low-voltage distribution grids [5], [52].

2.2.3 Battery Parameters

Different BESSs with capacities ranging from 4 to 16 kWh and maximum charging and discharging power ranging from 2.5 to 8.5 kW are chosen to evaluate their impact on the grid. As distributed storages, two types of a top-rated Li-ion battery [53], the sonnenBatterie system [54], have been selected according to the manufacturer's recommendation for an annual household consumption. At node 21 and 24, the type "eco 8/6" [55] is used since the annual household consumption is about 4000 kWh. For the household at node 37, an "eco 8/4" [55] is used since the annual consumption is less than 3300 kWh.

If a single, central storage is used at node 19 as grid-balancing measure, it is assumed that its capacity and maximum charging and discharging power equals the sum of all selected distributed BESSs. The possible depth of discharge (DOD), the charging and discharging converter efficiency η_{con} as well as the battery efficiency η_{bat} for all batteries are taken from the original system and assumed to be constant. The round-trip efficiencies (converter–battery–converter) for the presented systems are about 90%. Detailed battery parameters used for the battery model and the optimization (cf. section 2.1.1) are listed in Table 2.

Table 2: Node position and corresponding specification (type, capacity, depth of discharge (DOD), battery efficiency, nominal power and converter efficiency) for the integrated BESSs in the simulation study.

Node	Model	Battery characteristic			Converter characteristic	
		Capacity (kWh)	DOD (%)	Efficiency η_{bat} (%)	Power $P_{\mathrm{AC,max}}$ (kW)	Efficiency η_{con} (%)
37	eco 8/4	4	100	98	2.5	96
21, 24	eco 8/6	6	100	98	3.0	96
19	-	16	100	98	8.5	96

Using the nominal AC power, the constant battery loss P_{loss} can be estimated by calculating the average value between losses for charging, $P_{\mathrm{loss,in}}$, and discharging, $P_{\mathrm{loss,out}}$:

$$P_{\mathrm{loss}} = \frac{\overbrace{\left(P_{\mathrm{AC,max}} \cdot \frac{(1-\eta_{\mathrm{bat}})}{2}\right) \cdot \eta_{\mathrm{con}}}^{P_{\mathrm{loss,in}}} + \overbrace{\left(P_{\mathrm{AC,max}} \cdot \frac{(1-\eta_{\mathrm{bat}})}{2}\right) \cdot \frac{1}{\eta_{\mathrm{con}}}}^{P_{\mathrm{loss,out}}}}{2} \qquad \text{Eq. 9}$$

Note that (1-η_{bat}) has to be divided by two in Eq. 9 since η_{bat} describes the round-trip efficiency of the battery. When executing the simulation, the battery is assumed to be fully charged at $t = t_o$. Results for the optimization are achieved using MATLAB's *linprog* routine [56].

2.2.4 Evaluation Criteria

Three evaluation criteria are used as quality measure: the peak-to-average power ratio (PAPR), the maximum voltage drop/rise, and the distribution losses. PAPR is a measure for the maximum occurring power at the slack node. Voltage drop/rise is analyzed at each individual node as its deviation has to be in a certain range based on standards for electrical grids [57]. The distribution losses are the cumulative losses of the investigated grid section.

By improving the PAPR, it is possible to achieve a more uniform energy transmission reducing the need for expensive operating reserves. The voltage drop/rise is of interest for the grid operator to ensure that the voltage is kept within defined limits [57]. In addition to saving resources, both the utility company and the grid operator, are interested in reducing the distribution losses.

PAPR defines the maximum occurring apparent power, $S_{\mathrm{slack,max}}$, in relation to the average apparent power, $S_{\mathrm{slack,avg}}$, at the slack node during the observed period of n discrete time steps, $t \in \tau = \{t_0, \dots, t_n\}$, and is defined as:

$$\mathrm{PAPR} = \frac{S_{\mathrm{slack,max}}}{S_{\mathrm{slack,avg}}} = \frac{\max\limits_{t\in\tau} S_{\mathrm{slack}}(t)}{\frac{\sum_{t=t_0}^{t_n} S_{\mathrm{slack}}(t)}{|\tau|}} \qquad \text{Eq. 10}$$

The maximum voltage drop/rise can be determined by the relation of the maximum or minimum occurring voltage of all nodes during the observed period in relation to the constant slack node voltage, U_{slack}. It is given by:

$$U_{\mathrm{d/r}} = \frac{\max_{t \in \tau} |U_{\mathrm{slack}} - U_{\mathrm{node}}(t)|}{U_{\mathrm{slack}}} \qquad \text{Eq. 11}$$

The cumulative distribution losses are determined by the sum of all occurring distribution losses of the investigated grid section during the whole simulation period,

$$E_{\mathrm{losses}} = \frac{1}{2} \sum_{i \in N} \sum_{j \in C_i} \overbrace{\int_{t_0}^{t_n} Re\left(I_{i,j}^2(t) \cdot Z_{i,j}\right) dt}^{\text{losses for node } i \text{ to } j} \qquad \text{Eq. 12}$$

where N represents the total set of nodes and, C_i, the set of all neighboring nodes to node i. $I_{i,j}(t)$ and $Z_{i,j}$ are the current and impedance, respectively, at the branch connecting node i and j. Only effective losses are taken into account. Since by permutation of i and j, every branch would be accounted for twice, the total sum has to be divided in half.

3 Results

The grid simulation is conducted from 8 June 2016, 12:00 to 15 June 2016, 12:00 for the reference case without a BESS, as well as for a central BESS and multiple, distributed BESSs at load nodes with PV systems. The assignments of loads, as well as PV and battery parameters are unmodified throughout the simulations. This allows comparable results regarding load, distribution losses, and voltage levels. Detailed numerical results achieved can be found in Appendix. Investigated configurations (incentives, BESS position) are listed in Table 1. Fig. 2 depicts all incentives. All incentives are shown normalized to one, while the dashed line represents the zero line. The autonomous optimization attempts to charge the battery at the valleys and discharge it at spikes. Hence, the more valleys and spikes the incentive has, the more often the battery is in an active state. The timing of the incentives influences the battery's reaction rate; therefore, short resolutions are important for a fast response. The time resolution of the conducted simulation is 15 minutes.

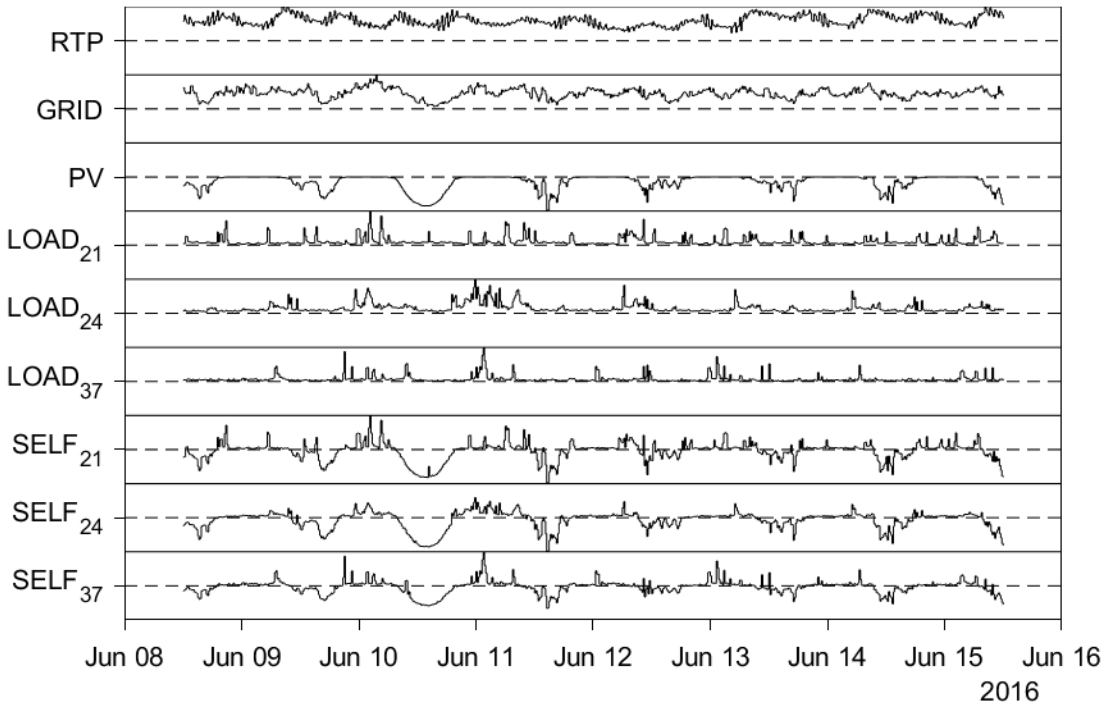

Fig. 2: Used and normalized incentives to drive the optimization of the BESS for a one-week period: EXAA day-ahead spot-market price for electricity (RTP); total grid load at the slack node (GRID); photovoltaic generation (PV); individual household loads (LOAD) for household at node 21, 24, and 37 comprising a distributed storage system; individual total household consumption including load and photovoltaic generation (SELF) for household at node 21, 24, and 37 comprising a distributed storage system.

Fig. 3 shows the PAPR, the voltage drop/rise as well as the corresponding distribution losses for all incentives and battery configurations. The PAPR is reduced in all operation modes with respect to the reference case except for RTP driven operation. In all modes other than RTP driven operation, while the maximum apparent power at the slack node, $S_{\mathrm{slack,max}}$, reduces, the mean value, $S_{\mathrm{slack,mean}}$, remains nearly the same since the required household load has to be transferred and the storages work as buffer capacities. Conversely, using RTP as incentive results in additional peak loads with respect to the reference case. In general, the cumulative distribution losses are nearly unaffected by introducing a central storage, whereas distributed storages lead to higher distribution losses for all incentives. RTP-driven operation of distributed storages exhibits the highest distribution losses. The voltage drop/rise as well as the maximum and minimum voltages indicate that regardless of the incentive, central storages do not deteriorate or significantly improve the power quality in terms of voltage deviation.

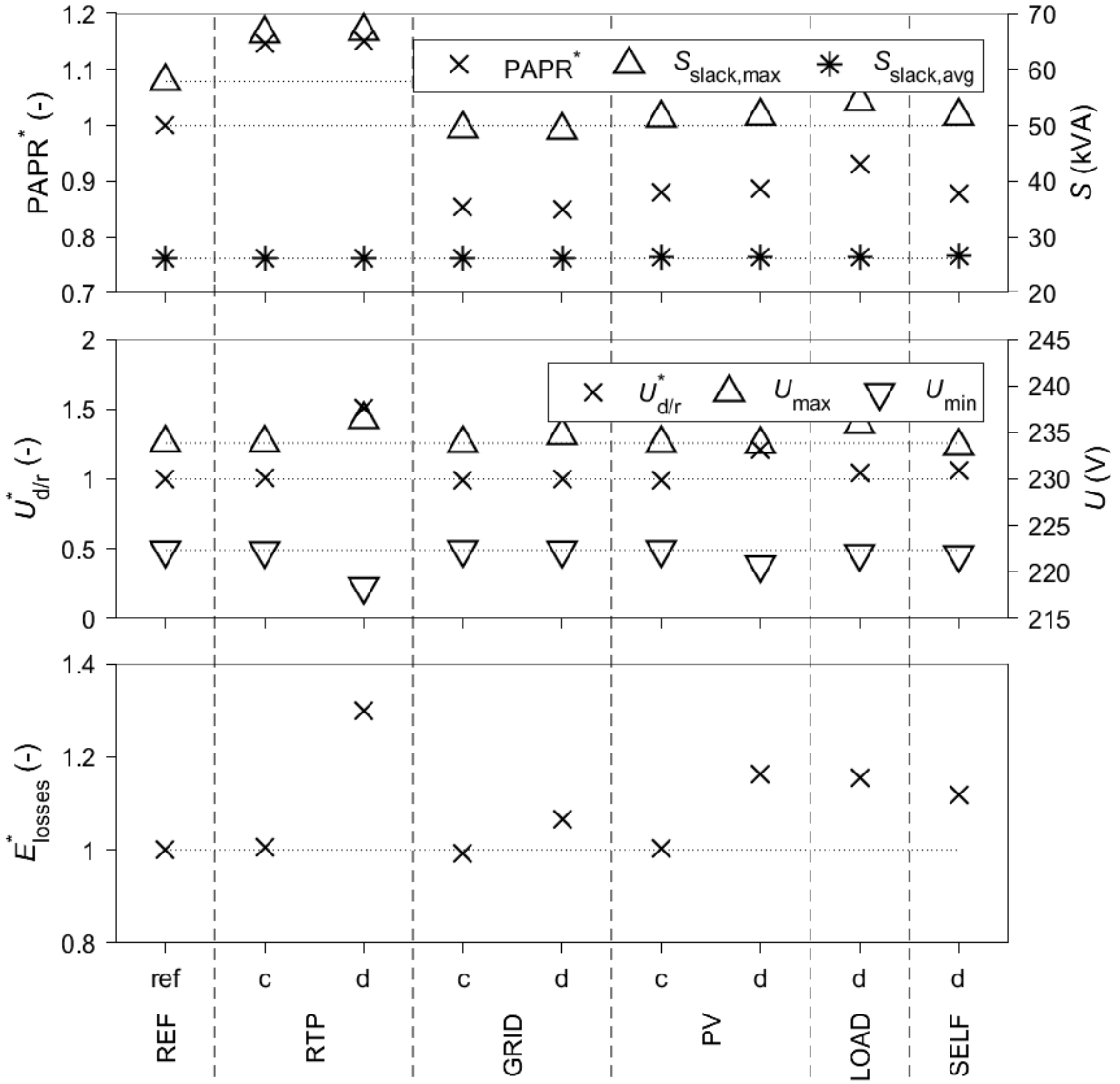

Fig. 3: Peak-to-average power ratio, voltages and cumulative distribution losses for all configurations for a single, central storage (c) and multiple, distributed storages (d). The superscript * refers to normed quantities with respect to the reference case, i.e. $E^*_{\mathrm{losses}} = \frac{E_{\mathrm{losses}}}{E_{\mathrm{losses,REF}}}$, analogously for $U_{\mathrm{d/r}}$ and PAPR.

Fig. 4 illustrates the power duration curves and Fig. 5 the voltage duration curves for all incentives and configurations. It shows the number of hours in which the feed-in apparent power is above a certain level. Better utilization of the grid is reflected by a straight curve. For both graphs, it can be seen that local, grid-motivated incentives (GRID, PV central) perform best, followed by consumer-motivated incentives (PV distributed, LOAD, SELF), the reference case, and RTP incentives. Simulations of a central storage, except in the RTP-driven case, have a positive impact on the voltage level and lead to a more uniform voltage distribution.

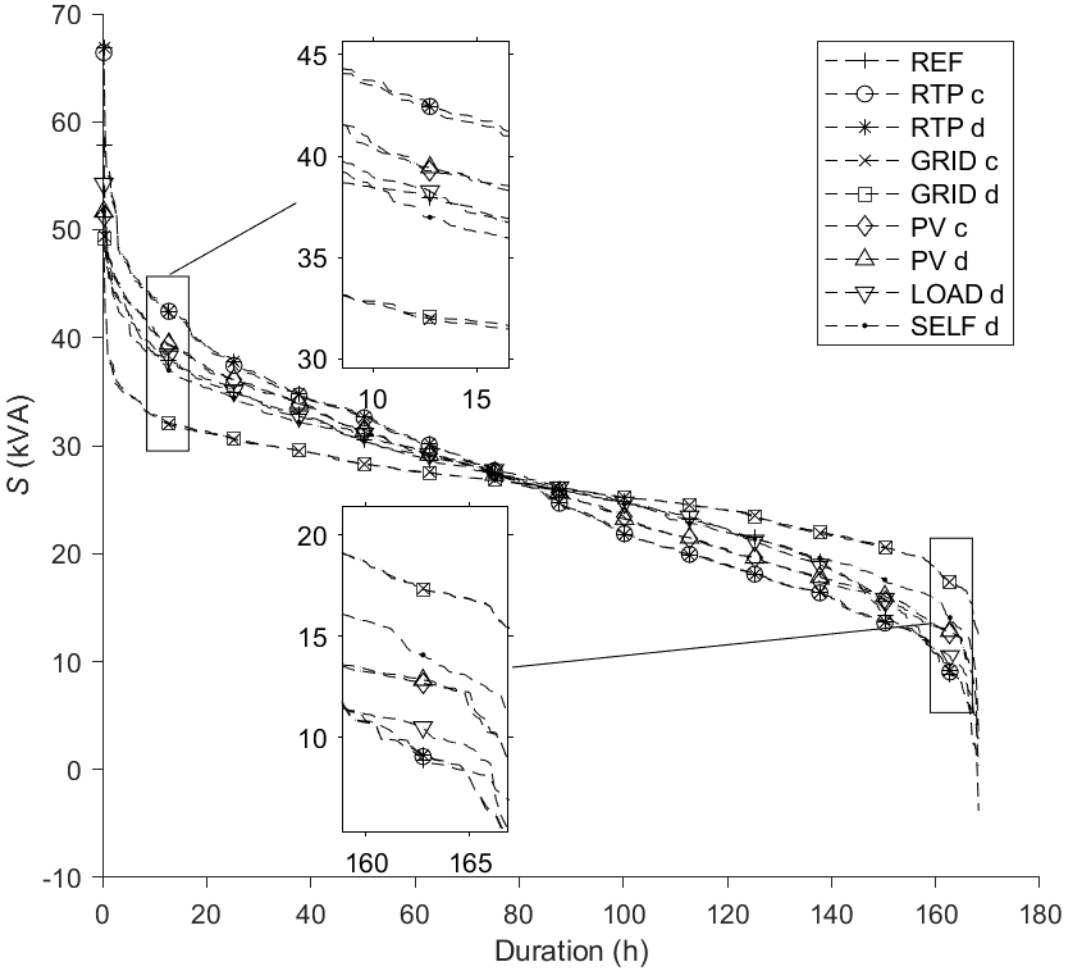

Fig. 4: Power duration curve for a single, central storage (c) and multiple, distributed storages (d) driven by different incentives.

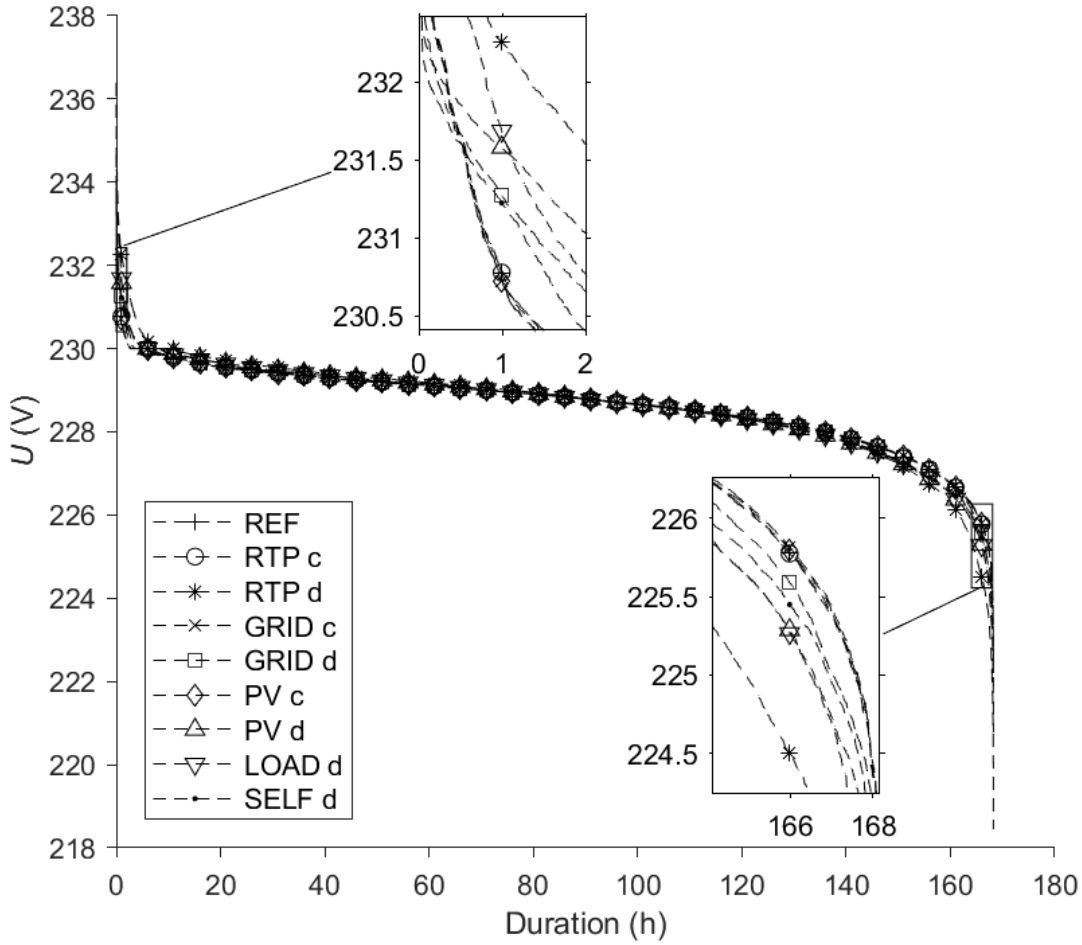

Fig. 5: Voltage duration curve for a single, central storage (c) and multiple, distributed storages (d) driven by different incentives.

4 Discussion

Results in section 3 show that local, grid-motivated incentives (GRID, PV central) help to improve the power quality in terms of the PAPR in the case of a single, central storage as well as in case of multiple, distributed storages. The distributed storages perform slightly better (15.0% reduction in PAPR for GRID distributed) than a central storage (14.5% reduction in PAPR for GRID central and 11.9% for PV central). This can be attributed to a higher probability that one of the distributed storages is close to a peak load at any given time as compared to a single, central storage. Hence, lower distribution losses occur for the transferred balancing energy. In addition, the cumulative distribution losses for distributed storages are higher than those for a central storage during the subsequent battery charging. In turn, the average slack node power is increased, which also leads to a further reduction of the PAPR. The voltage drop/rise is marginally better for central storages, however, for distributed storages, no significant change in the voltage quality is observed.

Consumer-motivated incentives (PV distributed, LOAD, SELF) for distributed storages lead to an improvement of the PAPR. This is because these incentives at least partially incorporate loads contributing to the total grid load. Combining household loads and photovoltaic generation reduces the PAPR most significantly (12.2% for SELF). This can be attributed to

the fact that the incentive represents more features of the total grid load than the individual photovoltaic or household loads. By applying photovoltaic generation as an incentive (PV), PAPR is improved by 11.4%; with individual household loads as the incentive (LOAD), the improvement is 7.0%. The voltage quality in terms of voltage drop/rise deteriorates only insignificantly compared to the reference.

Furthermore, we have proven that RTP incentives, as often used in literature, worsen the PAPR by 14.6% for a single, central storage and by 15.1% for multiple, distributed storages. This happens since supraregional markets do not reflect the local grid load situation. The voltage drop/rise for a single, central storage remains almost the same; for multiple, distributed storages, a deterioration of 1.8% of the minimum voltage compared to the minimum reference voltage is observed.

For distributed storages, the distribution losses of the investigated grid section increased. This can be attributed to the transmission of energy to the distributed storage resulting in higher losses compared to a feed-in-tied storage. This energy transfer also accounts for the greater deviation in voltage drop/rise of distributed storages compared to a central storage.

The round-trip efficiency used for the models was about 90%, which can only be achieved by very well-tuned systems. Lower round-trip efficiencies would increase the impact on the grid quality during discharging, due to the lower power output compared to systems that are more efficient.

5 Conclusion

In this work, the grid-balancing capability of a central battery storage was compared to distributed battery storage systems in a simulation study. Based on different incentives, the battery mode (charge, discharge, or idle) was determined by optimization. The simulation is based on a real grid topology in combination with smart meter household load data and distributed photovoltaics generation data. Evaluation criteria are the peak-to-average power ratio at the feed-in node, the maximum voltage drop/rise at all nodes of the grid, and the cumulative distribution losses of the investigated grid section.

The investigated cases show that incentives that reflect more general conditions, such as supraregional markets, may even deteriorate power quality. Thus, we proved that it is crucial to assess the impact of grid-balancing measures on all voltage levels of the electrical grid. Hence, to improve the power quality of low-voltage distribution grids by the use of autonomously optimized devices, local, grid-motivated and consumer-motivated incentives are preferable. In these cases, both a single, central storage as well as multiple, distributed storages have power quality related advantages in low-voltage distribution grids; the former configuration performs better in terms of the voltage drop/rise and shows lower distribution losses, the latter in terms of the reduction of the peak-to-average power ratio. Therefore, efforts should be made for grid and household load assessment, which account for contributions from distributed generation, in order to ensure grid reliability in the future.

Acknowledgements

The financial support by the Austrian Federal Ministry of Science, Research and Economy and the National Foundation for Research, Technology and Development is gratefully acknowledged.
The simulation study was conducted based on anonymized smart meter load data and PV generation data provided by Vorarlberger Kraftwerke AG and real, rural grid topology data provided by Vorarlberger Energienetze GmbH.
We thank Dr. Jörg Petrasch, the former Illwerke VKW Professor for Energy Efficiency and the former head of the Josef Ressel Center for Applied Scientific Computing in Energy, Finance, and Logistics at the Vorarlberg University of Applied Sciences, for his insightful contributions.

References

[1] B. Biegel, L. H. Hansen, J. Stoustrup, P. Andersen, and S. Harbo, "Value of flexible consumption in the electricity markets," *Energy*, vol. 66, pp. 354–362, Mar. 2014.

[2] M. Beaudin, H. Zareipour, A. Schellenberglabe, and W. Rosehart, "Energy storage for mitigating the variability of renewable electricity sources: An updated review," *Energy Sustain. Dev.*, vol. 14, no. 4, pp. 302–314, Dec. 2010.

[3] A. Pina, C. Silva, and P. Ferrão, "The impact of demand side management strategies in the penetration of renewable electricity," *Energy*, vol. 41, no. 1, pp. 128–137, May 2012.

[4] J. A. P. Lopes, N. Hatziargyriou, J. Mutale, P. Djapic, and N. Jenkins, "Integrating distributed generation into electric power systems: A review of drivers, challenges and opportunities," *Electr. Power Syst. Res.*, vol. 77, no. 9, pp. 1189–1203, Jul. 2007.

[5] C. Bucher, "Analysis and Simulation of Distribution Grids with Photovoltaics," ETH Zurich, 2014.

[6] J. V. Paatero and P. D. Lund, "Effects of large-scale photovoltaic power integration on electricity distribution networks," *Renew. Energy*, vol. 32, no. 2, pp. 216–234, Feb. 2007.

[7] L. F. Ochoa, A. Padilha-Feltrin, and G. P. Harrison, "Evaluating distributed generation impacts with a multiobjective index," *IEEE Trans. Power Deliv.*, vol. 21, no. 3, pp. 1452–1458, Jul. 2006.

[8] A. Woyte, V. V. Thong, R. Belmans, and J. Nijs, "Voltage fluctuations on distribution level introduced by photovoltaic systems," *IEEE Trans. Energy Convers.*, vol. 21, no. 1, pp. 202–209, Mar. 2006.

[9] T. Ackermann and V. Knyazkin, "Interaction between distributed generation and the distribution network: operation aspects," 2002, vol. 2, pp. 1357–1362.

[10] P. P. Barker and R. W. De Mello, "Determining the impact of distributed generation on power systems. I. Radial distribution systems," 2000, vol. 3, pp. 1645–1656.

[11] T. Stetz, F. Marten, and M. Braun, "Improved Low Voltage Grid-Integration of Photovoltaic Systems in Germany," *IEEE Trans. Sustain. Energy*, vol. 4, no. 2, pp. 534–542, Apr. 2013.

[12] P. Siano, "Demand response and smart grids—A survey," *Renew. Sustain. Energy Rev.*, vol. 30, pp. 461–478, Feb. 2014.

[13] P. Palensky and D. Dietrich, "Demand Side Management: Demand Response, Intelligent Energy Systems, and Smart Loads," *IEEE Trans. Ind. Inform.*, vol. 7, no. 3, pp. 381–388, Aug. 2011.

[14] L. Gelazanskas and K. A. A. Gamage, "Demand side management in smart grid: A review and proposals for future direction," *Sustain. Cities Soc.*, vol. 11, pp. 22–30, Feb. 2014.

[15] P. Richardson, D. Flynn, and A. Keane, "Optimal Charging of Electric Vehicles in Low-Voltage Distribution Systems," *IEEE Trans. Power Syst.*, vol. 27, no. 1, pp. 268–279, Feb. 2012.

[16] C. Pang, P. Dutta, and M. Kezunovic, "BEVs/PHEVs as Dispersed Energy Storage for V2B Uses in the Smart Grid," *IEEE Trans. Smart Grid*, vol. 3, no. 1, pp. 473–482, Mar. 2012.

[17] W. Zhang *et al.*, "Decentralized Electric Vehicle Charging Strategies for Reduced Load Variation and Guaranteed Charge Completion in Regional Distribution Grids," *Energies*, vol. 10, no. 2, p. 147, Jan. 2017.

[18] B. P. Roberts and C. Sandberg, "The Role of Energy Storage in Development of Smart Grids," *Proc. IEEE*, vol. 99, no. 6, pp. 1139–1144, Jun. 2011.

[19] M. Bragard, N. Soltau, S. Thomas, and R. W. De Doncker, "The Balance of Renewable Sources and User Demands in Grids: Power Electronics for Modular Battery Energy Storage Systems," *IEEE Trans. Power Electron.*, vol. 25, no. 12, pp. 3049–3056, Dec. 2010.

[20] H. Qian, J. Zhang, J.-S. Lai, and W. Yu, "A high-efficiency grid-tie battery energy storage system," *IEEE Trans. Power Electron.*, vol. 26, no. 3, pp. 886–896, Mar. 2011.

[21] L. Joerissen, J. Garche, C. Fabjan, and G. Tomazic, "Possible use of vanadium redox-flow batteries for energy storage in small grids and stand-alone photovoltaic systems," *J. Power Sources*, vol. 127, no. 1–2, pp. 98–104, Mar. 2004.

[22] O. M. Toledo, D. Oliveira Filho, and A. S. A. C. Diniz, "Distributed photovoltaic generation and energy storage systems: A review," *Renew. Sustain. Energy Rev.*, vol. 14, no. 1, pp. 506–511, Jan. 2010.

[23] R. S. Bhatia, S. P. Jain, Dinesh Kumar Jain, and B. Singh, "Battery Energy Storage System for Power Conditioning of Renewable Energy Sources," 2005, vol. 1, pp. 501–506.

[24] T. Borsche, A. Ulbig, M. Koller, and G. Andersson, "Power and energy capacity requirements of storages providing frequency control reserves," presented at the Power and Energy Society General Meeting, Vancouver, 2013, pp. 1–5.

[25] M. T. Lawder *et al.*, "Battery Energy Storage System (BESS) and Battery Management System (BMS) for Grid-Scale Applications," *Proc. IEEE*, vol. 102, no. 6, pp. 1014–1030, Jun. 2014.

[26] H. Chen, T. N. Cong, W. Yang, C. Tan, Y. Li, and Y. Ding, "Progress in electrical energy storage system: A critical review," *Prog. Nat. Sci.*, vol. 19, no. 3, pp. 291–312, Mar. 2009.

[27] T. Ma, H. Yang, and L. Lu, "Feasibility study and economic analysis of pumped hydro storage and battery storage for a renewable energy powered island," *Energy Convers. Manag.*, vol. 79, pp. 387–397, Mar. 2014.

[28] C. J. Barnhart and S. M. Benson, "On the importance of reducing the energetic and material demands of electrical energy storage," *Energy Environ. Sci.*, vol. 6, no. 4, p. 1083, 2013.

[29] M. O. Ramoni and H.-C. Zhang, "End-of-life (EOL) issues and options for electric vehicle batteries," *Clean Technol. Environ. Policy*, vol. 15, no. 6, pp. 881–891, Dec. 2013.

[30] B. Fäßler, P. Kepplinger, M. L. Kolhe, and J. Petrasch, "Decentralized on-site optimization of a battery storage system using one-way communication," presented at the International Conference on Renewable Power Generation, 2015, pp. 1–6.

[31] C. Heymans, S. B. Walker, S. B. Young, and M. Fowler, "Economic analysis of second use electric vehicle batteries for residential energy storage and load-levelling," *Energy Policy*, vol. 71, pp. 22–30, Aug. 2014.

[32] B. Faessler, P. Kepplinger, and J. Petrasch, "Decentralized price-driven grid balancing via repurposed electric vehicle batteries," *Energy*, vol. 118, pp. 446–455, Jan. 2017.

[33] P. Kepplinger, G. Huber, and J. Petrasch, "Demand Side Management via Autonomous Control-Optimization and Unidirectional Communication with Application to Resistive Hot Water Heaters," *ENOVA 2014*, p. 8, Dec. 2014.

[34] P. Finn and C. Fitzpatrick, "Demand side management of industrial electricity consumption: Promoting the use of renewable energy through real-time pricing," *Appl. Energy*, vol. 113, pp. 11–21, Jan. 2014.

[35] S. Gottwalt, W. Ketter, C. Block, J. Collins, and C. Weinhardt, "Demand side management—A simulation of household behavior under variable prices," *Energy Policy*, vol. 39, no. 12, pp. 8163–8174, Dec. 2011.

[36] T. Logenthiran, D. Srinivasan, A. M. Khambadkone, and H. N. Aung, "Multiagent System for Real-Time Operation of a Microgrid in Real-Time Digital Simulator," *IEEE Trans. Smart Grid*, vol. 3, no. 2, pp. 925–933, Jun. 2012.

[37] J. G. Roos and I. E. Lane, "Industrial power demand response analysis for one-part real-time pricing," *IEEE Trans. Power Syst.*, vol. 13, no. 1, pp. 159–164, Feb. 1998.

[38] EXAA Abwicklungsstelle für Energieprodukte AG, "EXAA Energy Exchange Austria," *EXAA Energy Exchange Austria*. [Online]. Available: www.exaa.at. [Accessed: 18-Dec-2015].

[39] G. Xu, S. Wu, and Y. Tan, "Island Partition of Distribution System with Distributed Generators Considering Protection of Vulnerable Nodes," *Appl. Sci.*, vol. 7, no. 10, p. 1057, Oct. 2017.

[40] C. Pötzinger, M. Preißinger, and D. Brüggemann, "Influence of Hydrogen-Based Storage Systems on Self-Consumption and Self-Sufficiency of Residential Photovoltaic Systems," *Energies*, vol. 8, no. 8, pp. 8887–8907, Aug. 2015.

[41] A. Ul-Haq, C. Cecati, and E. Al-Ammar, "Modeling of a Photovoltaic-Powered Electric Vehicle Charging Station with Vehicle-to-Grid Implementation," *Energies*, vol. 10, no. 1, p. 4, Dec. 2016.

[42] U. Ghatak and V. Mukherjee, "An improved load flow technique based on load current injection for modern distribution system," *Int. J. Electr. Power Energy Syst.*, vol. 84, pp. 168–181, Jan. 2017.

[43] H. Li, A. Zhang, X. Shen, and J. Xu, "A load flow method for weakly meshed distribution networks using powers as flow variables," *Int. J. Electr. Power Energy Syst.*, vol. 58, pp. 291–299, Jun. 2014.

[44] U. Ghatak and V. Mukherjee, "A fast and efficient load flow technique for unbalanced distribution system," *Int. J. Electr. Power Energy Syst.*, vol. 84, pp. 99–110, Jan. 2017.

[45] Jen-Hao Teng, "A direct approach for distribution system load flow solutions," *IEEE Trans. Power Deliv.*, vol. 18, no. 3, pp. 882–887, Jul. 2003.

[46] MATLAB, *MATLAB 2017a*. Natick, Massachusetts: The MathWorks Inc.

[47] M. Schuler, "Simulation Elektrischer Netze zur Beurteilung von Verbraucherseitiger Laststeuerung," Vorarlberg University of Applied Sciences, Dornbirn, Master's Thesis, 2017.

[48] Vorarlberger Energienetze GmbH, "Vorarlberger Energienetze GmbH." *Vorarlberger Netz*. [Online]. Available: www.vorarlbergnetz.at. [Accessed: 01-Jun-2017].

[49] Vorarlberger Kraftwerke AG, "VKW (Vorarlberger Kraftwerke AG)," *Vorarlberger Kraftwerke AG*. [Online]. Available: www.vkw.at. [Accessed: 01-Jun-2017].

[50] W. Gawlik *et al.*, "aDSM - Aktives Demand-Side-Management durch Einspeiseprognose," Vienna University of Technology - Institute of Energy Systems and Electrical Drives, Vienna, Endbericht, 2014.

[51] T. Erge, V. U. Hoffmann, and K. Kiefer, "The German experience with grid-connected PV-systems," *Sol. Energy*, vol. 70, no. 6, pp. 479–487, 2001.

[52] C. Bucher, "Wie viel Solarstrom verträgt das Niederspannungsnetz?," *Bulletin Electrosuisse*, no. 3/2014, pp. 37–40, Mar-2014.

[53] P. Vollmer, "Großer Vergleich - Das sind die 93 besten Stromspeicher für Zuhause," *WirtschaftsWoche*, 20-Jun-2016.

[54] sonnen GmbH, "sonnen GmbH - energy is yours," *sonnen*, 11-Feb-2016. [Online]. Available: www.sonnenbatterie.de. [Accessed: 31-May-2017].

[55] sonnen GmbH, "Technische Daten sonnenBatterie eco 8.0." sonnen GmbH, 17-May-2017.

[56] MATLAB, *Optimization Toolbox*. Natick, Massachusetts: The MathWorks Inc.

[57] EN Standard, "DIN EN 50160:2011-02," *Merkmale Spann. Öffentl. Elektrizitätsversorgungsnetzen*, Feb. 2011.

Appendix

Table 3: PAPR, power, and loss results achieved for a single, central storage (c) and multiple, distributed storages (d) driven by different incentives. The superscript * refers to normed quantities with respect to the reference case, i.e. $E^*_{\mathrm{losses}} = \frac{E_{\mathrm{losses}}}{E_{\mathrm{losses,REF}}}$ and analogously for PAPR.

		S_{avg} (kVA)	S_{min} (kVA)	S_{max} (kVA)	PAPR (–)	PAPR* (–)	E_{losses} (kWh)	E^*_{losses} (–)
REF		26.21	4.06	57.88	2.21	1.00	38.76	1.00
RTP	c	26.24	−3.84	66.41	2.53	1.15	38.97	1.01
	d	26.31	−3.62	66.85	2.54	1.15	50.38	1.30
GRID	c	26.14	12.56	49.35	1.89	0.85	38.50	0.99
	d	26.16	12.51	49.12	1.88	0.85	41.29	1.07
PV	c	26.38	2.80	51.32	1.95	0.88	38.83	1.00
	d	26.42	2.88	51.68	1.96	0.89	45.03	1.16
LOAD	d	26.42	0.37	54.26	2.05	0.93	44.72	1.15
SELF	d	26.63	3.10	51.68	1.94	0.88	43.35	1.12

Table 4: Voltage results achieved for a single, central storage (c) and multiple, distributed storages (d) driven by different incentives. The superscript * refers to normed quantities with respect to the reference case, i.e. $U^*_{\mathrm{d/r}} = \frac{U_{\mathrm{d/r}}}{U_{\mathrm{d/r,REF}}}$.

		U_{avg} (V)	U_{min} (V)	U_{max} (V)	$U^*_{\mathrm{d/r}}$ (–)
REF		228.67	222.35	233.87	1.00
RTP	c	228.67	222.29	233.87	1.01
	d	228.66	218.44	236.39	1.51
GRID	c	228.67	222.40	233.82	0.99
	d	228.67	222.35	234.68	1.00
PV	c	228.67	222.40	233.82	0.99
	d	228.65	220.77	233.72	1.21
LAOD	d	228.65	221.99	235.87	1.05
SELF	d	228.64	221.86	233.53	1.06